2025

U.S. Department of Transportation
Federal Highway Administration

NEBRASKA
DEPARTMENT OF TRANSPORTATION

NEBRASKA
TRANSPORTATION CENTER

Final Report SPR-FY23(024)

Repair/Preservation of Concrete Compression Members in Bridges Using Ultra-High-Performance Concrete (UHPC)

Mohammed Hedia, MS
Research Assistant
Durham School of Architectural Engineering and Construction
University of Nebraska-Lincoln

George Morcous, PhD
Professor
Durham School of Architectural Engineering and Construction
University of Nebraska-Lincoln

Nebraska Department of Transportation Research
Headquarters Address
1400 Nebraska Parkway
Lincoln, NE 68509
ndot.research@nebraska.gov
(402) 479-4697
https://dot.nebraska.gov/business-center/research/

Nebraska Transportation Center
262 Prem S. Paul Research Center at Whittier School
2200 Vine Street
Lincoln, NE 68583-0851
(402) 472-1932
http://ntc.unl.edu

This report was funded in part through grant from the U.S. Department of Transportation Federal Highway Administration. The views and opinions of the authors expressed herein do not necessarily state or reflect those of the U.S. Department of Transportation.

TECHNICAL REPORT DOCUMENTATION PAGE

1. Report No. SPR-FY23(024)	**2. Government Accession No.**	**3. Recipient's Catalog No.**
4. Title and Subtitle Repair/Preservation of Concrete Compression Members in Bridges Using Ultra-High-Performance Concrete (UHPC)		**5. Report Date** September 2025 **6. Performing Organization Code**
7. Author(s) Mohammed Hedia George Morcous		**8. Performing Organization Report No.** SPR-FY23(024)
9. Performing Organization Name and Address University of Nebraska-Lincoln 1110 South 67th St. Omaha, Nebraska 68182-0178		**10. Work Unit No.** **11. Contract**
12. Sponsoring Agency Name and Address Nebraska Department of Transportation Research Section 1400 Nebraska Parkway Lincoln, NE 68502		**13. Type of Report and Period Covered** Final Report July 2022 – May 2025 **14. Sponsoring Agency Code**
15. Supplementary Notes		

16. Abstract

As of 2024, approximately 36% of bridges across the United States require repair or replacement, with 7% classified as structurally deficient. The estimated cost to address these deficiencies exceeds $260 billion. In recent years, Ultra-High-Performance Concrete (UHPC) has emerged as a repair material for infrastructure preservation, drawing increased attention from transportation agencies and researchers worldwide. The Federal Highway Administration (FHWA) has notably advocated for UHPC's adoption in bridge preservation initiatives, recognizing its exceptional mechanical properties and durability.

This report presents a comprehensive literature review on the application of UHPC as a repair and strengthening material for bridge compression members. While significant progress has been made in employing UHPC for bridge decks and joints, its use in repair or strengthening bridge columns/piles remains relatively underexplored. To address this gap, the study introduces an analytical model designed to predict the axial and flexural capacities of reinforced or prestressed concrete compression members encased with UHPC jackets. The model is formulated based on strain compatibility and integrates idealized UHPC material behavior in both tension and compression, consistent with the latest UHPC design specifications. In addition, an experimental program was conducted to evaluate the structural benefits of UHPC encasement in compression members. The investigation consisted of two phases. Phase I assessed the confinement effect of UHPC on small-scale concrete cylinders with varying jacket thicknesses, revealing notable enhancements in compressive strength and ductility. Phase II focused on full-scale reinforced concrete columns subjected to axial loading and bending, examining the bond behavior at the UHPC–conventional concrete (CC) substrate interface under different surface preparation methods and the influence of transverse reinforcement within the UHPC jacket. Results confirmed a strong interfacial bond and underscored the role of transverse reinforcement in delaying failure and improving overall structural performance. The report concludes with a detailed design example, demonstrating the model's applicability and its predictive accuracy in estimating strength gains due to UHPC jacketing. Collectively, this study provides both a practical design framework and novel experimental insights, reinforcing UHPC's potential to enhance structural performance and extend the service life of aging bridge infrastructure.

17. Key Words Bridge repair, UHPC, AASHTO Guide Specifications, composite sections, Compression members, Interaction diagram, Confinement, Surface preparation, Bond.	**18. Distribution Statement** No restrictions. This document is available through the National Technical Information Service. 5285 Port Royal Road Springfield, VA 22161

19. Security Classification (of this report) Unclassified	**20. Security Classification (of this page)** Unclassified	**21. No. of Pages** 143	**22. Price**
Form DOT F 1700.7 (8-72)	Reproduction of completed page authorized		

Table of Contents

List of Figures

List of Tables

Disclaimer

The contents of this report reflect the views of the authors, who are responsible for the facts and the accuracy of the information presented herein. The contents do not necessarily reflect the official views or policies of the Nebraska Department of Transportations or the University of Nebraska-Lincoln. This report does not constitute a standard, specification, or regulation. Trade or manufacturers' names, which may appear in this report, are cited only because they are considered essential to the report's objectives.

The United States (U.S.) government and the State of Nebraska do not endorse products or manufacturers. This material is based upon work supported by the Federal Highway Administration under contract SPR-FY23(024). Any opinions, findings and, conclusions, or recommendations expressed in this publication are those of the author(s) and do not necessarily reflect the views of the Federal Highway Administration."

This report has been reviewed by the Nebraska Transportation Center for grammar and context, formatting, and compliance with Section 508 of the Rehabilitation Act of 1973.

Acknowledgments

The research presented in this project was supported by the Nebraska Department of Transportation (NDOT), and their contribution is gratefully appreciated. The authors would also like to express their sincere thanks to the members of the project advisory committee for their guidance, input, and review throughout the project duration.

Executive Summary

Challenge: Aging infrastructure remains a critical concern in the United States, with over 40% of the nation's bridges now exceeding 50 years in service life and approximately 7% classified as structurally deficient. This growing deterioration emphasizes the need for durable, cost-effective, and sustainable rehabilitation strategies. Ultra-High-Performance Concrete (UHPC), with its superior mechanical and durability characteristics, has emerged as a promising material for repair and strengthening. Its use has been actively promoted by the Federal Highway Administration (FHWA), particularly under the Everyday Counts (EDC-6) initiative, for applications including deck overlays, girder-end rehabilitation, and component jacketing. A preliminary review of the literature reveals a notable gap in the application of UHPC for the repair/strengthening of structural concrete components, particularly compression members like columns and piles. Moreover, the significant disparity between the material properties of UHPC jacket and conventional concrete (CC) member complicates the behavior of composite section.

Proposed model: An analytical approach to predict the capacity of reinforced/prestressed concrete compression members with UHPC encasement under combined axial and bending loads is presented in this report. The approach uses strain compatibility and idealized UHPC material models in tension and compression according to the AASHTO (2024). The approach uses integration to calculate the internal forces and develop interaction diagrams for any section, overcoming the approximations of the lamina approach.

Experimental Research: This research includes two phases: Phase I involved testing fourteen 4 in. × 8 in. CC cylinders with compressive strengths of 6 ksi and 7.5 ksi, confined by UHPC jackets of 1-in. and 2-in. thicknesses, to evaluate the impact of UHPC confinement on compression behavior; Phase II investigated eight full-scale CC columns strengthened with

UHPC jackets, focusing on the influence of common surface preparation techniques used in the bridge industry. Four specimens were jacketed with 2-in.-thick UHPC without transverse reinforcement, and four specimens had transverse reinforcement within the top 6 in. of the jacket to counteract splitting stresses observed in unreinforced specimens. Axial loading was applied to six specimens and interface slippage between CC and UHPC were measured, along with longitudinal and transverse strain in the UHPC jacket. Two specimens were tested in flexure to simulate members subjected to significant bending.

Observations: In the experimental program, Phase I and Phase II revealed consistent crack localization behavior in UHPC jackets. In Phase I, cracks typically formed at 60–65% of peak load, initiating at the top or bottom of the jacket and propagating vertically. Despite visible cracking, the fiber-bridging action of UHPC allowed the specimens to continue resisting load until fiber rupture led to sudden failure. In Phase II, interface slip was minimal, indicating a strong bond. Similar crack localization and fiber-bridging behavior were observed. Additional specimens with transverse reinforcement inside the UHPC jacket showed delayed crack formation and enhanced performance.

Summary: The results confirmed that UHPC jackets significantly improved mechanical properties. In Phase I, a 1-in. jacket increased compressive strength by up to 47.3%, strain capacity by 24.3%, and stiffness by 40.9%. A 2-in. jacket resulted in gains up to 84.2% in compressive strength, 27.1% in strain capacity, and 76.1% in stiffness. Phase II results demonstrated that adding transverse reinforcement to the UHPC jacket in CC compression members effectively increased the axial compressive capacity and prevented delay the crack localization. Together, the findings validate the use of UHPC jackets for repair and strengthening CC compression members.

Chapter 1 Introduction

1.1 Overview

Structural engineers are often faced with the challenge of required repair and strengthening projects for the ever-deteriorating concrete members in bridges. Strengthening projects are typically required when the structure's use is modified, requiring certain members to have higher capacity. Repair projects are typically required after incidents of deterioration, or incidental damage (i.e., impact damage) causing section loss in concrete or reinforcement.

As of 2024, around 36% of all bridges in the United States need repair/replacement work, and 7% are classified as structurally deficient. The cost of the identified repairs is estimated at $260 billion to restore their condition and maintain their service life (Bridge Report, 2024).

Recently, there were several repair and strengthening techniques using Ultra-High Performance Concrete (UHPC) that have been documented by several agencies in the United States and other countries and developed by different researchers for bridges. The Federal Highway Administration (FHWA) has been leading efforts in the past two years to encourage the use of UHPC in bridge preservation (FHWA-HRT-22-065, 2022). An interactive map has been created and frequently updated by FHWA to show cases where UHPC is used in bridge preservation in the United States.

UHPC is a relatively newly developed material and its use in the reinforced concrete construction industry has been growing rapidly in the past two decades, earning it the title of "Game Changer" (Binard, 2017). UHPC can be defined according to the AASHTO Guide Specifications for Structural Design with UHPC as "a cementitious composite material composed of an optimized gradation of granular constituents, a water-to-cementitious materials ratio less than 0.25, and a high percentage of discontinuous internal fiber reinforcement. The mechanical

properties include compressive strength greater than 17.5 ksi and sustained post-cracking tensile strength greater than 0.72 ksi." The presence of fibers in UHPC enhances all tension-driven failure modes, especially shear strength, which helps eliminate transverse reinforcement in beams and bridge girders.

One of the major challenges facing the growth of using UHPC is that it is a relatively new material compared to other cementitious materials. Limited cases using UHPC in the repair and strengthening of conventional concrete (CC) members have been reported. No cases of strengthening concrete beams have been reported to date. Table 1.1 lists some of the reported cases, the repair or strengthening that was required, and the advantages offered by UHPC compared to other options.

Table 1.1 Cases of using UHPC as a strengthening/repair material

Case	Requirement for Repair or Strengthening	Advantages offered by UHPC
Caderousse Dam's slab, 2010	Impact damage from heavy rocks	High impact and abrasion resistance. And high early-age compressive strength
Rail Bridge Pier Jacketing, Montreal, 2013	Spalling and deterioration	Jacket thickness was minimized compared to other options, maintaining adequate road clearances
Mission Bridge Piers Seismic Retrofit, 2014	Foundations in a high seismic zone and highly liquefiable soil	UHPC ductility would allow for high deformation capacity
Encasement of Bent Legs, 2015	Local corrosion at steel bent legs. Increase load capacity	Better mechanical properties than other options minimizing the required encasement area
Steel Bridge Girder, Zemtra, 2015	Corrosion damage	UHPC end-block increased shear and bearing resistance
Mud Creek Bridge Deck Overlay, Iowa, 2016	Cracking and spalling	High resistance to cracking and spalling, decrease water penetration, increasing deck rigidity, and girder flexural strength
Concrete bridge girder, 2016	Poorly consolidated closure pour	High bond strength with

		steel reinforcement and existing concrete. Highly flowable and self-consolidating for the congested area.
Ductal Shotcrete for Renovating a Metal Culvert	Deterioration	Minimizing jacket thickness (1.2 in.) and the reduction of the culvert cross-section
Precast Column Jacket	Additional load from 2 extra stories	Minimizing jacket thickness
Steel Bridge End Repair	Corrosion Damage	Provide 15-20 Years Additional Service Life

Using UHPC as a repair and strengthening material can offer several benefits over other techniques such as:

1. Marginal permeability, which increases durability and service life of the repaired/ strengthened section and has higher resistance to further damage/vandalism of the element.
2. Less sensitive to base concrete surface preparation than FRP wrapping.
3. Replace patching materials in restoring the loss in a concrete section (patching is required to be done prior to FRP wrapping).
4. High tension and shear resistance can eliminate the need for additional transverse reinforcement.
5. Increased bond strength to base concrete and reinforcement.
6. Highly flowable and self-consolidating for congested areas.
7. Smaller increase in section dimensions compared to CC jacketing.

1.2 Problem Statement

There is currently a lack of comprehensive design guidelines and standardized construction procedures for composite CC-UHPC components, particularly in the context of repairing and strengthening of compression members using NDOT-UHPC. In addition, the limited field applications and practical experience with UHPC in bridge compression members rehabilitation

pose further challenges for implementation. Few prediction models exist for evaluating structural behavior or facilitating the design of composite sections, such as CC compression members repaired or strengthened with UHPC.

A fundamental challenge lies in the significant mismatch between the mechanical properties of CC and UHPC, which complicates the prediction of composite behavior. As shown in Figure 1.1, the compressive stress-strain response of UHPC (with a compressive strength of 17.5 ksi) differs greatly from that of CC (with a compressive strength of 5 ksi). UHPC also exhibits a much higher elastic modulus than CC, resulting in higher stress concentrations in the UHPC at any given strain level. In tension, the disparity is even more pronounced: Figure 1.2 illustrates that UHPC maintains post-cracking tensile strength up to strain levels exceeding 0.01, whereas CC rapidly loses all tensile resistance upon cracking.

These differences underscore the need for analytical models and practical design guidance to ensure safe and effective use of UHPC in structural rehabilitation and strengthening of existing CC compression members.

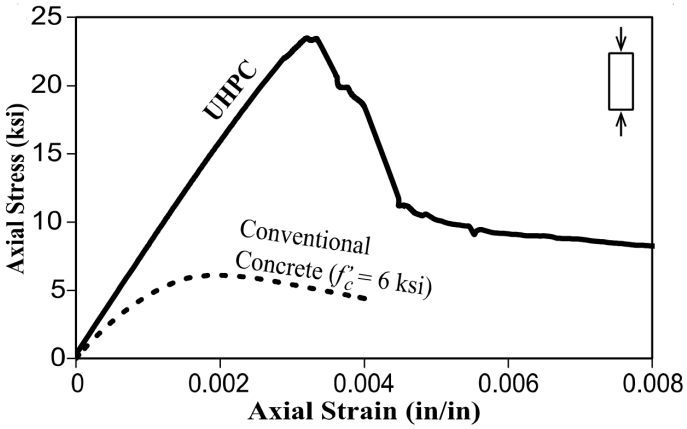

Figure 1.1 Stress-strain behavior of CC and UHPC in compression (El-Helou et al., 2019)

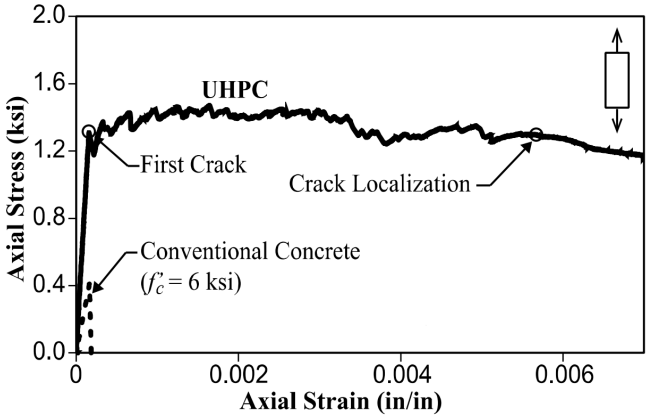

Figure 1.2 Stress-strain behavior of CC and UHPC in tension (El-Helou et al., 2019)

1.3 Research Objectives and Scope

The primary objective of this report is to establish a design methodology and construction procedure for utilizing UHPC in the repair and preservation of concrete bridge compression members. This involves developing a predictive model to determine the capacity of compression members encased in UHPC and generating an interaction diagram for such members. Additionally, the study examines the confinement effect of UHPC encasement on conventional concrete compression members, which is often overlooked in existing predictive models. The report also aims to streamline the construction process for using UHPC as a repair material in bridge components and to implement the proposed methodology in a demonstration project.

The developed prediction model applies to both prestressed and non-prestressed concrete bridge components. However, the experimental investigation is focused exclusively on non-prestressed components.

1.4 Report Organization

This report is structured as follows:

Chapter 2: Literature Review – Provides an overview of current practices in utilizing UHPC as a repair material for bridge compression members worldwide, with a focus on U.S. implementation projects and experimental studies on composite CC-UHPC compression members.

Chapter 3: Capacity of Compression Members Strengthened/Repaired with UHPC – presents a predictive model for evaluating the axial and flexural strength of compression members retrofitted or repaired using UHPC encasement. It also outlines the process for constructing interaction diagrams. The chapter details the adopted material modeling approach and highlights the key factors influencing the structural performance of the strengthened members.

Chapter 4: Experimental Investigation – Presents testing results of CC-UHPC cylinders to assess the confinement effect, along with full-scale specimen tests to evaluate compressive strength, interface shear and bond strength, and validate the developed model.

Chapter 5: Conclusions – Summarizes the key findings of the study, lessons learned from test specimen construction, and design recommendations based on structural testing outcomes.

Chapter 2 Literature Review

2.1 Introduction

This chapter explores current practices utilizing UHPC for repairing and strengthening bridge compression members. It also reviews experimental studies on reinforced concrete compression members repaired or strengthened with UHPC under cyclic and axial loading. This chapter also provides an overview of existing prediction models for conventional concrete (CC) compression members repaired using UHPC, highlighting their limitations. The insights presented in this chapter serve as a basis for developing improved prediction model for construction of interaction diagram of composite CC-UHPC compression members and experimentally investigate the effect of UHPC confinement on CC jacket and interface performance between CC and UHPC in compression members.

2.2 Current Practices of Using UHPC in Repair/Strengthening of Compression Members

This section presents a review of the reported practices of UHPC production and construction procedure used in repairing and strengthening CC compression members in bridges. Several cases have been reported with their construction procedures. These cases are presented for each construction practice discussed in this section.

UHPC has been reported in several strengthening projects because of its superior mechanical properties, durability, and ductility compared to conventional encasement materials. These superior properties enable the jacket dimensions to be minimized which can offer several advantages in tight areas. One case of adding a thin UHPC jacket over an impact damaged bridge pier is reported by Ductal (2020) and Doiron (2017) where UHPC was casted using a chute. The pier supported a railway bridge crossing over a two-lane ramp with narrow lanes. The existing bridge pier showed some spalling and deterioration, and the selected strengthening method was

adding a concrete jacket to protect against chloride ingress and freeze/thaw. The jacket thickness had to be optimized to maintain adequate clearances, which led to choosing UHPC. The deteriorated layer was removed, and a galvanized rebar cage was added. Afterwards, forms were installed to allow for a four-inch-thick concrete jacket of UHPC. Top openings were made in the forms around the pier and UHPC was cast from the top of the bridge deck as shown in Figure 2.1. Figure 2.2 shows the final UHPC jacket over the damaged bridge pier. In addition to the top form openings, intermediate openings were done to allow for mid-height UHPC pouring and better consolidation. This technique requires access from below the bridge and access to the top of the forms, which might be challenging in some projects. However, the advantage offered by this technique is that no opening is needed to be drilled in the deck slab as in the previous technique of steel bridge girder ends.

Figure 2.1 Casting UHPC using a chute for a thin jacket for a bridge pier from the top of formwork (Doiron, 2017)

Figure 2.2 UHPC jacket over the bridge pier (Doiron, 2017)

Another case of column encasement was reported by Doiron (2017) to cast a strengthening jacket for bridge columns subjected to significant seismic actions and the possibility of soil liquefaction. Two tapered, rectangular jackets with a height of approximately 10.5 feet from the base were cast around the V-shaped concrete piers as shown in Figure 2.3. Compared to other strengthening methods using traditional piles, a UHPC jacket provided significant cost savings, and allowed for a high seismic deformation capacity with a thin jacket. A conical shaped hopper allowed UHPC to be poured into tight places and small forms as shown in Figure 2.4. The main challenge facing this technique is the requirement for clear access from the top of the forms, as well as crane access to the casting location. The main advantage offered by this technique is the minimized pouring time and required labor during casting.

Figure 2.3 Seismic strengthening with UHPC jackets around bridge piers (Doiron, 2017)

Figure 2.4 Casting UHPC jacket around bridge pier using hopper (Doiron, 2017)

Another case of using precast UHPC jacket components to strengthen concrete columns in a shopping center in the United Kingdom was reported by Ductal (2020). The building required redevelopment to add two more stories to its existing structure which required the columns on the ground floor to be strengthened. Two components of the jacket were installed against each other and were linked to the existing element by anchors along the height of the element as shown in Figure 2.5. The use of thin UHPC jackets resulted in minimized added dimensions for the existing columns, as well as significantly reduced installation time.

Figure 2.5 Precast UHPC column encasement (Ductal, 2020)

2.3 Experimental Work

This section presents a review of collected test data of the experimental work of different CC compression members strengthened/repaired using UHPC, which includes seismic and compression testing.

2.3.1 Yuan et al., (2022)

Yuan et al. 2022 emphasized that strengthening normal reinforced concrete columns and piers of bridges using a jacket of UHPC around the columns having a specific height as shown in Figure 2.6 is promising and led to an increase in seismic-resistance capacity during the long-term service period.

Three circular column specimens were tested in this study (Figure 2.6). The first was a normal RC column without strengthening, while the other two were strengthened with UHPC jackets. In one strengthened specimen, the UHPC jacket replaced the existing one-inch concrete cover; in the other, the jacket extended an additional one inch beyond the cover, resulting in a two inches thickness. The height was designed so that $H_r > \frac{(M_{rc}-M_{uc})}{M_{rc}} * H$, where H_r is the height of the UHPC jacket, H is the total height of the column, M_{rc} is the moment capacity for the retrofitted part of the column, and M_{uc} is the moment capacity of the column without strengthening (Figure 2.7). Both variables M_{rc} and M_{uc} can be calculated based on the sectional analysis. Since all variables are known, therefore, the minimum UHPC jacket height, H, can be simply calculated. The height of the jacket for both columns was chosen to be the same for both.

The construction included casting of the UHPC jacket using reusable steel gage formwork for the column as illustrated in Figure 2.8. The fabrication was done in three distinct stages. The first was to erect the reinforcement steel of the two-foot-high column. In the second stage, one-inch-thick geotextiles were wound around the outside of the steel cage of the column. Finally, the

concrete for the pier shaft and pier cap was poured after the stainless-steel formwork was encased in the reinforcing cage. The column was produced with two different section sizes with heights ranging from 0-2 ft and 2-4.25 ft. The lower part was roughened to increase the bond with the UHPC jacket. The aim of this technique was to construct the column so that the lower part of the column would be without cover, and this was used instead of demolishing concrete after the construction as it is realistic in retrofit practice. To cast UHPC, two pieces of stainless-steel formwork were welded together after placing them around the lower part of the column.

Compared to the column without UHPC strengthening, the findings demonstrate that the pier's curvature distribution and damage modes were altered, the UHPC jackets stopped the outer concrete from breaking off early and reduced how quickly cracks spread in the most stressed zone. This made the cracks spread more evenly up the column and shifted the main bending zone higher, so the columns failed more gradually and with more ductility. Thanks to UHPC jacket strengthening, the strength and stiffness increased after being retrofitted with UHPC jackets. The research also suggested improved post-earthquake serviceability of rehabilitated piers considering the two-inch-thick UHPC jackets significantly reduced residual displacement and equivalent viscosity ratio. After that, a parametric study using 3D Finite element analysis (3D-NFEA) was conducted. This analysis showed that for fixed thickness or height, increasing the volume of the jacket did affect the strength of the retrofitted column after a certain point.

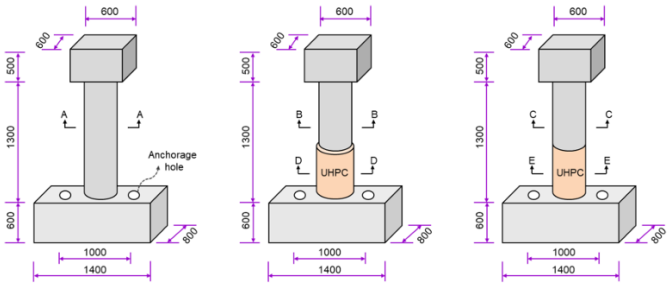

Figure 2.6 Three circular columns (Wenting et al. 2022)

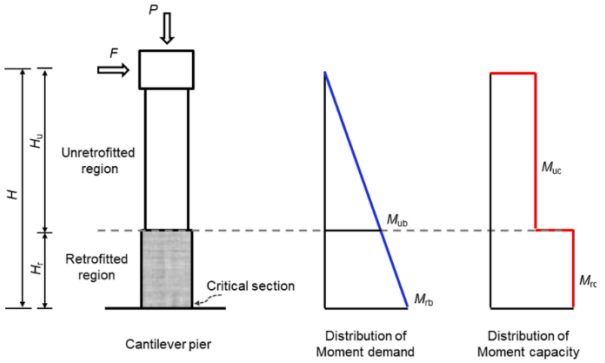

Figure 2.7 Straining actions of pier under seismic load (Wenting et al. 2022)

Figure 2.8 Construction of UHPC jacket (Wenting et al. 2022)

2.3.2 Susilorini et al., (2023)

Susilorini et al. performed an experimental and analytical investigation by testing 12 short-column specimens confined with UHPC with different fiber volume fractions (0%, 1%, and 2%) and subjected to axial loading with eccentricity 0 in, 1.4 in. and 2.8 in. The steel fibers measure 0.4 in. in length and 0.008 in. in diameter. Details of specimens are shown in Figure 2.9. A total of 12 short column specimens were fabricated using CC with a compressive strength of 5.2 ksi, with cross-sectional dimensions of 7.9 in. × 7.9 in. and a height of 29.5 in. Three unconfined specimens served as control columns, while the remaining nine were confined with UHPC jackets, each with a uniform thickness of 0.8 in. The longitudinal reinforcement consisted of four #4 deformed steel bars, while transverse reinforcement was provided using #3 ties spaced at 4 in. outside the lap zone and 2 in. within it. The UHPC achieved a target compressive strength of approximately 27 ksi, 27.36 ksi and 27.54 ksi corresponding to mixes with steel fibers volume fraction of 0%, 1% and 2% measured at 28 days. To ensure adequate bond and interface performance between the CC core and the UHPC jacket, all specimens underwent sandblasting prior to jacketing.

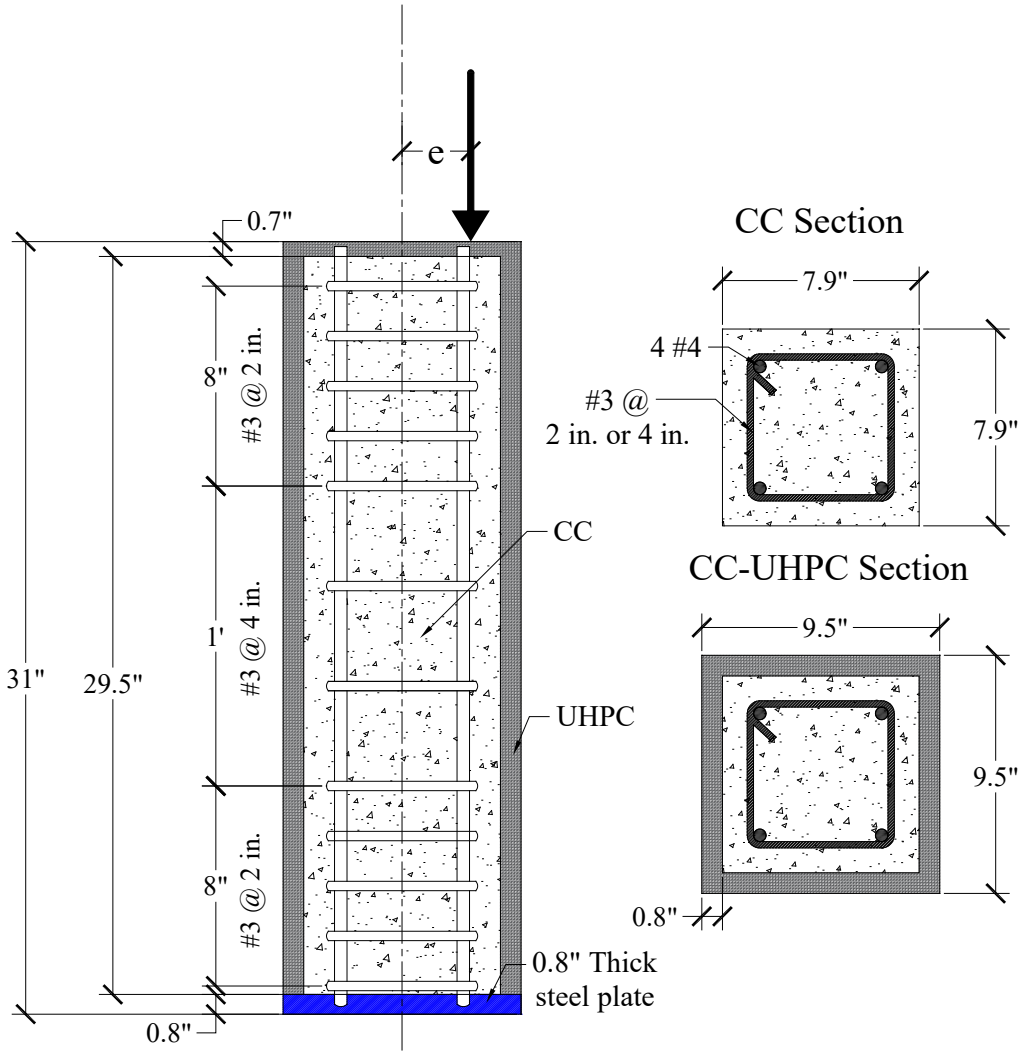

Figure 2.9 Geometry details of column specimen (Susilorini et al., 2023)

Table 2.1 presents the results of testing. The confinement systems demonstrated substantial improvements in axial capacity, vertical deformation, stress-strain response, and failure characteristics compared to unconfined control specimens. Notably, columns confined with UHPC containing 2% fiber under moderate eccentricity exhibited the highest strength and ductility, accompanied by a ductile failure mode and reduced cracking. The study also highlighted the efficacy of fiber inclusion in mitigating confinement spalling and enhancing structural resilience. Overall, the results affirm that UHPC confinement can significantly improve the mechanical

performance of CC columns, especially in terms of axial strength and energy dissipation, thereby supporting their use in structural retrofitting applications.

Table 2.1 Details of testing program and results (Susilorini et al., 2023)

Specimen ID	Volume of Fibers	Load Eccentricity (in.)	Max strength (ksi)	Corresponding strain
C-0	0	0	3.3321	0.0028
CF0-0	0		6.9397	0.0036
CF1-0	1		7.33555	0.0039
CF2-0	2		8.03735	0.0041
C-35	0	1.4	2.6854	0.0026
CF0-35	0		5.2171	0.0032
CF1-35	1		5.85655	0.0038
CF2-35	2		7.018	0.0042
C-70	0	2.8	1.7081	0.0032
CF0-70	0		3.46405	0.0045
CF1-70	1		3.73955	0.0036
CF2-70	2		4.1006	0.0037

2.3.3 Poncetti et al., (2023)

The experimental study done by Poncetti et al. investigated the compressive behavior of concrete cylinders strengthened with UHPC jackets, focusing on the influence of both concrete strength and jacket thickness on confinement effectiveness. A total of 24 specimens were tested, incorporating three grades of concrete (C25, C40, and C60) with average compressive strength of 4 ksi, 6.6 ksi and 9.0 ksi, respectively, and two jacket thicknesses (1 in. and 1.4 in.), to evaluate their interaction. The specimen height is 12 in., and the UHPC jacket was applied along the entire height except for the top and bottom 0.6 in. All specimen details and test results are presented in Table 2.2. The findings demonstrated that UHPC jacketing significantly enhances the compressive

strength of confined concrete across all tested grades. Analysis of the circumferential strain revealed that the confinement efficiency is not solely dependent on jacket thickness or concrete strength individually, but rather on their interrelation. This seems essential in comprehending the UHPC jacket with undersized or oversized dimensions, highlighting the need for proper sizing to optimize confinement performance.

The study evaluated the predictive capabilities of existing confinement models and proposed an empirical equation to estimate confined concrete strength, accounting for the behavioral differences observed with varying jacket thicknesses.

Table 2.2 Details of specimens and test results (Poncetti et al., 2023)

Specimen Diameter (in.)	Specimen Height (in.)	UHPC Jacket Thickness (in.)	Unconfined CC compressive Strength (ksi)	UHPC Tensile Strength (ksi)	Confined CC compressive Strength (ksi)	Strength increase (%)
6.0	12.0	1.0	3.92	1.0	5.13	30.87
			6.6		8.233	24.74
			8.88		10.12	13.96
		1.4	3.92	1.2	5.713	45.74
			6.6		9.02	36.67
			8.88		11.25	26.69

2.3.4 Ronanki et al., (2022)

Ronanki et al. (2022) conducted experimental investigations to assess the confinement effect of an unreinforced UHPC shell. The experimental investigation is composed of two phases. The first phase was conducted on nine short columns with a height of 4 in. and 8 in. and diameter of 4 in. and 6 in. as shown in Figure 2.10. The specimens were composed of one control specimen and eight specimens strengthened with a UHPC jacket. The thickness of UHPC jackets varied between 0.5 in. to 1.5 in. so the ratio between the area of UHPC shell to core area varied from 0.4

to 3. In the second phase, a total of 13 larger specimens were tested as shown in Figure 2.11: four specimens were 11.5 in. square columns, three specimens were 12 in. circular columns, three specimens were unreinforced 9 in. square columns, and three specimens were unreinforced 8 in. circular columns. All specimens had a height of 27 in. with a UHPC shell throughout the height except the top and bottom 2 in. Two specimens were considered control specimens with no UHPC confinement, and eleven other specimens were confined with UHPC shells with thicknesses of 1 in. and 2 in. The findings indicated that the peak compressive stress and crushing strain values of the core concrete increased by 15%–30% and 26%–46%, respectively, due to confinement effects of the unreinforced UHPC shell. The effectiveness of a UHPC shell in confinement was found to be higher in circular columns than square columns.

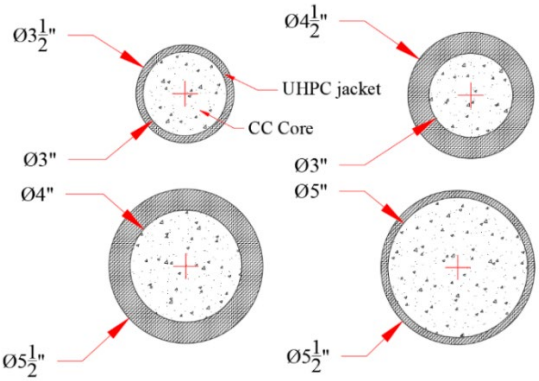

Figure 2.10 Phase 1 small specimens without reinforcement (Ronanki et al., 2022)

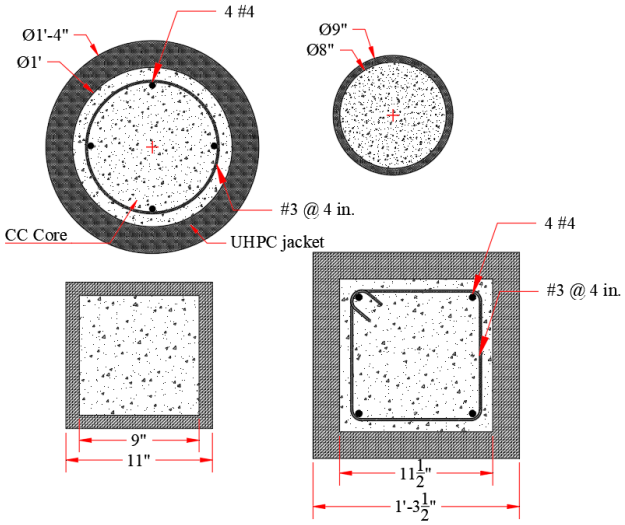

Figure 2.11 Phase 2 large reinforced and unreinforced specimens (Ronanki et al., 2022)

This research also compares experimental results with existing confinement models, including those proposed by Mander et al. (1988), Scott et al. (1982), and a modified version of Bousalem and Chick (2007) adapted for UHPC confinement. Among these, Mander's model showed the best agreement with the experimental peak stress. However, it overestimated the strain at peak stress by approximately 60% for rectangular specimens and 40% for circular ones. Although the models by Scott and Bousalem (2022) are simpler, they showed lower accuracy in predicting both peak stress and corresponding strain.

2.3.5 Farouk et al., (2023)

Farouk et al. (2023) conducted a comprehensive experimental and numerical investigation into the axial compressive behavior of CC-UHPC composite columns. The study fabricated and tested 23 circular column specimens with a diameter of approximately 4.8 in. and a height of 19.7 in. The investigation focused on the effects of three key parameters: longitudinal groove thickness at the interface, spacing of transverse reinforcement (i.e., shear reinforcement volumetric ratio) in

the UHPC jacket, and the compressive strength of the core CC. All the specimen details are shown in Figure 2.12. The findings revealed that increasing both the groove thickness and core concrete strength significantly enhanced the axial capacity of the composite columns. The surface layer of UHPC restrained the brittle crushing failure of CC core that is typically seen in concrete. However, increasing groove thickness does not improve the initial stiffness of the composite columns. In contrast, variations in hoop reinforcement spacing had minimal influence on compressive resistance. For CC core with a compressive strength of 46.35 MPa, increasing the hoop spacing from 75 to 150 and 225 mm decreased the ultimate resistance of the composite column by only 1.29% and 5.43% and the ductility index by 35.52% and 42.61%, respectively. Similarly, For CC core with a compressive strength of 36.77 MPa, the ultimate compressive resistance decreases by 1.34% and 9.70%, and the ductility index reduces by 49.65% and 50.24%, respectively. In addition, by increasing the CC compressive strength by 66.7%, compressive resistance improved by only 7.73%. Based on the experimental data, the authors proposed an analytical model of predicting the stress–strain response of UHPC-CC composite columns under axial loading. Additionally, a 3D finite element model was developed and validated against the experimental results, demonstrating strong agreement and confirming its effectiveness in simulating the compressive behavior of this novel composite column system.

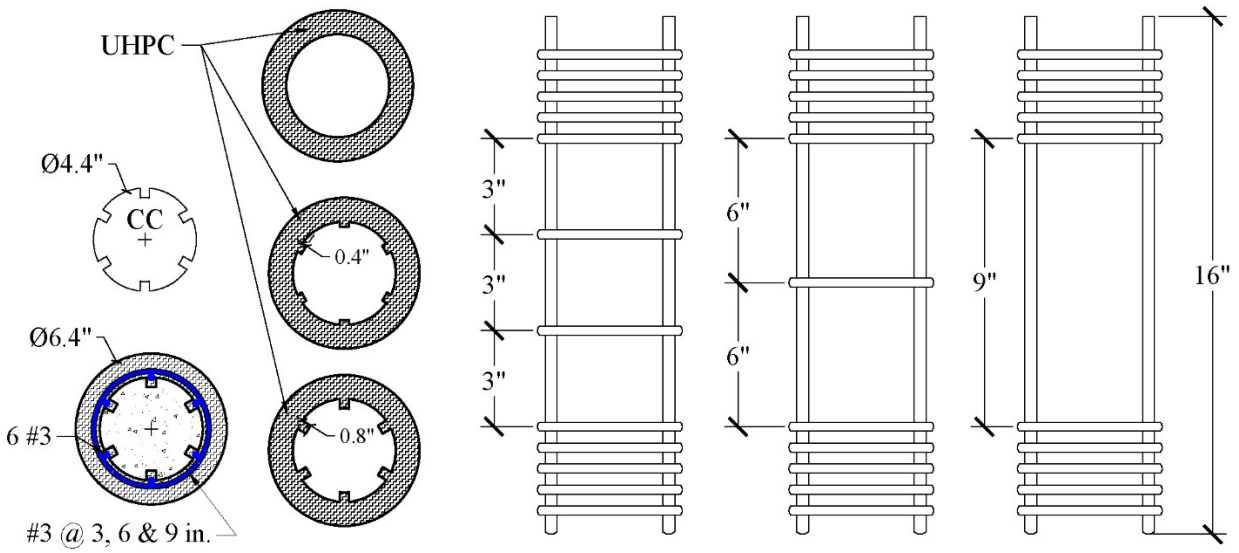

Figure 2.12 cross-section of groove thickness and reinforcement details (Farouk et al., 2023)

2.3.6 Dadvar et al. (2020)

Dadvar et al. (2020) investigated the axial performance of reinforced concrete columns strengthened using UHPC jacketing, with a focus on the influence of surface preparation and fiber type on bond quality and structural response. Fourteen circular columns, each 4.72 in. in diameter and 19.7 in. in height, were prepared, with ten specimens retrofitted using 0.6 in. thickness of UHPC jackets containing either steel fibers or synthetic macro-fibers (barchip), and three additional specimens strengthened with glass fiber-reinforced polymer (GFRP) hoop wraps for comparison. Various surface preparation techniques, including longitudinal grooving, horizontal grooving, sandblasting, and abrasion, were evaluated to determine their influence on the bond quality at the CC–UHPC interface. The vertical and horizontal grooving is shown in Figure 2.13. In this study, the longitudinal grooves had a smaller thickness of 0.24 in., and the applied UHPC jackets were unreinforced. Test results showed that longitudinal grooving achieved near-monolithic behavior, which means that the UHPC jacket and CC core act almost as if they were cast together, providing the highest performance, with approximately 33% higher axial

compression capacity and 34% greater energy absorption compared to sandblasted specimens. This is because the grooves ran parallel to the column axis, creating continuous mechanical interlock along the full height of the jacket. Horizontal grooving, although still improving the bond compared to untreated surfaces, was less effective because the grooves were perpendicular to the load direction and did not contribute as effectively to resisting axial slip between the core and jacket. Sandblasting enhanced the surface roughness by removing laitance and weak surface layers, which improved adhesion, but the lack of deep mechanical interlock limited its strengthening effect. Abrasion produced a similar outcome to sandblasting, as it created a roughened texture without forming distinct keying features, resulting in lower confinement efficiency compared to grooving. Overall, the results demonstrated that mechanical interlocking achieved through longitudinal grooving was superior to purely texturing methods such as sandblasting or abrasion, with horizontal grooving providing intermediate performance. The results also show that UHPC jacketing, particularly with steel fibers, significantly outperformed GFRP wrapping in strength enhancement, while GFRP-retrofitted columns demonstrated superior ductility. A stress–strain prediction model was developed and validated against existing experimental data, showing strong accuracy for CC columns strengthened with UHPC jackets.

Figure 2.13 Horizontal and longitudinal grooves (Dadvar et al., 2020)

2.3.7 Shehab et al. (2023)

Shehab et al. (2023) conducted an experimental program to investigate the structural performance of CC columns strengthened with UHPC jackets, with emphasis on the influence of surface preparation, jacket thickness, and the number of strengthened faces on axial load capacity. A total of nineteen square column specimens, each measuring 6.0 in. × 6.0 in. in cross-section and 39.5 in. in height, were fabricated and tested under axial compression. The strengthening schemes included two-sided, three-sided, and four-sided jacketing configurations, with jacket thicknesses of 0.80 in. and 1.60 in. To enhance the bond between the existing CC surface and the UHPC jacket, three interface preparation techniques were tested: vertical grooving (VG), horizontal grooving (HG), and no grooving (NG). Figure 2.14 present the details of specimens, grooving and number of strengthened sides. The results indicated that all strengthened columns exhibited brittle failure modes, but significant differences in axial capacity were observed depending on the interface treatment and jacketing configuration. Columns with vertical grooves consistently achieved the

highest ultimate load capacities, demonstrating the superior mechanical interlock provided by grooves aligned with the column's longitudinal axis. Horizontal grooving offered moderate performance gains over untreated surfaces for partially jacketed (two- and three-sided) columns but was less effective in fully jacketed specimens, where the NG configuration outperformed HG. This was attributed to potential weakening of the core concrete caused by horizontal groove cuts in fully confined columns. Overall, the study highlighted that optimal performance of UHPC jacketing depends on both the geometry of the jacket and the interface treatment, with vertical grooving being the most effective in enhancing bond and load resistance.

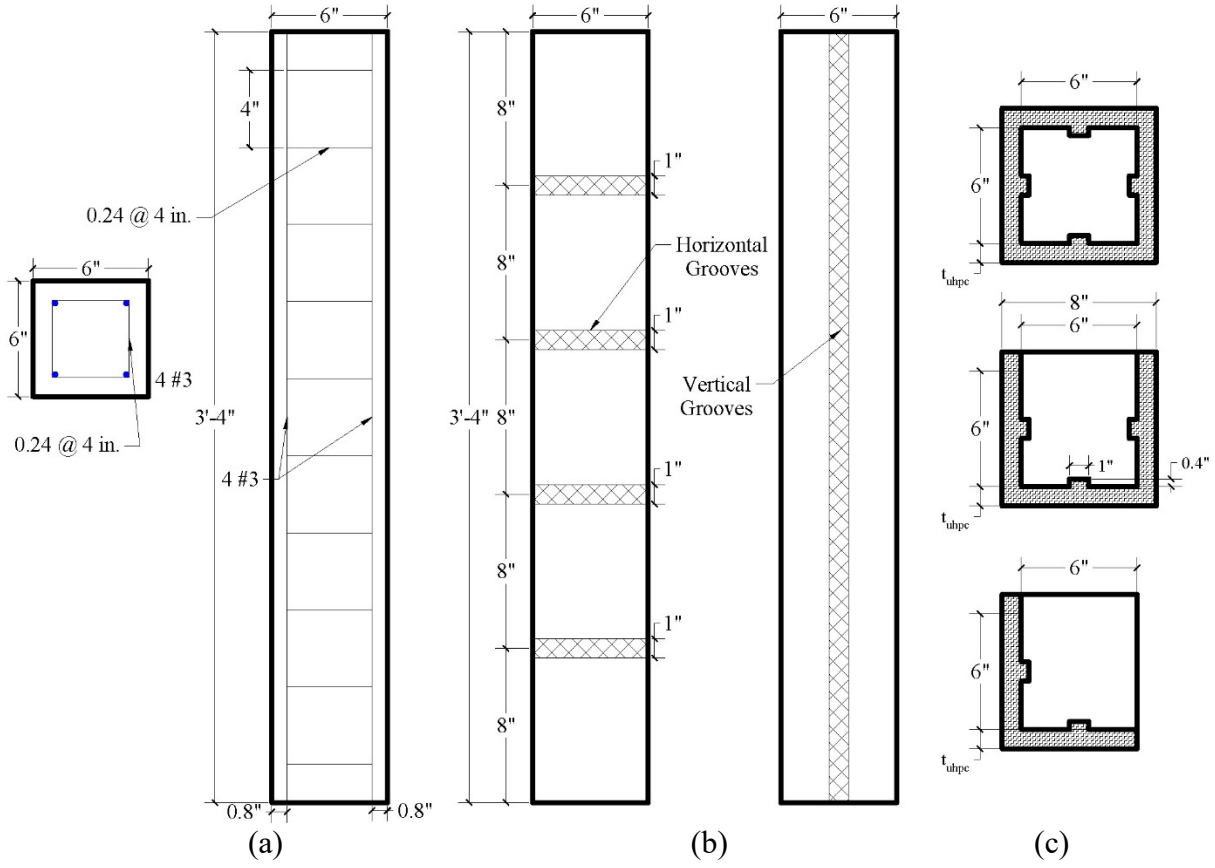

Figure 2.14 Specimen details a) longitudinal and cross section, b) surface preparation techniques and c) number of strengthened sides on cross sections (Shehab et al., 2023)

2.3.8 Farzad et al., (2019)

Farzad and Azizinamini proposed and experimentally validated a UHPC jacketing technique for rehabilitating CC bridge columns. The test matrix included eleven circular specimens, each 12 in. diameter and 60 in. height with a constant height-to-diameter ratio (H/D = 5), reinforced with eight #5 Grade-60 longitudinal bars and #3 hoops at 4 in. spacing. Each column was cast into an 83 in. × 83 in. × 24 in. footing with a free top end. Two undamaged columns and one damaged-but-unrepaired column served as controls. The remaining eight were intentionally damaged; seven of those were rehabilitated by backfilling the loss region with UHPC without increasing the cross-section, and one by filling with CC. Cover loss was simulated over the bottom 18 in. (1.5 times the original plastic-hinge length) by blocking concrete placement with an insulation roll as shown in Figure 2.15c, and in selected specimens the damage scenario was intensified by removing transverse ties or select longitudinal bars as shown in Figure 2.16. All deterioration was treated as corrosion-related for detailing purposes, although no corrosion was physically induced. Prior to casting, damaged substrates were sandblasted to exposed aggregate and conditioned to a dry-surface state. A commercial UHPC (Ductal JS1000) with 2% or 4% steel fibers was used. In some specimens, confinement was reintroduced by welding two half-hoops with a lap length of eight times the transverse-bar diameter ($8d_{bt}$), and a 2.5 in. hoop spacing was adopted for seismic detailing in others. Two specimens also replaced four extreme longitudinal bars with lap-spliced over a length equal to eight times the longitudinal-bar diameter ($8d_{bl}$). A two-piece, bolt-on form with side inlets facilitated placement and minimized finishing effort. The repair procedures are shown in Figure 2.17. Some specimens footing underwent repairing for a square of 24 in. x 24 in. x 4 in. around the column. The experimental program is presented in Table 2.3. All specimens were loaded with a constant axial force of 56 kips while imposing progressively larger

cyclic lateral drifts. UHPC-repaired members recovered or exceeded lateral strength, dissipated more hysteretic energy, and exhibited slower stiffness degradation relative to the damaged-unrepaired control. Failures were commonly governed by longitudinal bar buckling or fracture, and post-test examinations showed crushing localized within the CC core with no evidence of circumferential delamination at the UHPC–core interface. Modest increases in transverse (lateral) reinforcement markedly improved cyclic behavior, ductility, and deformability. The test results of the specimens with the lap splice in longitudinal reinforcements indicate that with proper design the required lap splice length in the UHPC repair area is noticeably short (8 d_{bl}). Moreover, from the strength standpoint, UHPC with 2% or 4% fiber content, resulted in similar behavior.

(a) (b) (c) (d)

Figure 2.15 Construction process of a typical specimen: (a) formwork and caging; (b) casting the footing; (c) simulating the damage; and (d) erecting the columns and casting the concrete substrate (Farzad et al., 2019).

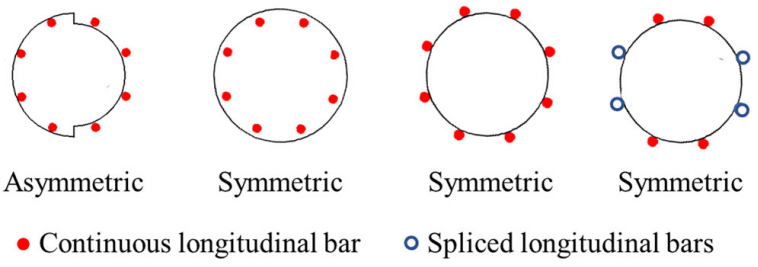

Figure 2.16 Damage geometry (Farzad et al., 2019)

Table 2.3 Details of specimens and test results (Farzad et al., 2019)

ID	Damage geometry	Shell thickness (in.)	Damage length (in.)	Repair material	Fiber content (%)	Transverse spacing in repair area (in.)	Footing repair
A-U2-0-F	(a)	0.5-2	18	UHPC	2	NA	Yes
A-U2-102-F	(a)	0.5-2	18	UHPC	2	4	Yes
S-U2-102-F	(b)	0.8	45	UHPC	2	4	Yes
A-D0-0-N	(a)	NA	18	No repair	NA	NA	No
R-102	NA	NA	NA	No repair	NA	4	No
R-64	NA	NA	NA	No repair	NA	2.5	No
S-N0-64-N	(c)	2	18	CC	0	2.5	No
S-U2-64-N	(c)	2	18	UHPC	2	2.5	No
S-U4-64-N	(c)	2	18	UHPC	4	2.5	No
S-U2-64-F	(d)	2	18	UHPC	2	2.5	Yes
S-U4-64-F	(d)	2	18	UHPC	4	2.5	Yes

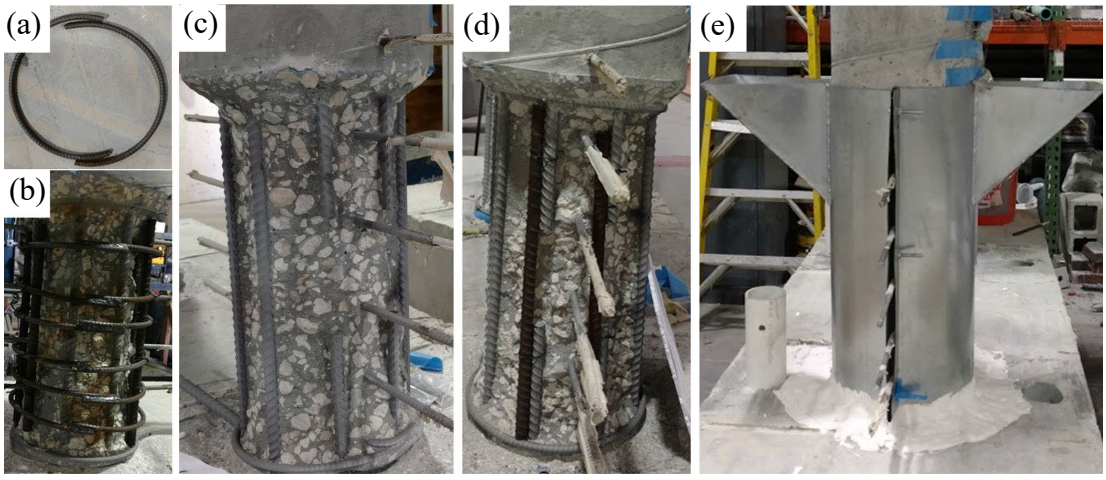

Figure 2.17 Repair process: (a) transverse reinforcement before placing in the damaged area; (b) transverse reinforcement placement in the damaged area; (c) specimens after cutting the rebar; (d) specimens after placing the spliced rebar; and (e) formwork used to place UHPC (Farzad et al., 2019)

2.3.9 Hossain et al., (2023)

Hossain et al. (2023) tested three circular columns with a core diameter of 6 in. and height of 3.3 ft and reinforced with three #3 bars in the longitudinal direction and #2 ties at 4 in. spacing

as transverse reinforcement to study the effect of UHPC jacket thickness on the structural behavior of the bridge columns as well as the effect of the jacket thickness to core diameter ratio. Figure 2.18-a shows the dimensions and reinforcement details of the original column considered as a control specimen, which was tested until failure to measure the axial capacity without a UHPC jacket. The other two specimens were loaded to cause damage, then repaired using UHPC jackets with a thickness of 1.5 in. and 2 in. and reinforced with three #3 bars as longitudinal reinforcement and ties with a diameter of 0.16 in. at 4 in. pacing as shown in Figure 2.18-b and c. The specimens were then tested again under concentric axial loading until failure. The results indicated that the axial capacity of the repaired specimens increased by 2.48 and 2.86 times the original capacity for jacket thicknesses of 1.5 in. and 2 in., respectively. However, the results also showed that increasing the ratio of UHPC thickness to core diameter resulted in a more brittle crushing failure and spalling of the UHPC jacket.

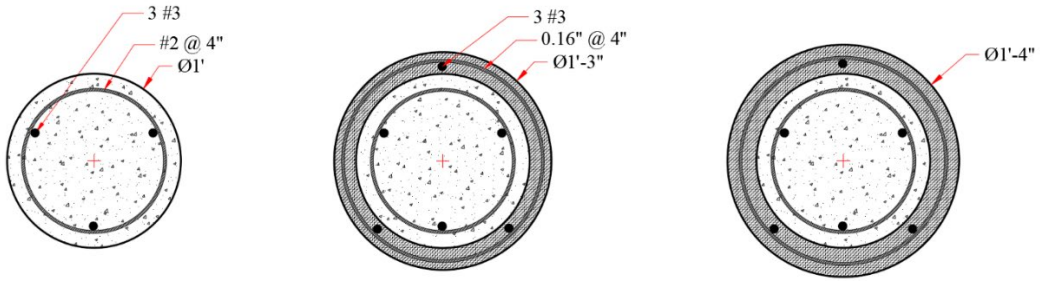

(a) (b) (c)

Figure 2.18 Dimensions and reinforcement details of a) original column b) repaired column with 1.5-in.-thick jacket, and c) repaired column with 2-in.-thick jacket (Hossain et al., 2023)

2.3.10 Hung et al., 2021

Hung et al. (2021) tested seven 13.78 in. square columns with a height of 47 in. to study seismic behavior under different axial load levels and the effect of adding reinforcement with a UHPC jacket. Two columns were control specimens without UHPC jackets, and five columns were retrofitted using 1.57-in.-thick UHPC jackets. Two jackets were reinforced with a sheet of

#3 welded wire mesh with a 3.93 in. grid size, two jackets were unreinforced, and one jacket was constructed using prefabricated panels as shown in Figure 2.19. The specimens were tested under biaxial bending at two levels of axial loads. The results indicated that increasing the level of axial loading resulted in a brittle failure for the control columns and the columns retrofitted with unreinforced UHPC jackets. However, the columns retrofitted with reinforced cast-in-place or precast UHPC jackets showed ductile behavior under high axial loads. The results also showed that using a UHPC jacket without reinforcement increased the shear capacity by only 20% and had no effect on the drift capacity due to the formation of the crack localization. However, adding reinforcement to cast-in-place or precast UHPC jackets increased the shear capacity by 50% as well as the drift capacity by 2% and 5% for specimens under low and high levels of axial load respectively.

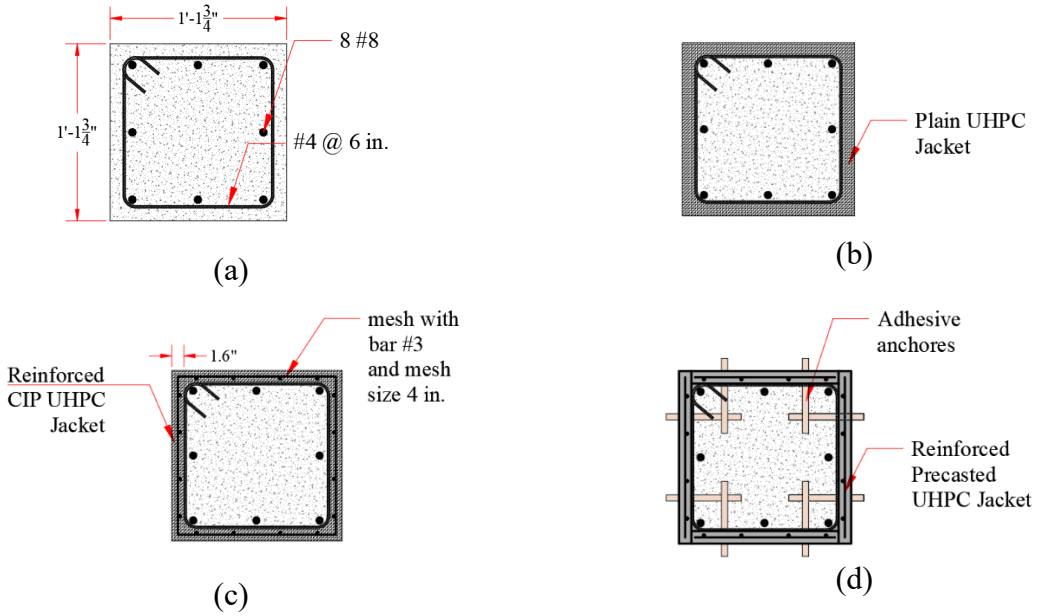

Figure 2.19 Dimensions and reinforcement details of a) original column, b) column repaired with plain UHPC jacket, c) column repaired with reinforced UHPC jacket, and d) column repaired with reinforced precast UHPC jacket (Hung et al. 2021)

2.3.11 Zhang et al., 2022

Zhang et al. (2022) tested seven columns, including two control columns and five UHPC strengthened columns under combined lateral cyclic load and constant axial load to study the effect of axial load level, fiber content, and the presence of steel reinforcement in UHPC. The results revealed that for the strengthened specimens, the effect of jacket reinforcement on the lateral load capacity is insignificant and the energy dissipation and post-peak ductility decreased with the reduction of either steel fibers or reinforcement mesh bars. This study also presented an approach for predicting the flexural capacity of strengthened columns, showing a good agreement with the test data. This approach ignored the tensile strength of UHPC in the tension zone and the confining effect of transverse reinforcement and the UHPC jacket. Additionally, the study employed idealized stress-strain relationships for UHPC, and CC as outlined in SETRA-AFGC (2002), and GB 50010 (2010), respectively.

2.3.12 Farzad et al., (2019)

Farzad et al. (2019) developed a method for predicting the flexural capacity of circular columns repaired with UHPC considering the tensile strength of UHPC based on a simplified assumption of the tension model. Also, the method assumed that all steel reinforcements were merged into an equivalent steel ring as suggested in Cosenza et al. (2011). Additionally, the reinforcement was assumed to be rigid–ideally plastic material and the stress distribution was constant at any height in a section as per Eurocode (2004). This method was assessed by comparing the results of the moment-curvature approach using the constitutive models proposed by Mander et al. (1988) for both confined and unconfined concrete. The method demonstrated superior

performance when applied to UHPC with smaller thicknesses and lower axial load levels (around 10%).

2.4 UHPC Vs. FRP Column Encasement

Column encasement is a widely adopted technique for strengthening and preserving deteriorated concrete bridge columns. Fiber-Reinforced Polymer (FRP) is a commonly used material for this purpose and can be applied using various techniques. In contrast, UHPC is a relatively new material that has recently gained attention as an effective solution for repairing and strengthening different types of reinforced concrete members. When used for column encasement, UHPC offers significant enhancements in both strength and ductility. Rabehi et al. (2014) conducted a comparative study on the compressive behavior of concrete columns repaired using two confinement methods: FRP jacketing and Ultra-High Performance Fiber-Reinforced Concrete (UHPFRC) encasement. Their experimental results showed that both techniques improved structural performance with distinct advantages. Columns encased with UHPFRC achieved the highest gains in compressive strength (up to 58%) and axial strain (50%) due to the superior bonding, compactness, and inclusion of steel fibers. In contrast, columns confined with Carbon FRP (CFRP) exhibited a remarkable increase in ductility (537%) and a moderate strength gain of 38%, while Glass FRP (GFRP) offered improved ductility with minimal strength enhancement. Although CFRP demonstrated exceptional ductility improvement, its higher cost makes it less economically viable compared to UHPC, which emerges as a more balanced and promising solution for structural rehabilitation.

Despite growing interest of using UHPC as a repair material, the behavior of UHPC-jacketed compression members remains insufficiently defined, especially regarding shear transfer

and bond at the UHPC-CC interface, the effect of UHPC confinement effects, and analytical models for axial–moment interaction of composite CC–UHPC sections. Existing tests consistently report gains in axial capacity and ductility attributable to UHPC confinement, which elevates the usable compressive strain of the core concrete; these trends can be represented with confinement-oriented constitutive models. To address these gaps, this study proposed an analytical model to construct the axial–moment interaction diagrams for CC–UHPC composite columns.

examines how CC substrate surface preparation governs interface shear strength and bond integrity in repaired/strengthened columns and experimentally evaluates the confinement provided by UHPC jackets. The results are synthesized into an adapted predictive model, originating from steel-confined concrete, to capture the distinctive confinement mechanics of UHPC.

Chapter 3 Capacity of Compression Members with UHPC Encasement

3.1 Introduction

This chapter presents a methodology developed by Hedia et al. (2024) for evaluating the combined axial and flexural capacity of CC compression members that have been repaired or strengthened using UHPC jackets, either with or without reinforcement. The method involves expressing all key parameters as functions of the neutral axis depth, *c*, measured from the compression face. By iterating through various assumed values of *c*, corresponding points on the interaction diagram can be determined.

The analysis assumes a perfect bond between the CC core and the UHPC jacket, allowing the cross-section to act as a fully composite section. To validate the perfect bond assumption, the interface shear stress between the CC and UHPC layers must be evaluated. The critical interface shear force is calculated at the strength limit state and compared with the interface shear resistance, as defined in the AASHTO (2024).

To achieve adequate bond performance, it is strongly recommended that UHPC be cast against a clean, laitance-free concrete substrate with a deliberately roughened surface, having a minimum amplitude of 0.25 inches. If necessary, post-installed concrete anchors can be employed to enhance the interface shear capacity. The influence of substrate surface preparation and the potential contribution of UHPC confinement are explored in detail in the following chapter.

3.2 Material Models

Compression and tension models of UHPC are shown in Figure 3.1 (AASHTO, 2024; PCI Report phase II, 2022), while the compression model of CC proposed by Thorenfeldt et al. (1987) and Collins et al. (1991) is shown in Figure 3.2. These models were selected due to their simplicity

and common use in design practices. However, the approach can be used with different models of UHPC, CC, and reinforcing steel.

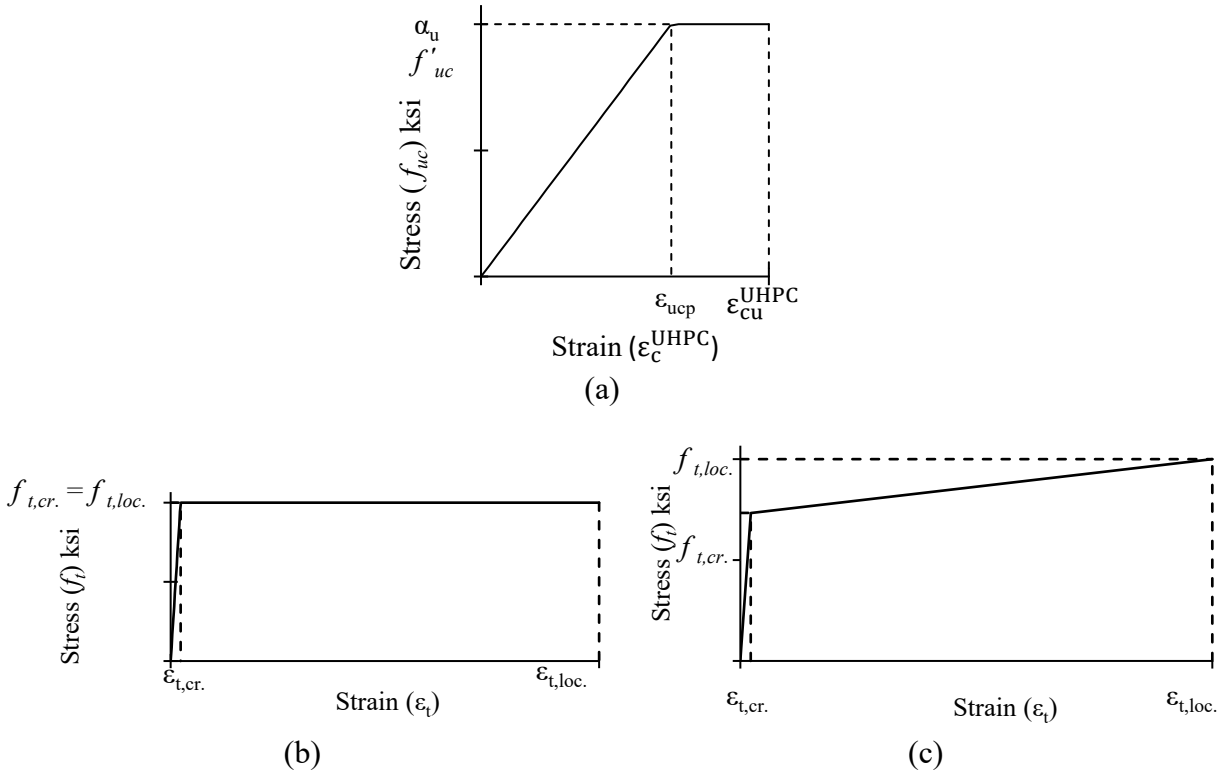

Figure 3.1 Material models of UHPC a) compression model; b) elastic perfectly plastic tension model; and c) bilinear strain-hardening tension model (AASHTO, 2024; PCI Report phase II, 2022)

Regarding UHPC, the idealized uniaxial stress-strain model in compression is defined by modulus of elasticity, E_{uc}, compressive strength, f'_{uc}, and ultimate compressive strain, ε_{cu}^{UHPC}, as shown in Figure 3.1a. Similarly, the idealized uniaxial stress-strain model in tension is defined by the same modulus of elasticity, effective cracking strength, $f_{t,cr}$, crack localization strength, $f_{t,loc}$, and crack localization strain, $\varepsilon_{t,loc}$, as shown in Figure 3.1b and Figure 3.1c based on the values of cracking strength and crack localization strength**.** If $f_{t,loc} \geq 1.20\, f_{t,cr}$, Figure 3.1c shall be used, otherwise, Figure 3.1b is used**.**

where

f'_{uc} = ultimate compressive strength of UHPC

ε_{cu}^{UHPC} = strain when f_{uc} reaches $\alpha_u f'_{uc}$

ε_{ucp} = elastic compressive strain limit, can be determined using Equation (3.2)

$f_{t,cr}$ = effective cracking strength of UHPC

$f_{t,loc}$ = crack localization strength of UHPC

$\varepsilon_{t,loc}$ = crack localization strain of UHPC

α_u = reduction factor to account for the nonlinearity of the compressive stress-strain response; it shall not be greater than 0.85

E_{uc} = modulus of Elasticity for UHPC, can be determined using Equation (3.1)

$$E_{uc} = 2{,}500K_1 f_{uc}'^{\,0.33} \tag{3.1}$$

where K_1 is a correction factor which shall be taken as 1.0 and f'_{uc} in ksi**.**

The ultimate compressive strain of UHPC, ε_{cu}^{UHPC}, shall be taken as the greater of the elastic compressive strain limit, ε_{ucp}, or 0.0035 (Figure 3.1a).

$$\varepsilon_{ucp} = \frac{\alpha_u f'_{uc}}{E_{uc}} \tag{3.2}$$

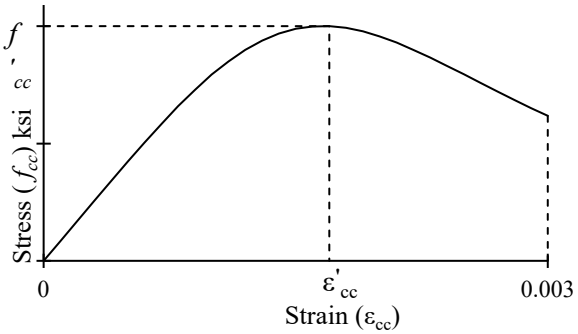

Figure 3.2 Material model of CC in compression (Thorenfeldt et al., 1987)

Likewise, the stress-strain curve for CC can be developed using Equation (3.3) proposed by Thorenfeldt et al., 1987.

$$f_{cc}(\varepsilon_{cc}) = \left(\frac{n\left(\frac{\varepsilon_{cc}}{\varepsilon'_{cc}}\right)}{n - 1 + \left(\frac{\varepsilon_{cc}}{\varepsilon'_{cc}}\right)^{nk}} \right) f'_{cc} \quad (3.3)$$

where

f'_{cc} = compressive strength of conventional concrete.

f_{cc} = stress at any strain ε_{cc}

ε'_{cc} = strain when f_{cc} reaches f'_{cc}.

ε_{cc} = strain at different loading and assumed (0 to ε_{ccu})

ε_{cu}^{CC} = ultimate strain of CC and equal to 0.003 (AASHTO 2020).

n = a curve-fitting factor equal to $0.8 + \left(\frac{f'_{cc}}{2500}\right)$ where f'_{cc} is in psi

k = a factor to control the slop of the ascending and descending branches of stress-strain curve, taken equal to 1.0 for $\frac{\varepsilon_{cc}}{\varepsilon'_{cc}}$ less than 1.0 and taken $0.67 + \left(\frac{f'_{cc}\,(psi)}{9000}\right)$ for $\frac{\varepsilon_{cc}}{\varepsilon'_{cc}}$ greater than 1.0

E_{cc} = modules of Elasticity for CC. Determined using Equation (3.4) (AASHTO 2020)

$$E_{cc} = 120{,}000\, K_1 \gamma_{cc}^2 f_{cc}'^{\,0.33}\ ksi \quad (3.4)$$

where γ_{cc} is the unit weight of CC in kcf, K_1 is a correction factor which shall be taken equal to 1 and f'_{cc} in ksi.

The material models of the commonly used non-prestressing steel and prestressing steel are shown in Figure 3.3 and Figure 3.4, respectively. Other material models can be used instead when other types of reinforcement are used, such as high strength steel.

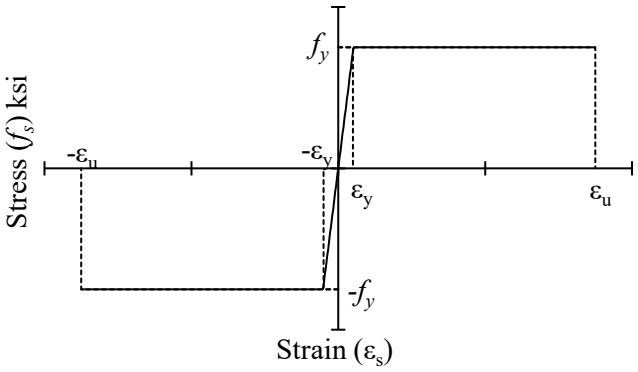

Figure 3.3 Material model of non-prestressing steel (ACI 318, 2019)

The elastic perfectly-plastic model of the non-prestressing steel is given by Equation (3.5) according to Mattock (1979).

$$f_s(\varepsilon_s) = \begin{cases} E_s.\varepsilon_s & \text{when } 0 < |\varepsilon_s| < |\varepsilon_y| \\ f_y & \text{when } |\varepsilon_y| < |\varepsilon_s| < |\varepsilon_u| \end{cases} \quad (3.5)$$

where

f_y = yield strength

ε_y = yield strain

ε_u = ultimate strain, which depends on the grade and diameter of bars

f_s = stress at a given strain ε_s

E_s = modulus of elasticity, equal to 29000 ksi

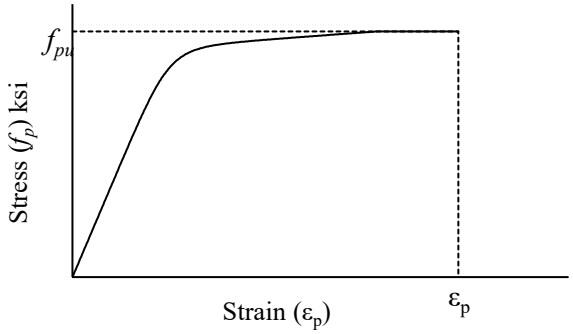

Figure 3.4 Material model of prestressing steel (Mattock, 1979)

Prestressing steel is modeled using a power formula shown in Equation (3.6) according to Mattock (1979) and Devalupura (1992).

$$f_p(\varepsilon_p) = E_p.\varepsilon_p \left(Q + \frac{1-Q}{\left(1+\left(\frac{E_p.\varepsilon_p}{K.f_{py}}\right)^R\right)^{\frac{1}{R}}} \right) \leq f_{pu} \tag{3.6}$$

where

f_{py} = yield strength of prestressing steel, equal to 0.9 f_{pu}

f_{pu} = ultimate strength of the prestressing steel

f_p = stress at a given strain ε_p

ε_{pu} = ultimate strain of prestressing steel

ε_{pe} = effective strain of prestressing steel, equal to $\frac{f_{pe}}{E_p}$

E_p = modulus of elasticity of prestressing steel

Q = power formula factor, equal to 0.031 for grade 270 low-relaxation strands

K = power formula factor, equal to 1.043 for grade 270 low-relaxation strands

R = power formula factor, equal to 7.36 for grade 270 low-relaxation strands

3.3 Section Properties

To determine compression member section properties, the width is expressed as a function of the distance from the compression side to allow calculating the properties of any section by integration. For example, a typical section of a circular CC column with radius, r, and outer UHPC shell with thickness, $t_{uhpc,}$ will have a total height, h, of the composite section equal to $2(r + t_{uhpc})$, as shown in Figure 3.5. Equations (3.7) and (3.8) express the width of the outer shell and inner

circular core as a function of height, z, measured from the compression side as shown in Figure 3.5.

$$b_o(z) = 2\sqrt{zh - z^2} \tag{3.7}$$

$$b_{cc}(z) = 2\sqrt{r^2 - \left(z - \frac{h}{2}\right)^2} \tag{3.8}$$

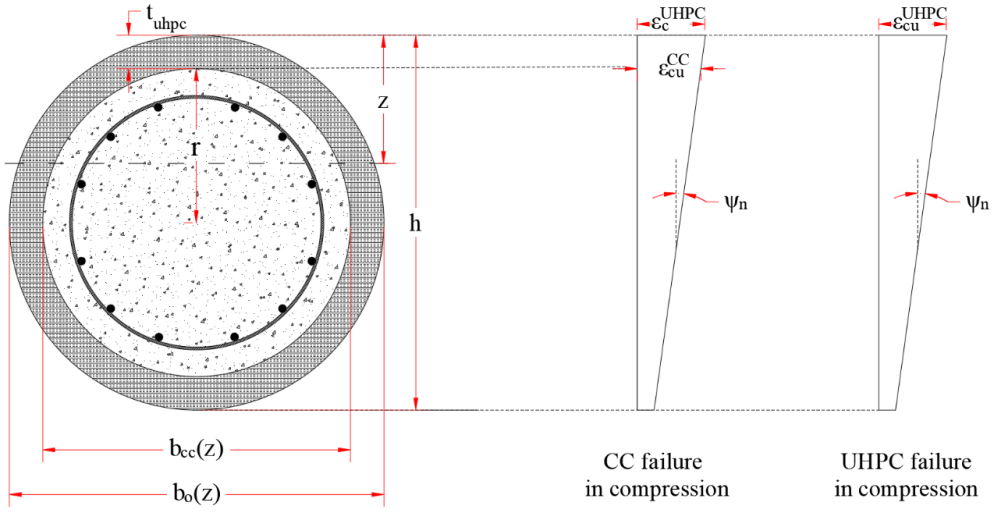

(a)

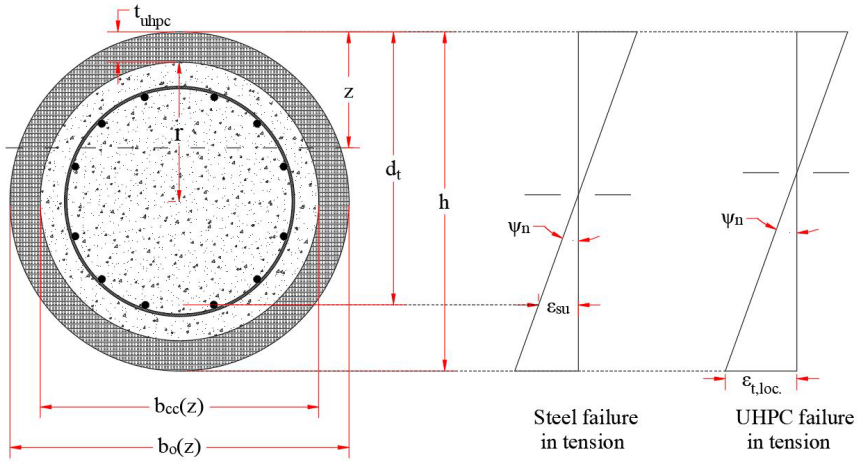

(b)

Figure 3.5 Strain distributions of a composite section for a) compression failure of CC and UHPC, and b) tension failure of steel and UHPC

The following equations are used to determine the section properties using the defined width of the section, $b(z)$, at any level, z, as the difference between $b_o(z)$ and $b_{cc}(z)$ as shown in Equation (3.9).

$$b(z) = b_o(z) - b_{cc}(z) \tag{3.9}$$

Equations (3.10) and (3.11) are used to determine the section area, A_g, and the center of gravity, cg.

$$A_g = \int_0^h b(z) \, . \, dz \tag{3.10}$$

$$cg = \frac{\int_0^h b(z) \, . \, z. \, dz}{A_g} \tag{3.11}$$

3.4 Methodology

3.4.1 Modes of Failure

For CC-UHPC composite sections, the failure mode may occur by crushing of UHPC in compression, crushing of CC in compression, crack localization of UHPC in tension, or tension rupture of reinforcement. The mode is marked by whichever occurs first for a given location of the neutral axis as shown in Figure 3.5. These modes of failure are determined by evaluating the calculated values of the lesser sectional curvature, ψ_n, when:

1. The compressive strain at the extreme compression fiber of the composite section is equal to the compression strain limit, ε_{cu}^{UHPC},
2. The compressive strain at the extreme compression fiber of the core is equal to the compression strain limit, ε_{cu}^{CC},

3. The net tensile strain at extreme tension fiber of the composite section is equal to the UHPC crack localization strain limit, $\varepsilon_{t,loc}$, and
4. The strain in the extreme tension steel is equal to the ultimate strain of reinforcing steel, ε_{su}.

Figure 3.5 illustrates the strain profiles for different modes of failure and describes the sectional curvature. The value of the sectional curvature, $\psi_n(c)$, can be calculated from Equation (3.12):

$$\psi_n(c) = \begin{cases} \text{min of } \left(\frac{\varepsilon_{t,loc}}{h-c}, \frac{\varepsilon_{su}}{d_t-c}\right) \text{ when } c \le c_b \\ \text{min of } \left(\frac{\varepsilon_{cu}^{UHPC}}{c}, \frac{\varepsilon_{cu}^{CC}}{c-t_{uhpc}}\right) \text{ when } c > c_b \end{cases} \quad (3.12)$$

where:

ε_{cu}^{UHPC} = strain in the extreme compression fiber of the composite section when the UHPC tensile strain limit, $\varepsilon_{t,loc}$, at extreme tension fiber is reached (in./in.)

ε_{cu}^{CC} = strain in the extreme compression fiber of the core (in./in.)

c = distance from the extreme compression fiber of the composite section to the neutral axis at different values of strain

d_t = distance from the extreme compression fiber of the section to the centroid of the extreme tension steel, equal to either the maximum depth of non prestressing steel, d, or the maximum depth of prestressing steel, d_p (in.)

c_b = distance from the extreme compression fiber to the neutral axis determined by the first occurrence of either the UHPC crack localization strain limit, $\varepsilon_{t,loc}$, or reinforcement

yield strain limit, ε_y, simultaneous with either UHPC compression strain limit, ε_{cu}^{UHPC}, or CC compression strain limit, ε_{cu}^{CC}, can be determined using Equation (3.13)

This equation demonstrates that the sectional curvature depends on the neutral axis depth at balanced point, c_b. If the neutral axis depth, c, is less than the neutral axis depth at the balanced point, c_b, either UHPC crack localization failure or yield of steel reinforcement occurs. Conversely, if the neutral axis depth, c, is greater, compression failure mode occurs, which might be in UHPC or CC, depending on whether the lesser sectional curvature is corresponding to UHPC crushing or CC crushing. c_b can be determined using Equation (3.13).

$$c_b = \max \text{of} \begin{cases} \dfrac{\varepsilon_{cu}^{UHPC}}{\varepsilon_{cu}^{UHPC} + \varepsilon_{t,loc}} \text{ x } h \\ \dfrac{\varepsilon_{cu}^{CC}}{\varepsilon_{cu}^{CC} + \varepsilon_{t,loc}} \text{ x } (h - t_{uhpc}) \\ \dfrac{\varepsilon_{cu}^{UHPC}}{\varepsilon_{cu}^{UHPC} + \varepsilon_y} \text{ x } d_t \\ \dfrac{\varepsilon_{cu}^{CC}}{\varepsilon_{cu}^{CC} + \varepsilon_y} \text{ x } (d_t - t_{uhpc}) \end{cases} \tag{3.13}$$

3.4.2 UHPC Confinement Effect

This section presents the effect of UHPC confinement on CC. Traditional confinement models, originally developed for concrete confined with steel ties, have been adapted to account for UHPC confinement. The model utilized in this study was initially proposed by Richart et al. (1928) for concrete confined by steel ties or hoops. The UHPC confinement effect is assumed to affect the compressive strength of concrete and the corresponding strain.

Equations (3.16) and (3.17) are used to estimate the compressive strength and strain of CC compression members confined with UHPC jackets. These equations account for the additional strength and ductility provided by the confinement mechanism.

A key aspect of this model is the arching action that develops within the UHPC jacket, as illustrated in Figure 3.6. This arching mechanism arises from the interaction between the core concrete and the surrounding UHPC, which redistributes the vertical compressive forces laterally toward the jacket. As the core attempts to expand under axial load, the UHPC jacket resists this lateral dilation, inducing tensile hoop stresses that generate lateral confining pressure. This pressure, in turn, enhances the axial load-carrying capacity of the core concrete.

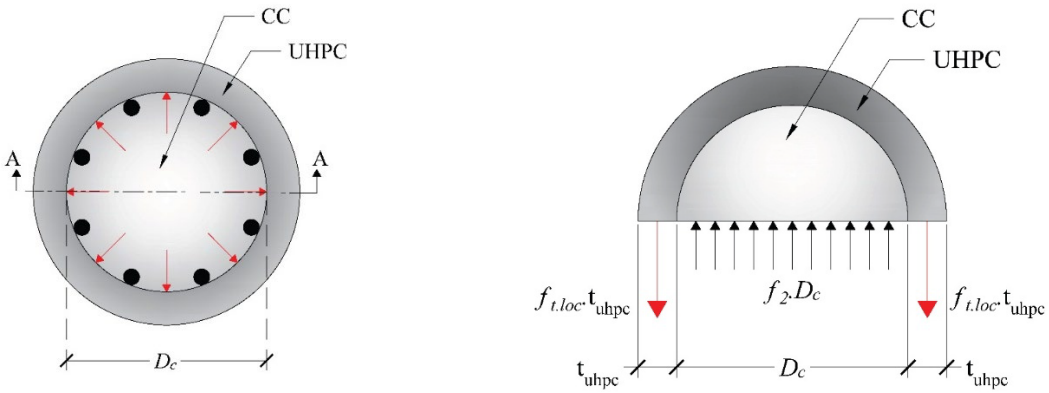

Figure 3.6 Effective arching action for transversely unreinforced UHPC encasement

The confinement-induced lateral pressure, denoted as f_2, is determined through equilibrium between the internal arching force paths and the tensile resistance provided by the UHPC jacket. For unreinforced jackets, the lateral pressure is expressed as:

$$f_2 = \frac{2\ x\ f_{t.loc}\ x\ t_{uhpc}}{D_c} \tag{3.14}$$

When reinforcing steel is embedded within the UHPC jacket, its contribution to confinement is also considered, yielding the modified expression:

$$f_2 = \frac{2\ x\ f_{t.loc}\ x\ t_{uhpc} + A_{st}\ x\ f_s(\varepsilon_{t.loc})}{D_c} \tag{3.15}$$

The modified compressive strength and strain of the confined concrete, $f_{ccc}^{'}$ and ε_{ccc}', are estimated as:

$$f_{ccc}' = f_{cc}' + k_1 f_2 \tag{3.16}$$

$$\varepsilon_{ccc}' = \varepsilon_{cc}' + k_2 \varepsilon_{cc}' \frac{f_2}{f_{cc}'} \tag{3.17}$$

where

f_{ccc}' is the maximum compressive strength of the confined concrete

f_{cc}' is the maximum compressive strength of the unconfined concrete

f_2 is the lateral pressure provided by confinement.

ε_{ccc}' is the concrete strain corresponding to f_{ccc}'

ε_{cc}' is the concrete strain corresponding to f_{cc}'

k_1 and k_2 are confinement effectiveness coefficients. These coefficients directly relate to concrete properties, lateral pressure, and reinforcement arrangement. The average values of the confinement effectiveness coefficients are taken equal to 4.1 and 5, which was found by Richart et al. (1928)

A_s is the total area of transverse reinforcement within spacing *s*

$f_{t.loc}$ is the crack localization strength of UHPC

t_{uhpc} is the thickness of the UHPC jacket

D_c is the confined diameter of the core of the column

The proposed formulation follows the foundational confinement model developed by Richart et al. (1928), which was originally established to account for the effects of transverse steel reinforcement (e.g., ties or spirals) on concrete confinement. To adapt this approach for UHPC jackets, several modifications were introduced while preserving the core logic of the original model.

In particular, the UHPC jacket is conceptually divided into one-inch-wide horizontal strips, analogous to the spacing of transverse reinforcement in traditional confinement systems. This results in an assumed one-inch center-to-center spacing between confining layers along the height of the column. The confinement effectiveness coefficients k_1 and k_2 remain consistent with Richart's original values, i.e., 4.1 and 5, respectively.

For steel-reinforced confinement, the lateral confining force per unit height is expressed as the product of the transverse reinforcement area A_s and its yield strength f_y, i.e., $A_s \cdot f_y$.

In the case of UHPC confinement, a similar analogy to conventional steel confinement is adopted. For an unreinforced UHPC jacket, as shown in Figure 3.6, the tensile force per strip is calculated by multiplying the localized tensile strength of UHPC ($f_{t.loc}$) by the effective cross-sectional area of a one-inch-high strip, which is equal to the jacket thickness (t_{uhpc}) multiplied by one inch (the assumed strip height).

In the case of a reinforced UHPC jacket, as shown in Figure 3.7, the total tensile force per strip additionally includes the contribution of embedded steel reinforcement. This is calculated as the product of the cross-sectional area of transverse reinforcement (A_s) and the steel stress corresponding to the crack localization strain of UHPC, $f_s(\varepsilon_{t.loc})$.

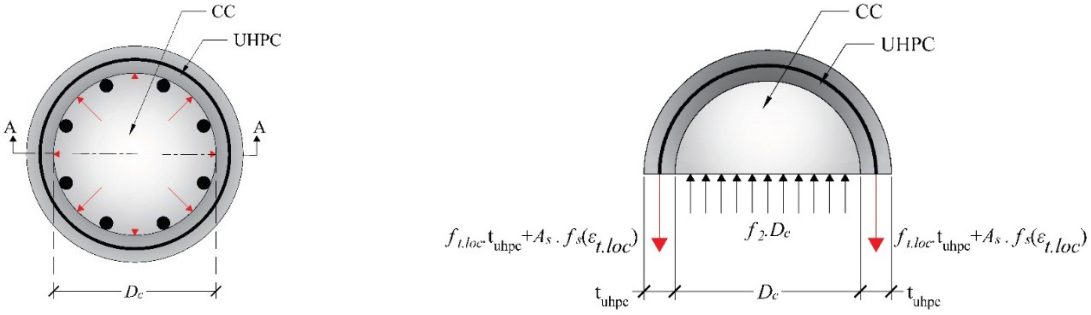

Figure 3.7 Effective arching action for transversely reinforced UHPC encasement

This approach results in a confinement formulation that reflects the logic of steel-based confinement models but replaces discrete ties with the continuous tensile resistance of UHPC, either with or without reinforcement.

These modifications are further examined in the next chapter through a comparison with experimental test results to validate the approach.

3.4.3 Nominal axial capacity

Figure 3.8 shows the resultant internal forces of the composite section which are composed of CC compressive force (C_{cc}), UHPC compressive and tensile forces (C_{uc}, T_c), and either reinforced steel tensile and compressive forces, T_{si}, or prestressing steel tensile forces, T_{pi}. To determine the contribution of each material to the axial capacity of a member, it is necessary to utilize its stress-strain relationship and integrate it over the corresponding area. It is permissible to ignore the tensile stresses in CC according to Devalupura (1992); however, it is crucial to account for the tensile stresses in UHPC due to its enhanced ductility and higher tensile strength. Static equilibrium of the section requires that the sum of internal forces be equal to the nominal axial capacity of the section. Equation (3.18) can be used to determine the axial capacity of a compression member expressed as a function of c.

$$P_n(c) = C_{uc}(c) + C_{cc}(c) - T_c(c) - \sum_{0}^{i} T_{si}(c) - \sum_{0}^{i} T_{pi}(c) \tag{3.18}$$

where

$P_n(c)$ = nominal axial capacity of the section as a function of the neutral axis depth, c

$C_{uc}(c)$ = resultant compressive force in the UHPC as a function of the neutral axis depth, c

$C_{cc}(c)$ = resultant compressive force in the CC as a function of the neutral axis depth, c

$T_c(c)$ = resultant tensile force in UHPC as a function of the neutral axis depth, c

$T_{si}(c)$ = force of the reinforcement steel in row (i) as a function of the neutral axis depth, c

$T_{pi}(c)$ = force of the prestressing steel in row (i) as a function of the neutral axis depth, c

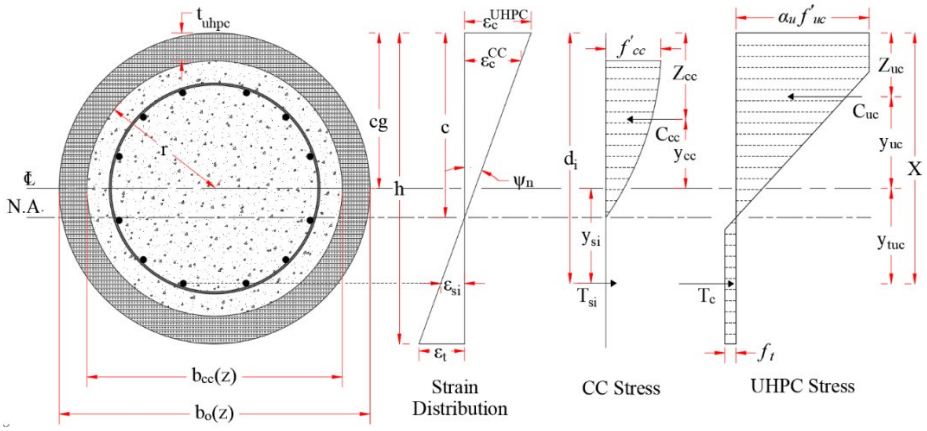

Figure 3.8 Stress and strain distributions of a composite section at a given neutral axis depth

Figure 3.9a and Figure 3.9b show a strip in the UHPC shell and CC core at a height y, which might be above or below the neutral axis. The strip thickness is dy and the width is equal to $b(c-y)$ and $b_{cc}(c-y)$ for the UHPC shell and the CC core, respectively, above the neutral axis. Below the neutral axis, the strip has the same thickness while its width is $b(c+y)$ for UHPC shell and zero for CC core since tension is neglected in CC. Equations (3.19) and (3.20) show the resultant compressive forces of CC and UHPC respectively. These equations use the integration of the stress distribution over the area at the top part with intervals beginning from the extreme top fibers of the section at $y = c$, down to the neutral axis level at $y = \text{zero}$. Equation (3.21) shows the resultant tensile strength of UHPC calculated using the integration of stress distribution over the area below the neutral axis with intervals beginning from neutral axis level at $y = 0$, down to the extreme bottom of the section at $y = h - c$. Figure 3.9a shows the calculation of the resultant compression and tensile forces of UHPC shell while Figure 3.9b shows the calculation of the resultant compression force of CC core.

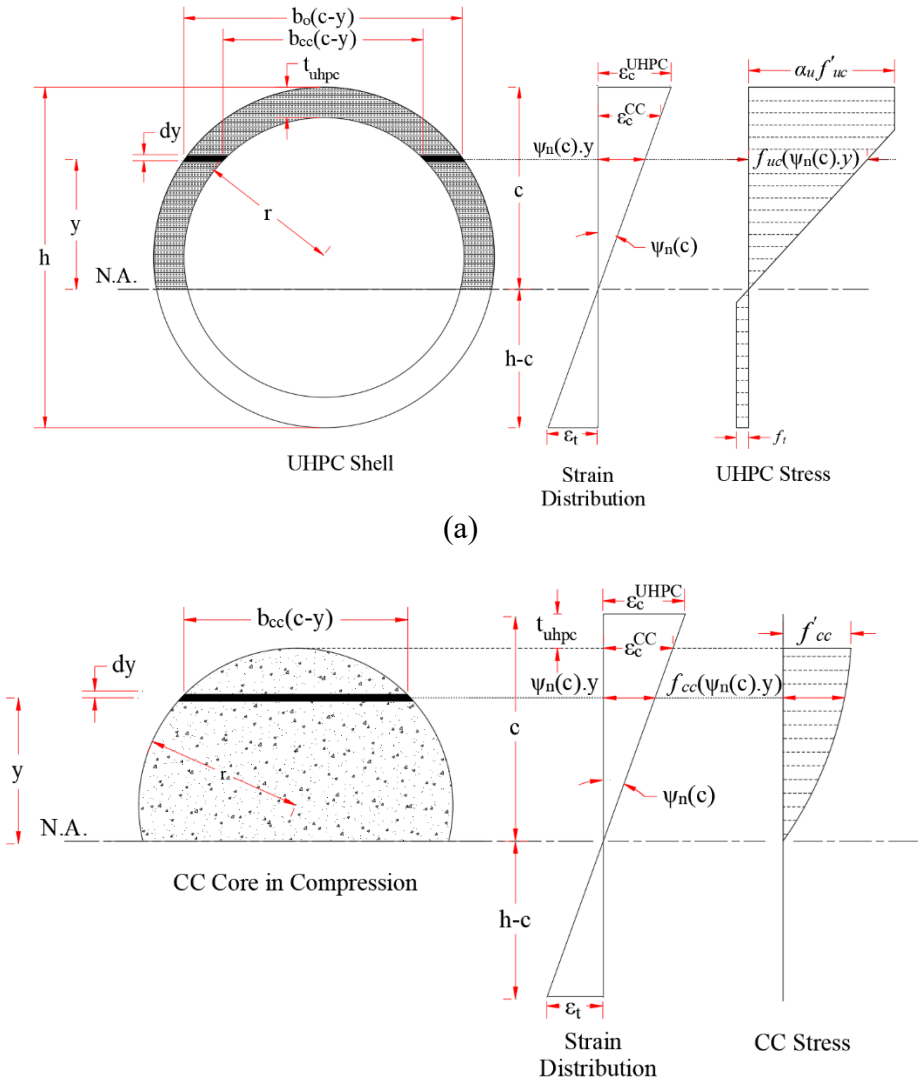

Figure 3.9 Calculation of forces in a) UHPC shell, and b) CC core

The resultant force in reinforcement steel and/or prestressing strands are calculated as the sum of forces in each individual row (i) as shown in Equations (3.22) and (3.24) respectively. Equations (3.23) and (3.25) may be used to determine the stress in each row based on the corresponding strain. The stress calculation includes the effect of the concrete stress corresponding to the strain in the steel.

$$C_{cc}(c) = \int_0^c f_{cc}(\psi_n(c).y).\, b_{cc}(c-y)\,.\,dy \tag{3.19}$$

$$C_{uc}(c) = \int_0^c f_{uc}(\psi_n(c).y).\, b(c-y)\,.\,dy \tag{3.20}$$

$$T_c(c) = \int_0^{h-c} f_t(\psi_n(c).y).\, b(c+y)\,.\,dy \tag{3.21}$$

$$T_s(c) = \sum_1^i T_{si}(c) = \sum_0^i A_{si}.f_{si}(c) \tag{3.22}$$

$$f_{si}(c) = \begin{cases} f_s(\varepsilon_s(c)_i) & \text{when } c < d_i < h \\ f_s(\varepsilon_s(c)_i) + f_{cc}(\varepsilon_s(c)_i) & \text{when } 0 < d_i < c \end{cases} \tag{3.23}$$

$$T_{ps}(c) = \sum_1^i T_{pi}(c) = \sum_0^i A_{pi}.f_{pi}(c) \tag{3.24}$$

$$f_{pi}(c) = \begin{cases} f_p(\varepsilon_{ps}(c)_i) & \text{when } c < d_{pi} < h \\ f_p(\varepsilon_{ps}(c)_i) + f_{cc}(\varepsilon_{ps}(c)_i - \varepsilon_{pe}) & \text{when } 0 < d_{pi} < c \end{cases} \tag{3.25}$$

where

$f_{cc}(\psi_n(c).y)$ = compression stress in CC corresponding to a strain at level y measured from neutral axis level and equal to $\psi_n(c).y$

$b_{cc}(c-y)$ = width of CC core above neutral axis at a–distance c - y measured from the top

$f_{uc}(\psi_n(c).y)$ = compression stress in UHPC corresponding to strain at level y measured from neutral axis level and equal to $\psi_n(c).y$

$b(c-y)$ = width of UHPC shell above neutral axis at a–distance c - y measured from the top

$f_t(\psi_n(c).y)$ = tensile stress in UHPC corresponding to strain at level y measured from neutral axis level and equal to $\psi_n(c).y$

$b(c+y)$ = width of UHPC shell below neutral axis at a distance c + y measured from the top

$f_{si}(c)$ = stress in reinforcement steel in row (i) at a given c, determined using Equation (3.23)

A_{si} = area of reinforcement steel in row (i)

d_i = depth of row (i) of reinforcement steel

$f_{pi}(c)$ = stress in prestressing steel in row (i) at a given c, determined using Equation (3.25)

A_{pi} = area of prestressing steel in row (i)

d_{pi} = depth of row (i) of prestressing steel

3.4.4 Nominal flexural capacity

The moment capacity of the section (M_n) is determined by summing the moments of each force about the centerline of the section. Equation (3.26) shows the calculation of the moment capacity of a CC-UHPC composite section in terms of the neutral axis depth, c.

$$M_n(c) = C_{cc}(c).\left(cg - Z_{cc}(c)\right) + C_{uc}(c).\left(cg - Z_{uc}(c)\right) + T_c(c).\left(X(c) - cg\right) + \sum_{1}^{i} T_{si}(c).(d_i - cg) + \sum_{1}^{i} T_{pi}(c)\left(d_{pi} - cg\right) \quad (3.26)$$

where

$Z_{cc}(c)$ = depth of resultant compression force of CC measured from extreme top fibers as a function of c

$Z_{uc}(c)$ = depth of resultant compression force of UHPC measured from extreme top fibers as a function of c

$X(c)$ = depth of resultant tension force of UHPC measured from extreme top fibers as a function of c

Figure 3.8 depicts the distance between the centroid of the resultant compression CC and UHPC forces and the extreme top fiber of the composite section which can be determined using Equations (3.27) and (3.28) respectively. Additionally, it shows the distance between the resultant tensile force of UHPC, and the extreme top fibers, which can be determined using Equation (3.29). The equations are expressed as a function of neutral axis depth, c, so that different flexural and axial capacities for various locations of neutral axis could be calculated.

$$\mathrm{Z_{cc}(c)} = \frac{\int_0^{\mathrm{c}} f_{cc}(\psi_{\mathrm{n}}(\mathrm{c}).\mathrm{y}).\,\mathrm{b_{cc}(c-y)}.\,(\mathrm{c-y})\,.\,\mathrm{dy}}{\mathrm{C_{cc}(c)}} \tag{3.27}$$

$$\mathrm{Z_{uc}(c)} = \frac{\int_0^{\mathrm{c}} f_{uc}(\psi_{\mathrm{n}}(\mathrm{c}).\mathrm{y}).\,\mathrm{b(c-y)}.\,(\mathrm{c-y})\,.\,\mathrm{dy}}{\mathrm{C_{uc}(c)}} \tag{3.28}$$

$$\mathrm{X(c)} = \frac{\int_0^{\mathrm{h-c}} f_t(\psi_{\mathrm{n}}(\mathrm{c}).\mathrm{y}).\,\mathrm{b(c+y)}.\,(\mathrm{c+y})\,.\,\mathrm{dy}}{\mathrm{T_c(c)}} \tag{3.29}$$

3.4.5 Pure axial capacity

For the pure compression point, the axial capacity could be determined using Equation (3.30) (AASHTO, 2024). This capacity is the nominal axial capacity when the nominal flexural capacity is zero (no eccentricity).

$$\mathrm{P_o(c)} = \mathrm{k}\left(\alpha_u.f'_{uc}.A_g + \alpha_1.f'_{cc}.\left(A_{gc} - \sum_0^i A_s\right) + f_y.\sum_0^i A_s\right) \tag{3.30}$$

where

k = confinement factor taken 0.8 for ties and 0.85 for spirals

α_1 = compressive strength factor and taken equal to 0.85

3.4.6 Ultimate design axial and flexural capacities

To determine the ultimate design capacity of a compression member, Equations (3.31) and (3.32) could be used.

$$P_u = \phi . P_n \tag{3.31}$$

$$M_u = \phi . M_n \tag{3.32}$$

where ϕ is a resistance factor which depends on the curvature ductility ratio, μ.

The resistance factor ϕ, shall be taken equal to 0.9 for sections with curvature ductility ratio, μ, greater than the curvature ductility ratio limit, μ_ℓ, which is equal to 3.0; and 0.75 for compression members, tension members, members subjected to combined tension and flexure, and sections with curvature ductility ratio, μ, less than 1.0. When curvature ductility ratio, μ, is between the curvature ductility ratio limit, 3.0 and 1.0, the value of ϕ associated with the ductility ratio may be obtained by a linear interpolation from 0.75 to 0.90. as shown in Figure 3.10 using Equation (3.33) (AASHTO, 2024):

$$\phi(c) = \begin{cases} 0.75\,, & 1.0 > \mu(c) \\ 0.75 + 0.15\dfrac{(\mu(c) - 1.0)}{(\mu_\ell - 1.0)}, & 1.0 \le \mu(c) \le \mu_\ell \\ 0.9\,, & \mu(c) > \mu_\ell \end{cases} \tag{3.33}$$

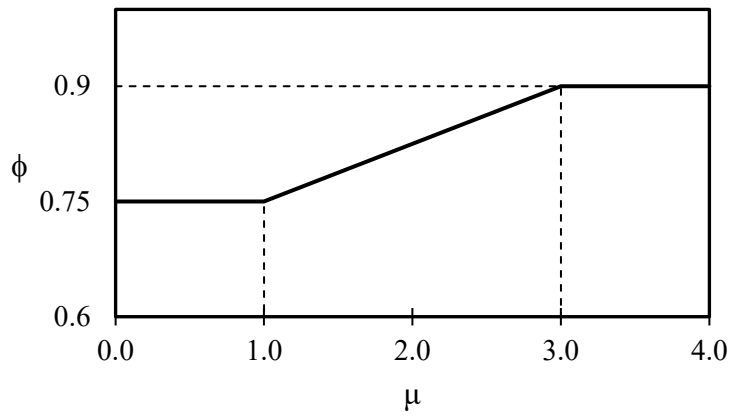

Figure 3.10 Relation between resistance factor, ϕ, and curvature ductility ratio, μ (AASHTO, 2024)

The curvature ductility ratio, μ, is defined as the ratio of the sectional curvature at the nominal moment resistance over the baseline sectional curvature and can be computed using Equation (3.34) (AASHTO, 2024).

$$\mu = \frac{\psi_n}{\psi_{s\ell}} \tag{3.34}$$

$$\psi_{s\ell} = \frac{\varepsilon_{s\ell}}{d_t - c_{s\ell}} \tag{3.35}$$

where

$\psi_{s\ell}$ = sectional curvature of the composite section when the steel stress in the extreme tension steel is equal to the steel service stress limit, $f_{s\ell}$, calculated using Equation (3.35) (1/in.)

$\varepsilon_{s\ell}$ = service strain in the tension steel when the steel stress in the extreme tension steel is equal to the steel service stress limit, $f_{s\ell}$ (in./in.)

$f_{s\ell}$ = stress limit in steel at service loads (ksi)

$c_{s\ell}$ = distance from the extreme compression fiber of the section to the neutral axis when the steel stress in the extreme tension steel is equal to the steel service stress limit, $f_{s\ell}$ (in.)

3.4.7 Interaction Diagram

The interaction diagram could be constructed using Equations (3.18) and (3.26) by substituting different values for the neutral axis depth, c. The range of neutral axis depth begins from the depth corresponding to pure flexural failure and ends at a depth corresponding to a pure compression failure which could happen at c > h.

3.5 Design Example

3.5.1 Introduction

This section presents a practical illustration example demonstrating the design of a bridge pier that has been repaired or strengthened using UHPC jacket, following the proposed numerical

model outlined above. Through this example, the effectiveness and practicality of the proposed model are evaluated under assumed real-world conditions. The detailed calculation is shown in Appendix A which shows the Mathcad sheet for the proposed model.

The authors selected a bridge column that needs to be repaired and assumes that it may be repaired using UHPC jacket. This is to apply the proposed method on that column. This column is located on the Adams Street bridge in Lancaster County, over Highway I-180, Nebraska. The assumed plan is to remove the damaged section and concrete cover, shown in Figure 3.11, then cast a jacket of UHPC around the column that has the same cover thickness so the column cross section does not changed. The proposed approach is used to construct the interaction diagram for that column after repair and show the effect of adding a UHPC cover on the capacity of the column.

Figure 3.11 Deteriorated bridge column considered in this example

3.5.2 Details of the bridge column

The bridge column has a 28 in. diameter and is reinforced with 12 #7 bars in the longitudinal direction and #4 ties in the transverse direction at 12 in. spacing. Section dimensions and reinforcement details are shown in Figure 3.12. The repair procedures began with removing the 2-in.-thick CC cover of the column, cleaning the surface, forming for UHPC encasement, and finally casting UHPC. The assumed material properties of CC, UHPC, and steel reinforcement are listed in Table 3.1.

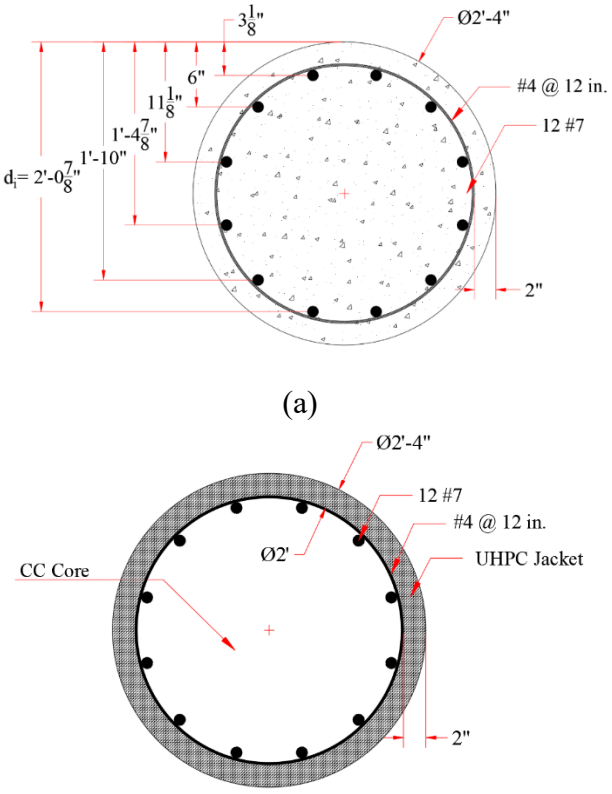

Figure 3.12 Cross section and reinforcement of the example column a) before repair and b) after repair

Table 3.1 CC, UHPC and reinforcing steel properties

Property	CC	UHPC
Compressive Strength, ksi	5.0	17.5
Modulus of Elasticity, ksi	4,291	6,249
Tensile Strength, ksi	neglected	0.75
Localized Strength, $f_{t,loc}$, ksi	N/A	0.75
Maximum Strain in Compression	0.003	0.0035
Localized Strain, $\varepsilon_{t,loc}$	N/A	0.005
Property	Reinforcing Steel (A615)	
Yield Strength, ksi	60	
Modulus of Elasticity, ksi	29,000	
Yield Strain, ε_y	0.002	
Service Strain, ε_{sl}	0.00166	
Ultimate Strain, ε_u	0.09	

3.5.3 Section Properties

The area of the shell, A_g, is 163.38 in.^{2} and the area of the core, A_{gc}, is 452.37 in^2. The centroid of both is at the mid-height of the section.

3.5.4 Calculating a Point in the Interaction Diagram for a Given Neutral Axis Depth

For a given depth of the neutral axis, c = 10 in., the axial and flexural capacities are calculated as follows: The sectional curvature is first computed to capture the mode of failure. The result showing c = 10 in. is less than the balanced neutral axis depth, c_b = 15.63 in. so that the curvature at the given neutral axis depth, ψ_n (10 in.) = 0.00028, which corresponds to crack localization failure of the UHPC jacket. Thus, the actual compressive strains in UHPC and CC, ε_c^{UHPC} and ε_c^{CC}, corresponding to the crack localization strain are calculated using strain compatibility and are equal to 0.0028 and 0.0022, respectively. The pre-existing strain and curvature in the CC column are ignored for simplicity, but they can be determined by analyzing the loads on the column when UHPC jacketing is applied. This strain impacts the ultimate strain

of the CC column and needs to be subtracted accordingly. The strain in each row of the reinforcing steel is then calculated using strain compatibility. Consequently, the stresses and the capacity of the reinforcing steel are determined for each row of steel as shown in Table 3.2

Table 3.2 Strain, stress, and force at each reinforcement row

Row (i)	Number of bars (n_i)	Area of bars (A_{si}) (in^2)	Depth of bars from the top (d_i) (in)	Strain in bars* (ε_{si}) $\varepsilon_{si} = (d_i - c).\psi_n(c)$	Stress in bars** (f_{si}) (ksi)	Force in bars* (T_i) (kip) $T_i = f_{si}A_{si}$	Distance between CG of bars to CG of section ** (in.)
1	2.0	1.2	3.125	-0.00191	-55.38	-66.46	+10.875
2	2.0	1.2	6.0	-0.00111	-32.22	-38.67	+8.0
3	2.0	1.2	11.125	+0.00031	+9.06	+10.87	+2.875
4	2.0	1.2	16.875	+0.00191	+55.38	+66.46	-2.875
5	2.0	1.2	22.0	+0.00333	+60.0	+72.0	-8
6	2.0	1.2	24.875	+0.00413	+60.0	+72.0	-10.875
TOTAL						**+116.21**	

* Positive sign is tension and negative sign is compression.
** positive sign is above centerline of the section and negative sign is below.

Equations (3.19) and (3.20) are used to determine the resultant compression forces in CC and UHPC respectively, while Equation (3.21) is used to determine the tensile force in UHPC. Substituting for c = 10 in., internal forces are as follows: C_{uc} (10 in.) = 665.8 kip, C_{cc} (10 in.) = 422.2 kip, and T_c (10 in.) = 72.8 kip. Substituting these forces in Equation (3.18) lead to nominal axial capacity, P_n = 902.6 kip. By substituting in Equations (3.27) to (3.29) for c = 10 in., the depth of the internal forces measured from the top are Z_{uc} (10 in.) = 2.86 in, Z_{cc} (10 in.) = 5.68 in., and X (10 in.) = 20.67 in. Consequently, the nominal flexural capacity, M_n (10 in.) in Equation (3.26) is equal to 1160.82 kip.ft.

Another point on the interaction diagram, point of pure axial, is determined. The nominal axial load capacity should not exceed the pure compression capacity, P_o (10 in.) = 3803.4 kip, given in Equation (3.30).

3.5.5 Interaction diagram

To develop the interaction diagram, the neutral axis depth, c, is assumed to range from the pure flexural value, c_{eq}, to about 3h, which represents the pure compression value. The c_{eq} value is equal to 6.064 in. for this example. The nominal and ultimate interaction diagrams for the original and repaired sections are shown in Figure 3.13.

The diagram in Figure 3.13 illustrates that the ultimate pure axial and flexural capacities of the repaired column section increased by 82% and 20%, respectively, compared to their original column. The limited increase in the flexural capacity is due to the controlling failure mode of UHPC in tension, which is reaching crack localization strain.

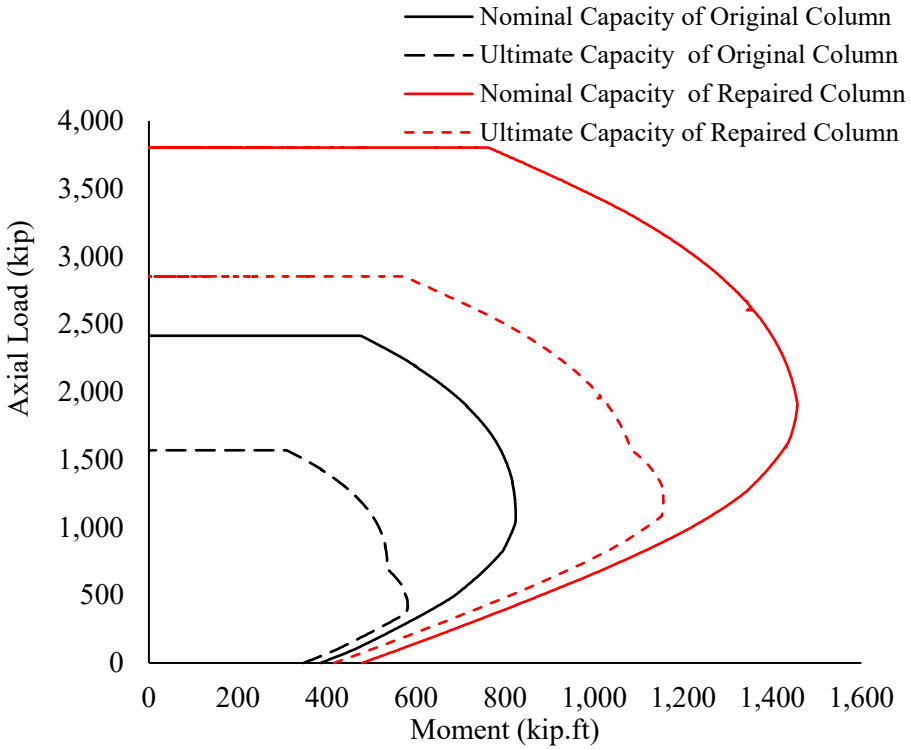

Figure 3.13 Interaction diagrams of the bridge column before and after repair

3.5.6 Effect of increasing UHPC jacket

Figure 3.14 shows the effect of increasing the thickness of the UHPC jacket, t_{uhpc}, on the column interaction diagram. The figure indicates a significant increase in the column's capacity above the balanced failure line. Conversely, below the balanced failure line, the capacity slightly increases because the UHPC crack localization strain controls the design even with an increased overall height of the column section, which could limit the strain in the reinforcement steel. For example, in comparison to a UHPC jacket with a thickness of 2.0 in., the diagram depicts a 14% increase in the ultimate pure axial capacity and a 9% increase in the pure flexural capacity for a UHPC cover thickness of 2.5 in. Furthermore, a UHPC cover thickness of 3.0 in. exhibits an increase of 28.5% and 19% in the ultimate pure axial capacity and the pure flexural capacity, respectively, compared to the 2.0-in. thickness.

It should be noted that the capacity calculations shown in the study assume a short column. As the column gets slender, P-δ analysis needs to be conducted to consider the secondary moments associated with the deformations of the composite CC-UHPC column, which will result in capacity reduction depending on the slenderness ratio and end conditions.

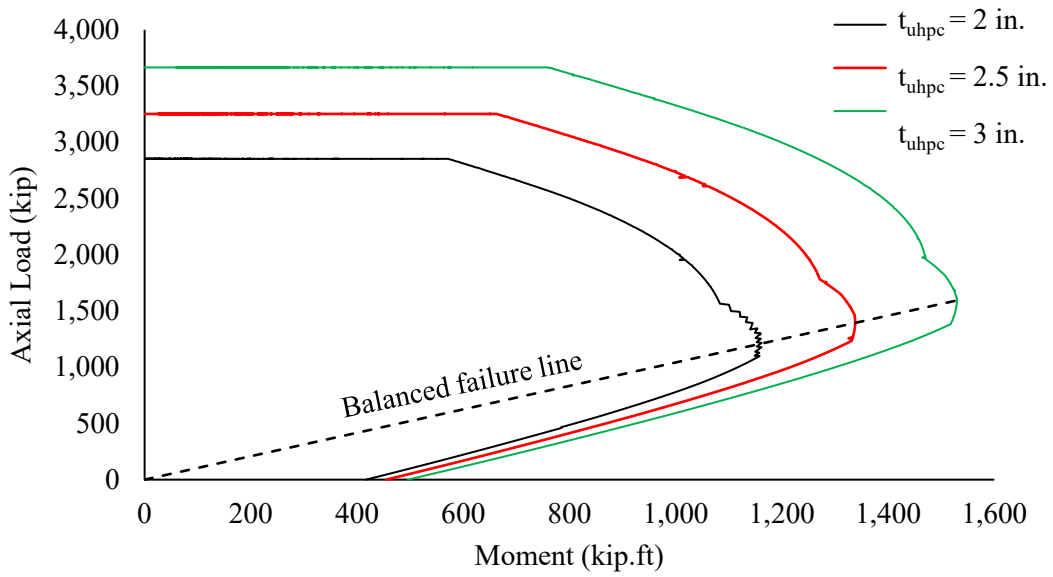

Figure 3.14 Ultimate capacity interaction diagrams for repaired columns with different UHPC jacket thicknesses

3.5.7 Effect of UHPC confinement

In this section, the modified methodology introduced in section 3.4.2 is employed to evaluate the influence of UHPC confinement on the axial capacity of the bridge column used in the example neglecting the contribution of UHPC jacket in axial capacity of the composite CC-UHPC section. The analysis considers both unreinforced and transversely reinforced UHPC jackets. For the case of transversely reinforced, #4 ties spaced at 6 inches are embedded within the mid-thickness of the UHPC layer, as illustrated in Figure 3.15.

A parametric investigation is conducted by varying the UHPC jacket thickness from zero inches (i.e., no confinement) to 4 in. in 0.5-in. increments. For jackets incorporating transverse reinforcement, the thickness range is limited to 2–4 in., reflecting constructible and field-practical configurations. The computed results shown in Figure 3.15 demonstrate that UHPC confinement substantially enhances the axial strength of the column, with thicker jackets yielding progressively greater improvements. Moreover, at any given thickness, the presence of transverse reinforcement further amplifies the axial capacity, underscoring its structural effectiveness.

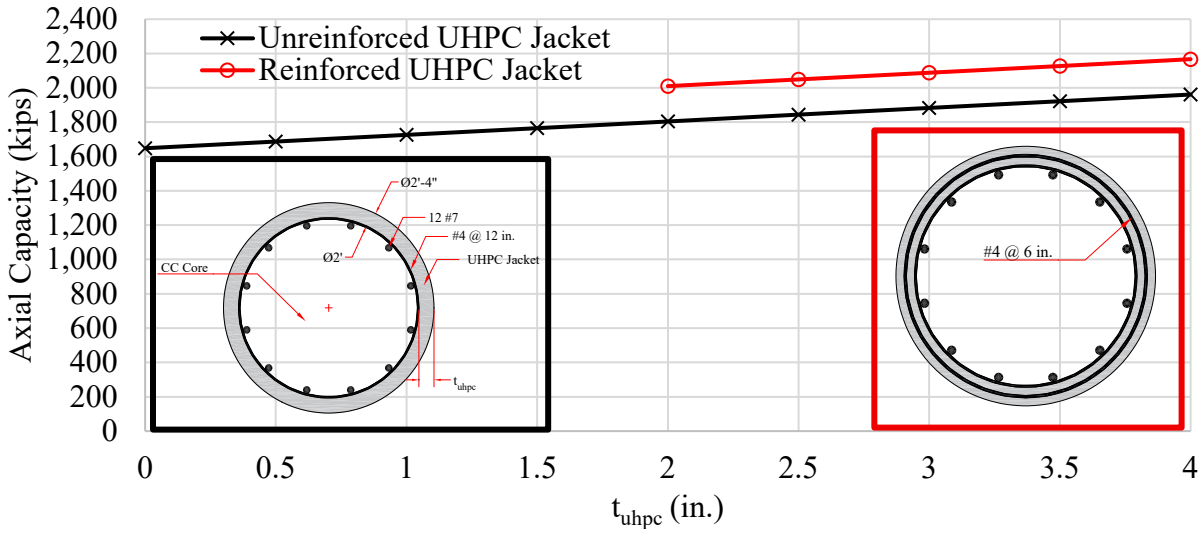

Figure 3.15 Transversely reinforced and unreinforced UHPC confinement effect

Chapter 4 Experimental Investigation

4.1 Introduction

The experimental investigation consists of two primary test phases: (I) UHPC-confined CC cylinders tested under compressive loading and (II) full-scale CC columns strengthened with UHPC jackets, subjected to compressive and flexural loading. The objective of the first phase of testing is to assess the effect of UHPC confinement on the compressive behavior of CC compression members. The second phase of testing aims to evaluate the influence of different substrate CC surface preparation techniques on the interface shear strength and bond performance between UHPC and CC in compression members when tested under axial and flexural loading.

This study contributes to the field of bridge engineering by enhancing the understanding of the compressive behavior of compression members repaired or strengthened with UHPC. This chapter presents an overview of specimen geometry, construction procedures, material characterization, test setup, instrumentation, and experimental results.

4.2 Experimental Work Details

4.2.1 General Description

The experimental program consists of two primary test phases. The first phase includes 14 cylindrical specimens as follows: a group of seven cylinders constructed from concrete with a compressive strength of 6 ksi and a group of seven cylinders constructed from a compressive strength of 7.5 ksi. Each group of specimens is further categorized into three subgroups. Each subgroup consists of one unconfined cylinder, three confined with a 1-in.-thick UHPC jacket, and three confined with a 2-in.-thick UHPC jacket. Samples of this phase are shown in Figure 4.1.

Figure 4.1 Samples of the small cylinders confined with UHPC

The second phase of testing includes eight full-scale reinforced concrete columns strengthened with UHPC jackets. Two different surface preparation techniques for the CC substrate were used. Six of the specimens are encased in UHPC without additional reinforcement, while jackets in the remaining two specimens are transversely reinforcement within the end 0.5 ft of the jacket. Samples of full-scale specimens are shown in Figure 4.2. Despite the specified compressive strength of CC bridge columns in Nebraska is more than or equal to 3 ksi, the concrete strength of tested specimens in phase I and II is high as self-compacting concrete (SCC) was used in the construction of all the specimens, which often result in higher strength due to the high powder content and this is intentionally as lower compressive strength are covered in different studies in the literature while higher strength are not investigated properly.

Figure 4.2 Samples of the full-scale compression members encased with UHPC

4.2.2 Specimens Details

Specimens in the first phase are measuring 4 in. diameter and 8 in. height. This phase is designed to examine the influence of confinement on the compressive behavior of CC compression members. Two distinct CC mixtures are utilized, with compressive strengths of 6.0 ksi and 7.5 ksi, respectively. The inclusion of different concrete strengths aims to develop a comprehensive understanding of how UHPC confinement affects the axial capacity and deformation of compression members constructed from higher compressive strength concrete. Details of the specimen are shown in Figure 4.3.

Table 4.1 presents the nomenclature and specifications of the specimens in the first phase. The designation system follows a structured format to clearly convey the key parameters of each specimen. The abbreviation CC denotes conventional concrete, followed by a numerical value representing its designed compressive strength, which is either 6 ksi or 7.5 ksi. The next identifier specifies whether the specimen is confined with a UHPC jacket or remains unconfined. If UHPC is present, the subsequent number indicates the thickness of the UHPC jacket, either one inch or two inches. Finally, an index number (one, two, or three) is assigned to distinguish individual specimens within each category.

Table 4.1 Details of first phase of experimental programs

Specimen ID	#	Dimensions	f_c' (ksi)	UHPC Confinement thickness
CC6	1	4 in. × 8 in.	6	No confinement
CC6-UHPC 1	1			1 in.
	2			
	3			
CC6-UHPC 2	1			2 in.
	2			
	3			
CC7.5	1		7.5	No confinement
CC7.5-UHPC 1	1			1 in.
	2			
	3			
CC7.5-UHPC 2	1			2 in.
	2			
	3			

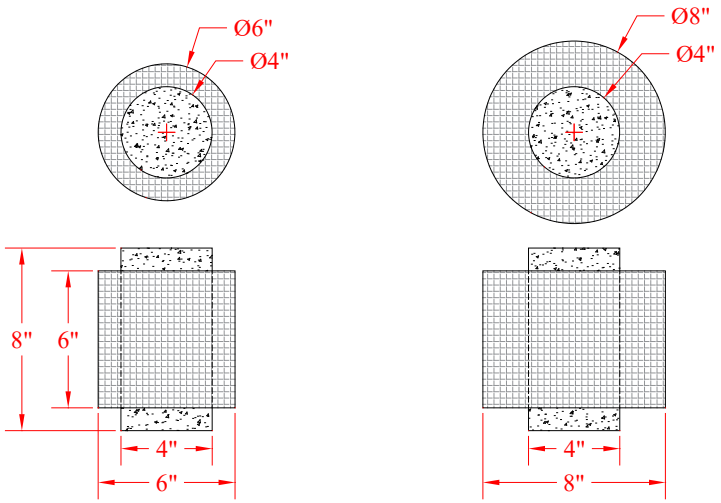

Figure 4.3 Details of phase I specimens

In The second phase, each column has a height of four feet and a diameter of eight inches, with a two-inch-thick UHPC jacket extending along the full column height, except for the bottom two inches, as illustrated in Figure 4.4. The unjacketed part of the specimen is intended and designed to be inserted into a steel ring, with the UHPC jacket providing structural support. This

setup is specifically configured to facilitate an interface shear test for six specimens which are axially tested, evaluating the bond performance between the UHPC and the CC. Two specimens are tested under flexural loading. All specimens are designed according to AASHTO LRFD Bridge Design Specifications (2020).

Each column is reinforced with eight #5 longitudinal bars and #3 transverse ties spaced at 9.6 inches. A clear cover of two inches measured from the steel ties face is incorporated into the design. This phase of testing primarily investigates the influence of surface preparation on the interface shear behavior and bond strength between UHPC and the underlying CC, effect of adding transverse reinforcement at the ends of the UHPC jacket and the investigate the behavior under axial and flexural loading. Two columns undergo sandblasting, while six are roughened by mechanically removing the concrete cover with a jackhammer. Table 4.2 outlines the nomenclature and details of the specimens. The designation of each specimen is based on the type of loading and surface preparation technique as follows: “A” stands for specimens tested axially, while “F” denotes for the specimens tested under flexural loading and "S" denotes specimens prepared through sandblasting, while "R" and "RT" represent specimens with a roughened surface achieved by removing the concrete cover using jackhammering without transverse reinforcement and with transverse reinforcement, respectively. The numerical designation represents the specimen index. Specimens which are transversely reinforced have #3 transverse ties in the upper 0.50 feet of the UHPC jacket, spaced at 1.0 in. The transverse reinforcement configuration is determined based on UHPC jacket transverse strain concentration and modes of failure of testing specimens without transverse reinforcement. Strain distribution along the jacket is recorded from top to bottom, providing data for transverse reinforcement design to accommodate the part with highest strain concentration (at the two ends) effectively.

Table 4.2 Details of second phase of experimental programs

Series	#	Type of testing	CC column diameter	CC column height	UHPC jacket thickness	UHPC jacket height	Reinforcement		Surface preparation	UHPC jacket transverse reinforcement
							Longitudinal	Transverse		
AS	1	Axial loading	8 in.	48 in.	2 in.	46 in.	8#5	#3@9.6in.	Sand Blasting	No
	2									
AR	1								Cover removal by jack hammering	No
	2									
ART	1									#3@1in. ties in the top
	2									
FR	1	Flexural loading								No
	2									

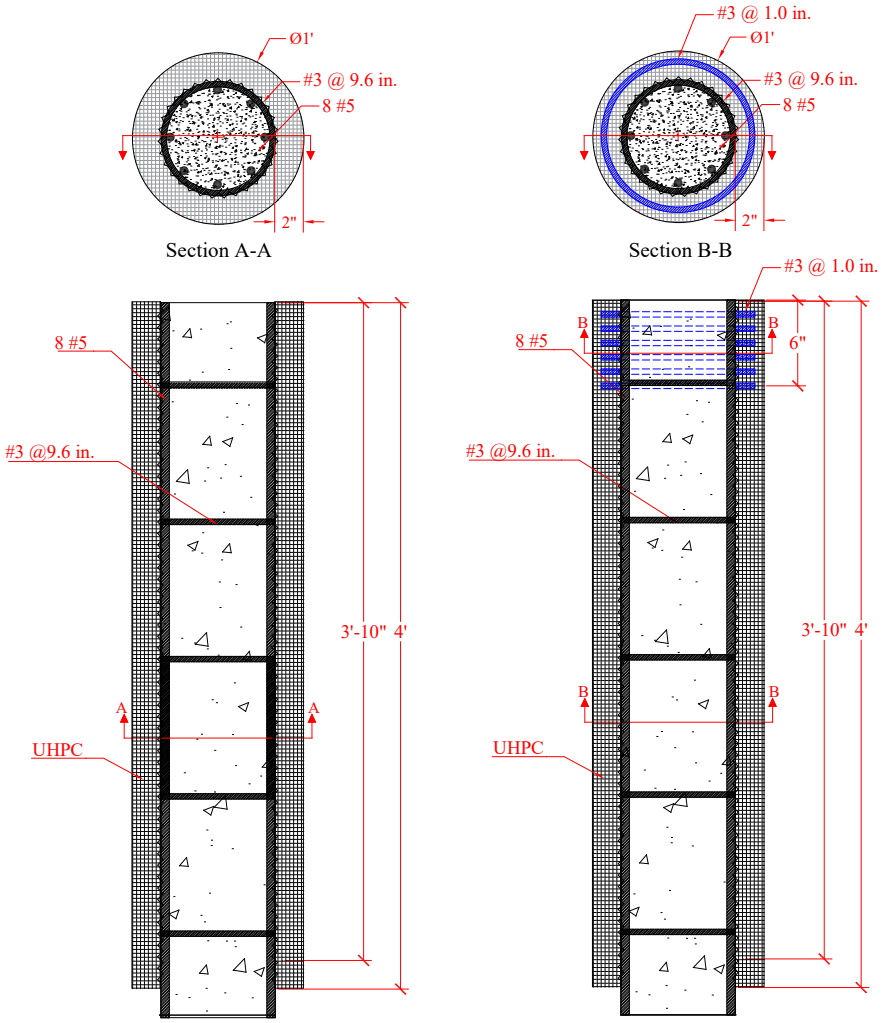

UHPC jacket w/o transverse reinforcement at the top.

UHPC jacket with transverse reinforcement at the top 6 in.

Figure 4.4 Details of the full-scale specimens

4.2.3 Materials

All specimens in phase I and II are cast using plant-produced ready-mix SCC with a specified compressive strength of 6 ksi and 7 ksi for phase I and 6 ksi for phase II and subsequently encased with CIP-NDOT UHPC, which is mixed in the structural laboratory at the University of Nebraska–Lincoln. Phase I specimens are not reinforced while the second phase's specimens are reinforced with *ASTM A615/A615M-24* steel in both longitudinal and transverse directions.

UHPC mix is developed based on particle packing theory to optimize strength and minimize permeability (El-Tawil, 2018). A cast-in-place (CIP) UHPC mix design, originally formulated by Flavia et al. (2020) and later refined by Hu et al. (2023), is adopted and further validated by the Nebraska Department of Transportation (NDOT) based on prior research and empirical testing conducted at UNL. The mix proportions used for casting the UHPC encasement of all specimens are presented in Table 4.3.

Table 4.3 Details of second phase of experimental programs (Hu et al., 2023)

Ingredient	**Type**	**Quantity lb/cy**
Cement	Ash Grove Type I/II	1,213
Silica Fume	Force 10,000 D	162
Slag	Central Plains GGBFS	589
Fine Sand	No.10	1,612
Water	30% Ice	291
Workability Retaining Admixture (WRA)	Chryso Optima 100	25
High Range Water Reducer (HRWR)	Chryso Premia 150	65
Fibers	13 mm Steel	264

The UHPC mixing process begins by pre-mixing sand and silica fume for 5 to 10 minutes to enhance silica fume dispersion, prevent agglomeration, and improve particle packing efficiency. Then the remaining fine ingredients are added to the sand-silica fume mixture.

The ingredients are mixed for three minutes, after which cold water is gradually added from the top of the mixer. Initially, the mix may exhibit balling behavior, but as mixing continues,

it transitions into a flowable and well-dispersed consistency. At this stage, steel fibers are gradually introduced from the top of the mixer to ensure even distribution throughout the mix. The mixing process continues until a homogeneous distribution of fibers is achieved, ensuring uniform mechanical properties throughout the UHPC matrix.

4.3 Materials Characterization

This section presents the material characterization of CC, reinforcing steel, and UHPC. Regarding CC, according to *ASTM C39/C39M-21* the average compressive strength was determined by testing three 4 in. × 8 in. cylindrical specimens at 28 days for each phase, as well as three cylinders are tested on the day of phase II specimens cover removal. The individual and average results are summarized in Table 4.4. Regarding phase I, two grades of concrete are used 6 ksi and 7.5 ksi while regarding phase II the columns are constructed from the 6 ksi concrete. Despite the specified compressive strength of CC bridge columns in Nebraska is equal to 3 ksi, the concrete strength of tested specimens in phase I and II is high as SCC was used in the construction of all the specimens, which often result in higher strength due to the high powder content and this is intentionally as lower compressive strength are covered in different studies in the literature while higher strength are not investigated properly.

Table 4.4 Compressive strength of CC at for two phases of experimental work

Mix	6 ksi Mix			7.5 ksi Mix
Experimental Phase	Phase I	Phase II		Phase I
Age	28 days	At cover removal	28 days	28 days
#1	6.37	4.72	6.37	7.42
#2	6.03	4.43	6.03	7.78
#3	6.12	4.65	6.12	7.65
Average	**6.17**	**4.60**	**6.17**	**7.61**
Standard Deviation	**0.17**	**0.15**	**0.17**	**0.18**
COV	**0.028**	**0.033**	**0.028**	**0.024**

Regarding NDOT CIP-UHPC, a flow test of UHPC is performed and the resulting spread ranges from 9 in. to 10 in. The average compressive strength was measured by testing three cylinders after seven days, three cylinders after 28 days, and three cylinders after 56 days. The results of each set are shown in Table 4.5. The average compressive strength is more than 17.0 ksi after 56 days, which satisfies the ASTM C1856- requirements for UHPC.

Table 4.5 Compressive strength of UHPC at different ages

Specimen No.	Compressive Strength (ksi)		
Age (day)	7	28	56
#1	13.8	16.2	20.8
#2	13.6	16.6	21.4
#3	13.4	16.7	21.2
Average	**13.6**	**16.5**	**21.1**
Standard Deviation	**0.20**	**0.26**	**0.30**
COV	**0.014**	**0.016**	**0.014**

The flexural tensile properties of UHPC are estimated according to ASTM C1609-19 as shown in Figure 4.5. Figure 4.6 shows the stress-deflection plot of three prisms, while Figure 4.7 shows the cracking, peak and residual strengths of UHPC. Table 4.6 presents the test results of the prisms alongside the PCI-UHPC performance requirements, as outlined by Sim et al. (2020). These requirements specify that the peak flexural strength must be at least 2,000 psi, the flexural strength at first crack (cracking strength) must not be less than 1,500 psi, the ratio of peak to cracking flexural strength should exceed 1.25, and the residual flexural strength must be greater than 75% of the cracking strength. It can be noted that the results in the table and all plots satisfy these requirements with a considerable safety margin. Figure 4.8 shows the tested prisms after failure for prisms. All failures occur within the middle third of the specimens and the fibers are uniformly distributed throughout the cross-section.

Figure 4.5 Flexural testing of UHPC prism

Table 4.6 Flexural Properties of UHPC

Specimen ID	Cracking Strength (psi)	Peak Strength (psi)	Residual Strength (psi)	Peak Strength /Cracking Strength	Residual Strength/Cracking Strength (psi)
#1	1,837	2,411	1,556	1.31	0.84
#2	1,705	2,215	1,526	1.30	0.89
#3	1,805	2,709	1,745	1.50	0.96
Average	**1,782**	**2,445**	**1,609**	**1.40**	**0.90**
Standard Deviation	**68.9**	**248.7**	**118.7**	**0.11**	**0.06**
COV	**0.04**	**0.10**	**0.07**	**0.08**	**0.07**

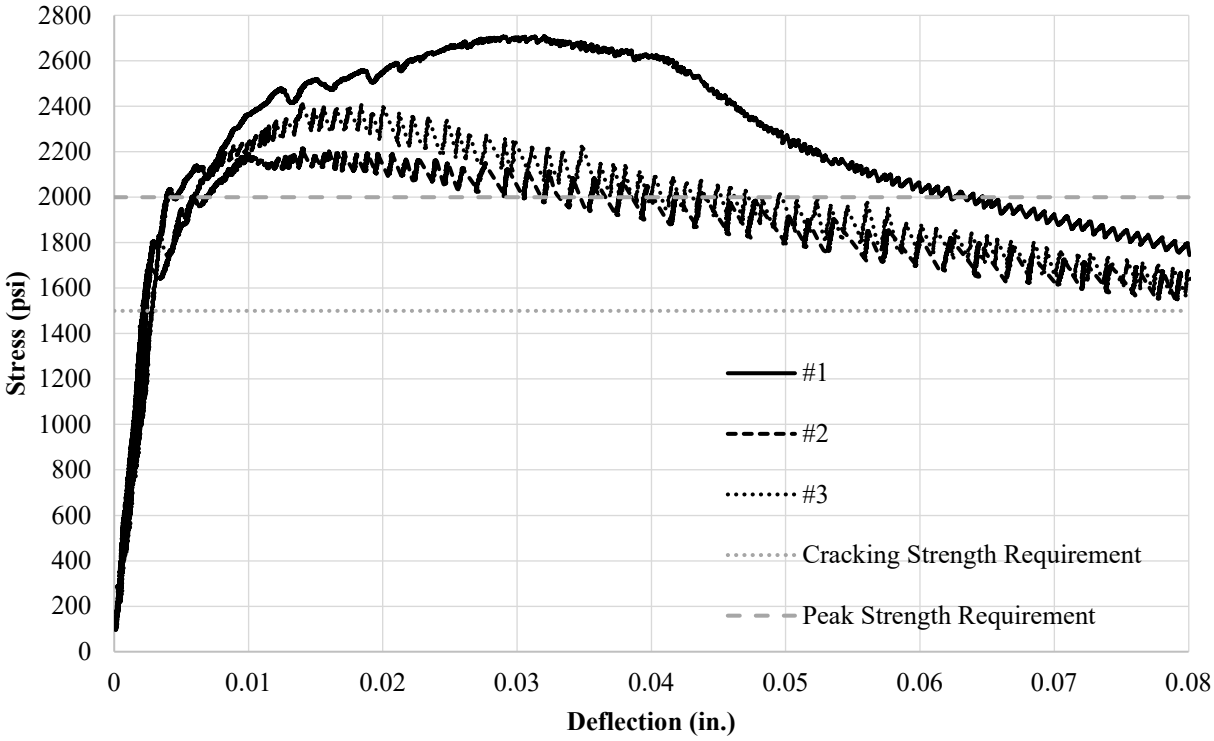

Figure 4.6 Stress-deflection plot of the UHPC prisms

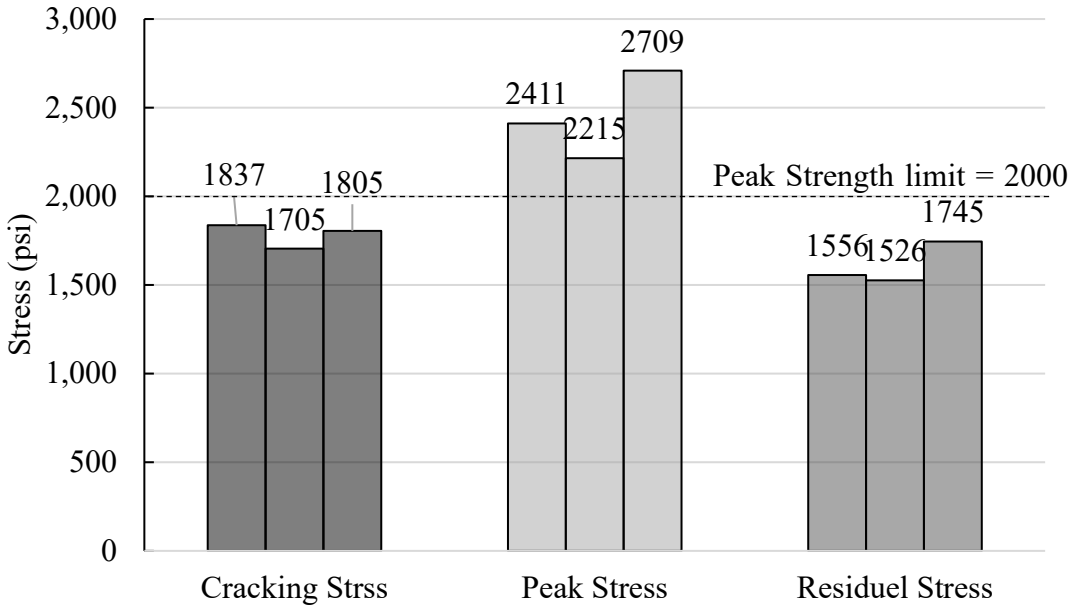

Figure 4.7 Flexure strength result of UHPC

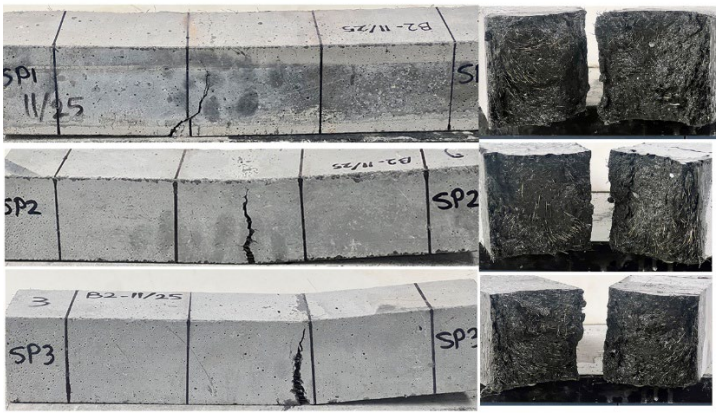

Figure 4.8 Tested flexural prisms after failure.

The tensile properties of UHPC are determined according to AASHTO T397-22, as illustrated in Figure 4.9. Figure 4.10 presents the stress-strain plot for the six prism specimens, and Table 4.7 lists the tensile properties of each specimen, along with the average values of the three successful specimens. In the table, the specimens written in red are excluded and did account in the average calculations, as failure either occurs outside the gage length or is attributed to alignment issues. The results confirm that the tested specimens meet the requirements set by AASHTO T397-22.


Figure 4.9 Direct tension testing of UHPC prism

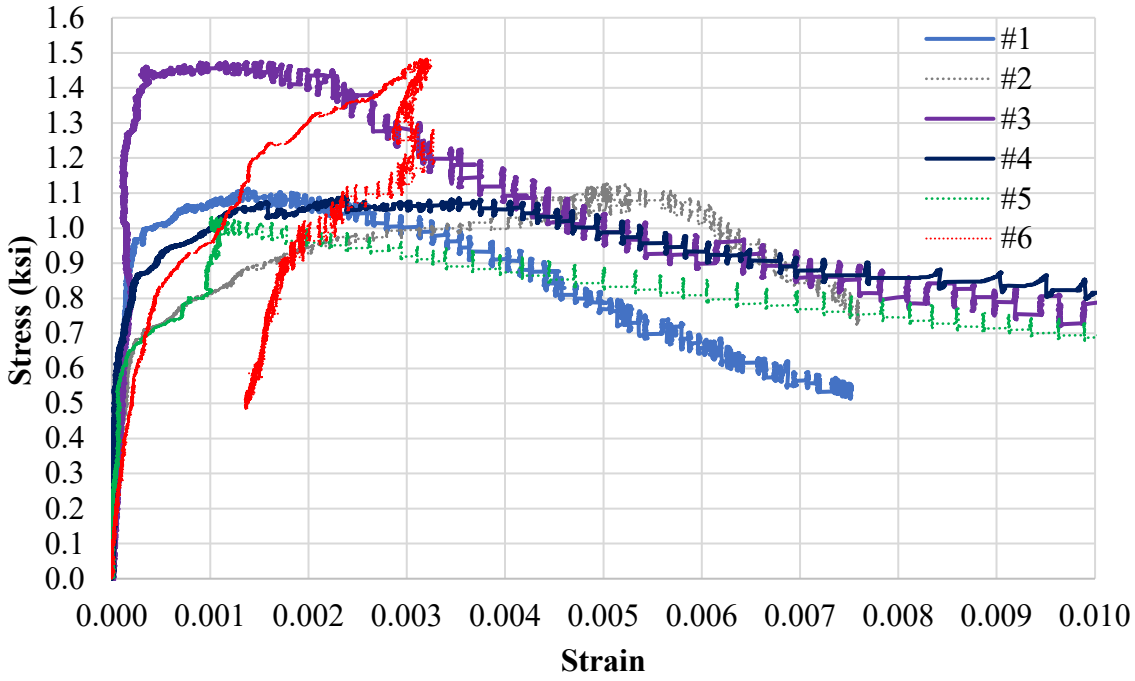

Figure 4.10 Tensile stress-strain plot of the UHPC prisms

Table 4.7 Tensile properties of tested tension prisms

	Cracking		Crack localization		Peak		
Specimen	Cracking Stress	Cracking Strain	Crack Localization Stress	Crack Localization Strain	Peak Stress	Peak Strain	Location of failure
#1	1.00	0.00037	1.07	0.0032	1.11	0.0032	within the gage length
#2	0.72	0.00047	1.08	0.0056	1.12	0.005	*Two Cracks
#3	1.43	0.00050	1.43	0.0025	1.47	0.0015	within the gage length
#4	0.87	0.00032	1.05	0.0041	1.09	0.0024	within the gage length
#5	0.69	0.00034	1.03	0.00101	1.03	0.00101	*Two Cracks
#6	0.83	0.00049	N/A	N/A	1	N/A	*Two Cracks
Average	**1.10**	**0.0004**	**1.18**	**0.0033**	**1.25**	**0.0025**	
Standard Deviation	**0.29**	**0.00009**	**0.21**	**0.0008**	**0.21**	**0.00085**	
COV	**0.266**	**0.234**	**0.181**	**0.246**	**0.175**	**0.359**	

*Failure occurs outside the gage length, and two cracks form, indicating flexural behavior and misalignment with the machine's axis

Figure 4.11 displays the left, front, back and right faces view of the tensile-tested prisms after failure. Notably, for specimens #2, #5, and #6, failure occurs outside the gage length, and two cracks form, indicating flexural behavior and misalignment with the machine's axis. This suggests a potential issue with specimen alignment during testing. Therefore, the results of these specimens are excluded.

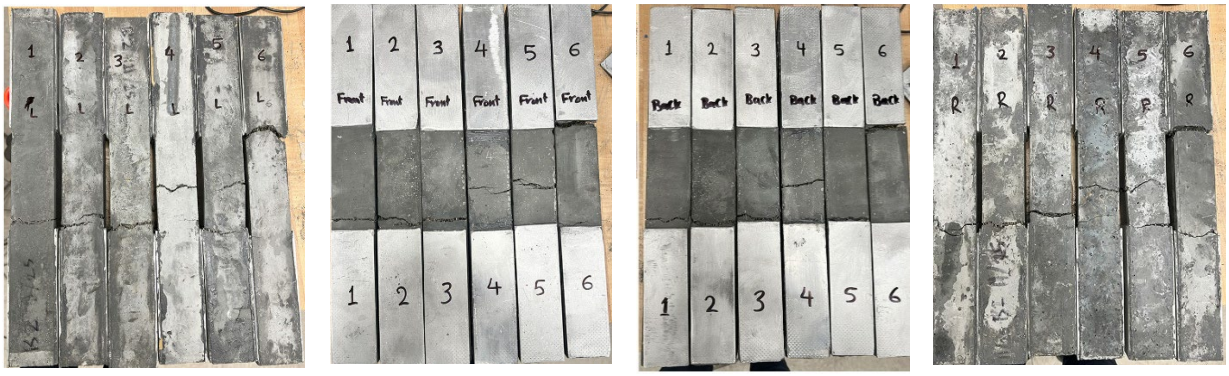

Left face Front face Back face Right face

Figure 4.11 Tested tension prisms after failure

4.4 Fabrication of Test Specimens

In this section procedures of the specimen's construction are detailed showing the installation of steel bars in phase II specimens, formwork of the two phases, casting CC, different types of surface preparation in the second phase, and casting UHPC for phase I and II specimens.

4.4.1 Reinforcement Layout

Regarding phase I specimens, no reinforcement is used, whereas those in phase I are reinforced with details shown in Figure 4.4 and Table 4.3.

For each specimen in phase II, steel bars are cut into eight 4.0-ft segments. Circular ties are then installed at a 9.6-inch spacing, ensuring that each longitudinal bar is securely attached to the inner circumference of the tie using steel ties, as shown in Figure 4.12. The assembled reinforcement cage is placed inside a rigid paper concrete form tube, as shown in Figure 4.13, maintaining proper positioning during casting using plastic spacers.

Figure 4.12 Steel reinforcement layout

Figure 4.13 Steel cage of column and the concrete tube form

4.4.2 Formwork

As previously discussed, phase I specimens have dimensions of 4.0 × 8.0 in², which corresponds to the standard size specified in ASTM C39/C39M-21 and prepared in accordance with ASTM C192/C192M-16. After the cylinders harden, they are demolded and moist cured for a period of 28 days.

In phase II, specimens are cast in rigid paper form tubes with nominal diameters of 8 inches for specimens which their surface is prepared via sandblasting and 12 inches for specimens which their surface prepared by cover removal. The larger diameter accommodated the 2-inch cover that is subsequently removed as part of the roughening process. All specimens are cured until the concrete attained sufficient strength for surface preparation. The use of two form sizes ensured a consistent final diameter of 8 inches across all specimens following surface treatment and prior to UHPC jacketing. Sandblasted specimens retained their original dimensions, while roughened specimens undergo cover removal to achieve the same target geometry. This methodology ensured uniformity in specimen dimensions for subsequent testing and analysis.

No spacers are required for specimens which their surface prepared by sandblasting as the surface preparation technique as shown in Figure 4.14. However, spacers are used to ensure 2 in. UHPC thickness for specimens that cover removal is the surface roughening technique.

Figure 4.14 Specimen with surface sand blasted before cast CC

4.4.3 Surface preparation

In phase I, no intentional surface preparation is done. All specimens are prewetted only before UHPC placing.

In phase II, removing 2 in. concrete cover around the circumference of the column until the transverse reinforcement is exposed, as shown in Figure 4.15-b, was the technique used for roughening surface of six specimens. The concrete cover removal process is performed at concrete compressive strength of 4.70 ksi. While for two specimens, the surface of the specimen sandblasted until the surface appeared roughened and uniformly textured with a thin cement paste layer partially removed and the fine aggregate slightly exposed as shown in Figure 4.15-c. This is done by using fine sand passing through sieve #10 which is compressed using abrasive blaster.

a) b) c)

Figure 4.15 Surface preparation of columns a) original column, b) column after cover removal, and c) column after surface sand blasting.

4.4.4 UHPC jacket Reinforcement

The UHPC jackets in the first phase are not reinforced while in the second phase two specimens are reinforced in the top 6.0 in. This reinforcement was designed based on the failure mode observed in the UHPC-jacket-unreinforced tested specimens. The failure mode is described in detail in a later section; in general, cracks initiate from the top of the UHPC jacket.

To assess this behavior, the transverse strain in the UHPC jacket was measured 2 in. from the top. This strain value is then used to determine the required amount of steel tie reinforcement necessary to control strain development and prevent crack initiation. The height of the steel ties

and its distribution is determined based on the depth of cracking that initiated from the top of the UHPC jacket, measured from the top to the crack termination point and the strain at a second transverse measurement point, located 12 inches from the top.

The results indicate that #3 steel ties should be placed at 1 in. spacing over a 6 in. vertical distance to effectively mitigate cracking. Figure 4.16 shows the installation of reinforcement on the top 6.0 in. of the column and adding the form to the column.

Figure 4.16 Top reinforcement of UHPC jacket

4.4.5 Construction of UHPC Jacket

In phase I, a rigid paper concrete form tube with a diameter of 8 in. is used to ensure a 2 in. thickness of the UHPC jacket, as shown in Figure 4.17. To construct a 1 in. thick UHPC jacket, 6.0 in. diameter plastic molds are utilized, also shown in Figure 4.17. All specimens are prewetted before UHPC placement and no preparation was performed for the surfaces of these cylinders. To ensure that the load acts only on the CC during testing, 1.0 in. clearance is maintained at both the top and bottom ends of the cylinders as shown in Figure 4.3. This is achieved by placing the cylinders inside a slotted Styrofoam ring at the bottom, while at the top, the UHPC casting stops approximately 1.0 in. beyond the CC cylinder's top edge.

Figure 4.17 Formwork for the first phase specimens

In phase I, the UHPC jacket is constructed using the same type of formwork, maintaining a uniform 12-inch diameter to encase an 8.0 in. diameter CC core, whether sandblasted or with cover removal. This setup creates a composite CC-UHPC section with a CC core diameter of 8.0 in. and a UHPC jacket diameter of 12.0 in., as illustrated in Figure 4.18. To evaluate the transfer shear between UHPC and the CC substrate, the bottom 2.0 in. of the CC core are left without a UHPC jacket, as depicted in Figure 4.2.

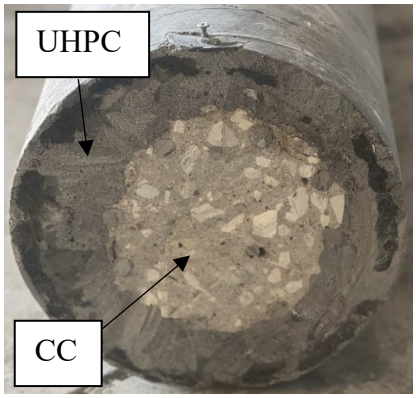

Figure 4.18 Cross section of CC-UHPC composite section of the specimen

To test the interface shear and bond between CC substrate and UHPC, the specimens are designed to be supported from the bottom of the UHPC jacket on a slotted circular steel plate, with the load applied at the top of the CC column. Each column is placed in a 12.0 in. diameter form, which is terminated by a 2.0 in. thick Styrofoam ring with an outer diameter of 12.0 in. and an

inner diameter of 8.0 in. The CC column's bottom is inserted in the Styrofoam ring slot and supported on a flat surface. A 2.0 in. spacer was installed between the CC column and the form to maintain a consistent UHPC jacket thickness of 2.0 in.

To provide structural stability for the entire setup, including the column and form, a supportive skeleton is constructed around the column, as shown in Figure 4.19. This ensures that the form remains securely in place during casting.

Figure 4.19 Supportive skeleton for the form work

All specimens in phases I and II are prewetted and cleaned from dust before casting UHPC. The UHPC is mixed using a high-shear Imer 750 mixer available at UNL, which has a capacity of 5.12 ft^3 (0.145 m^3) per batch as depicted in Figure 4.20. The casting process involves pouring UHPC from the top of the form using buckets, as shown in Figure 4.21, ensuring continuous flow from one side to minimize air entrapment until the form is filled. A sample of the final specimens, after UHPC hardening and form removal, for the first and second phases are presented in Figure 4.1 and Figure 4.2, respectively. The surface of the specimens shows good and high-quality finishing. The specimens are then prepared for the testing.

Figure 4.20 UHPC high shear mixer at UNL (Imer 750)

Figure 4.21 Formwork and casting of UHPC jacket

4.5 Test Setup

This section describes the test setup for both phases of specimens. For phase I, the specimens are tested using a Material Testing System (MTS) machine. The primary objective of this test is to develop stress-strain relationships for both confined and unconfined concrete specimens, to study the effect of UHPC confinement on the compression behavior of CC.

The MTS machine, known for its precision and reliability, is utilized to measure the longitudinal deformation of the specimens. To ensure accurate load measurements, a load cell is attached to an independent system, verifying the recorded loads from the MTS machine and the external load cell are consistent.

Initially, the test is conducted at a loading rate of 35 psi/sec. However, after testing the first specimen, it becomes evident this rate is fast, making it difficult to observe crack formation. Consequently, the loading rate is reduced to 10 psi/sec, which is found to be optimal for crack observation. Figure 4.22 illustrates the test setup for phase I.

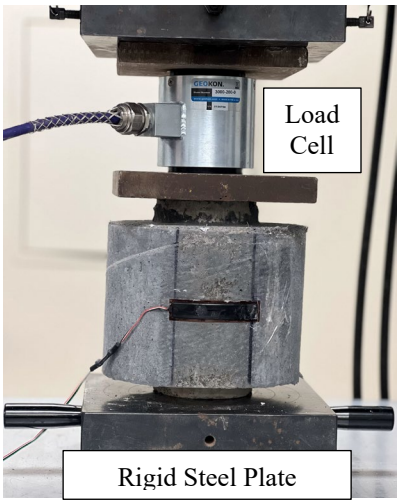

Figure 4.22 Test set up of specimens in first phase

Regarding phase II, the axial experimental test setup is illustrated in Figure 4.23-a. The specimen is supported on a slotted steel plate ring, which is designed to carry the UHPC jacket while allowing the uncovered tip of the CC core to be inserted into the central hollow slot. The plate has an outer diameter of 12.0 in. and an inner diameter of 8.5 in., ensuring proper fit and stability without contacting of CC core. The slotted steel plate carrying the column is mounted on a 400-kip steel frame, providing a rigid testing base. The load is applied at the top of the specimen directly onto the CC core using an 8.0-inch diameter rigid steel plate, ensuring axial compression of the core and enabling the UHPC jacket to resist any potential interfacial sliding, thereby simulating shear transfer at the CC-UHPC interface. A string potentiometer is used to monitor the relative displacement between the CC column and the UHPC jacket. This device is attached to the UHPC jacket at height of 4.0 in. measured from the bottom of the jacket, with its string connected to a steel bar anchored to the CC core within the slotted steel plate, ensuring accurate measurement of differential movement. To ensure uniform load distribution and surface flatness, neoprene pads are placed beneath the applied load and between the UHPC jacket and the slotted steel plate,

enhancing the accuracy of the test results. Figure 4.23-b shows a schematic drawing of the test set up. Transverse strains are recorded using strain gauges mounted horizontally along the height of the UHPC jacket for each specimen. The horizontal gauges are positioned starting at 2.0 in. from the top of the jacket, followed by one at 12.0 in. from the top, and then at 6.0 in. intervals down to a level of 36.0 in measured from the top. An additional horizontal gauge is placed at 46.0 in. from the top to capture lateral strain behavior near the lower end of the jacket. This layout is used for longitudinal strain gauges without adding two longitudinal strain gauges at the top and bottom ends as shown in Figure 4.23-a.

a) instrumentation photo

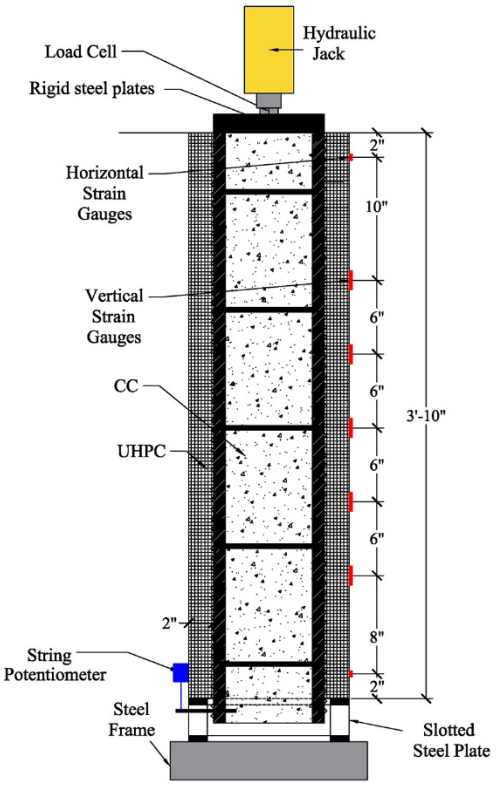

b) location of gauges and test components

Figure 4.23 Axial loading test setup: a) instrumentation photo and b) schematic drawing showing locations of gauges

The flexural experimental test setup is shown in Figure 4.24-a. The specimen was simply supported with a clear span of 38.0 inches, measured from the centerline of one roller support to the centerline of the other. The supports rested on two rigid steel base beams capable of safely transferring the applied loads to the steel testing frame. To prevent lateral displacement or rolling of the circular specimen under load, threaded rods were anchored to the steel beams and secured against the specimen. A rigid U-shaped steel frame was constructed in the lab to apply the load vertically at the mid-span of the specimen, ensuring accurate application of the loading point without sliding or instability. The test was conducted using the 400-kip capacity hydraulic steel loading frame which was used in the axial testing. To record mid-span deflections, a string potentiometer was installed directly below the specimen. Neoprene pads were placed between the specimen, and the steel roller supports, as well as under the U-frame loading point, to promote uniform load distribution and accommodate any minor surface irregularities. A schematic of the setup is presented in Figure 4.24-b. Strain in the extreme tension fibers of the section is recorded using strain gauge mounted at the bottom of the specimen.

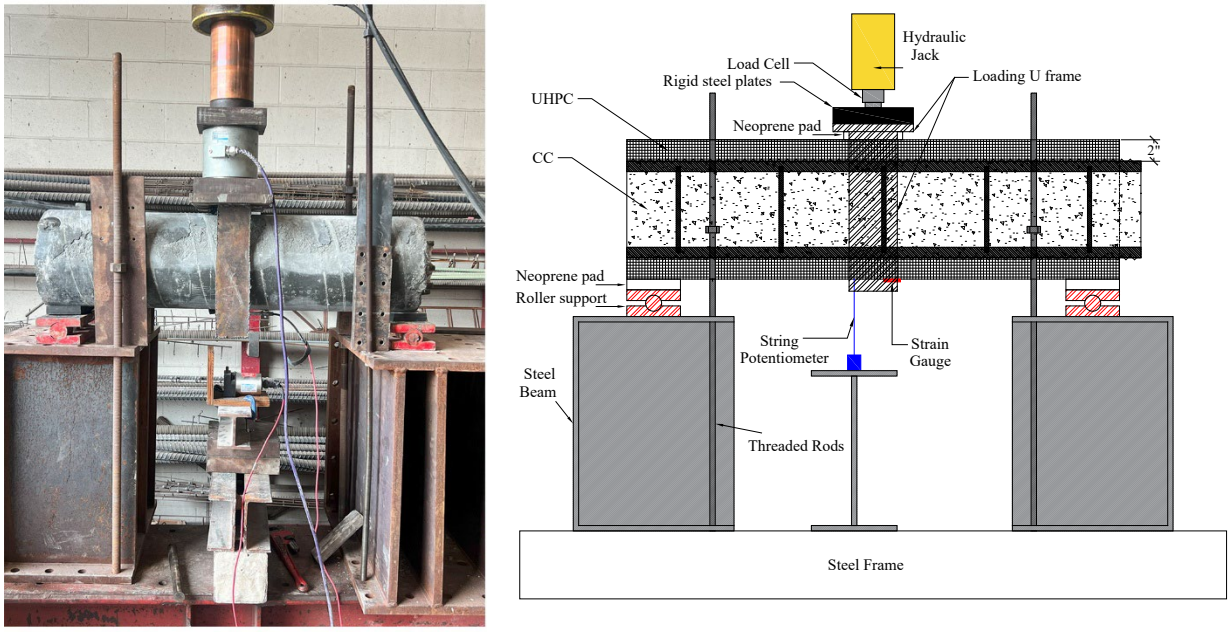

a) Test setup photo b) Test setup components

Figure 4.24 Flexural test setup: a) actual photo and b) schematic drawing showing components

4.6 Results

4.6.1 Phase I

This phase consists of 14 specimens, divided into two groups of seven specimens each. The designed compressive strengths of these groups are 6.0 ksi and 7.5 ksi. Utilizing two different compressive strengths allows for a more comprehensive understanding of the effect of UHPC confinement on the behavior of CC with higher compressive strength. This testing program aims to enhance the understanding of CC behavior when confined with UHPC.

Each group includes seven specimens: one cylinder with no confinement, which is considered a control specimen, three cylinders confined with 1-in. UHPC, and three cylinders confined with 2-in. UHPC.

4.6.1.1 Stress-strain curves

Figure 4.25, Figure 4.26, along with

Table 4.8, show the results of phase I and demonstrate the effects of UHPC confinement on the mechanical behavior of CC. Figure 4.25 compares the average stress-strain curves for 6 ksi concrete specimens in three conditions: unconfined, confined with 1.0 inch of UHPC, and confined with 2.0 inches of UHPC. Similarly, Figure 4.26 presents the average stress-strain diagram for 7.5 ksi concrete under the same confinement conditions.

Table 4.8 present key findings, including maximum compressive strength, strain at peak stress, and modulus of elasticity (MOE) for individual specimens and their respective averages across confinement conditions. The data clearly demonstrates that UHPC confinement significantly enhances both strength and ductility. Specifically, a 1.0 in. UHPC jacket increases compressive strength by 33% and 35% for the 6 ksi and 7.5 ksi specimens, respectively, while also improving strain capacity by 65% and 64%. The modulus of elasticity exhibits a corresponding rise of 26% and 23%. Increasing the confinement thickness to 2.0 in. further amplifies these effects, yielding strength enhancements of 66% and 55%, peak strain improvements of 69% and MOE increases of 49% and 76% for the 6 ksi and 7.5 ksi specimens, respectively. These results underscore the effectiveness of UHPC confinement in substantially improving the mechanical performance of conventional concrete, with greater confinement thickness yielding more pronounced gains in both strength and stiffness.

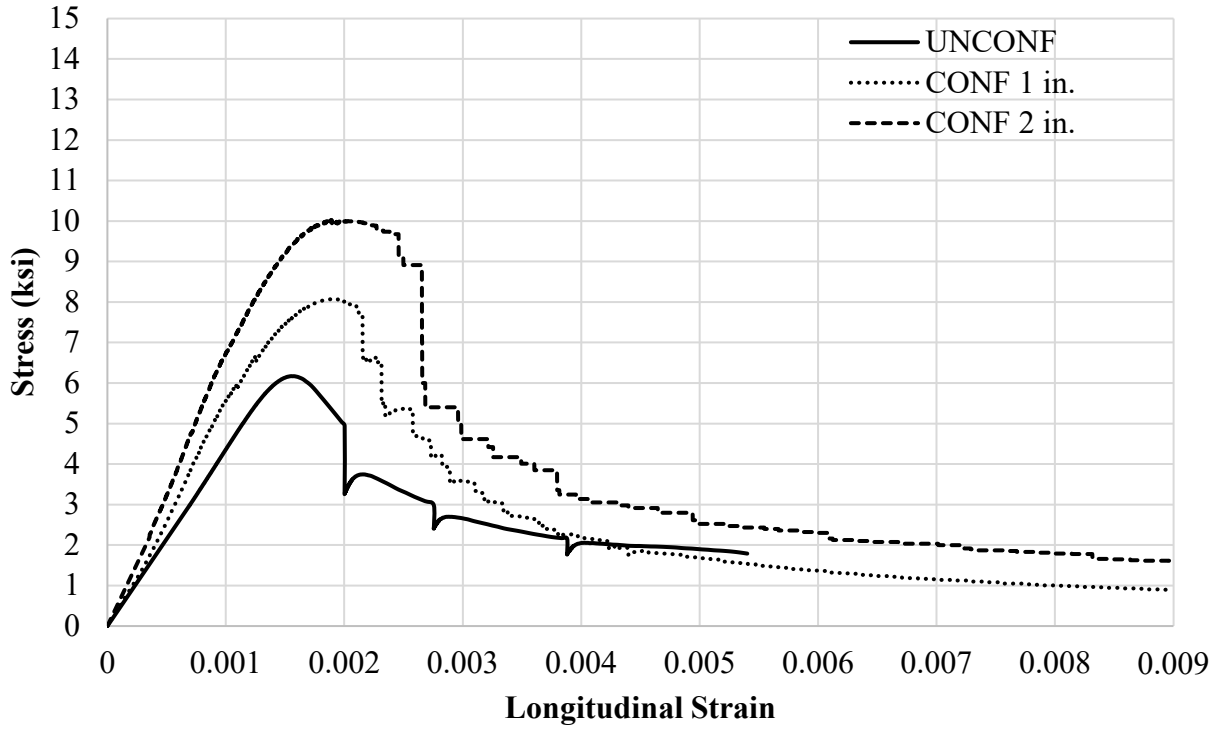

Figure 4.25 Average stress-strain curve of CC6 ksi specimens

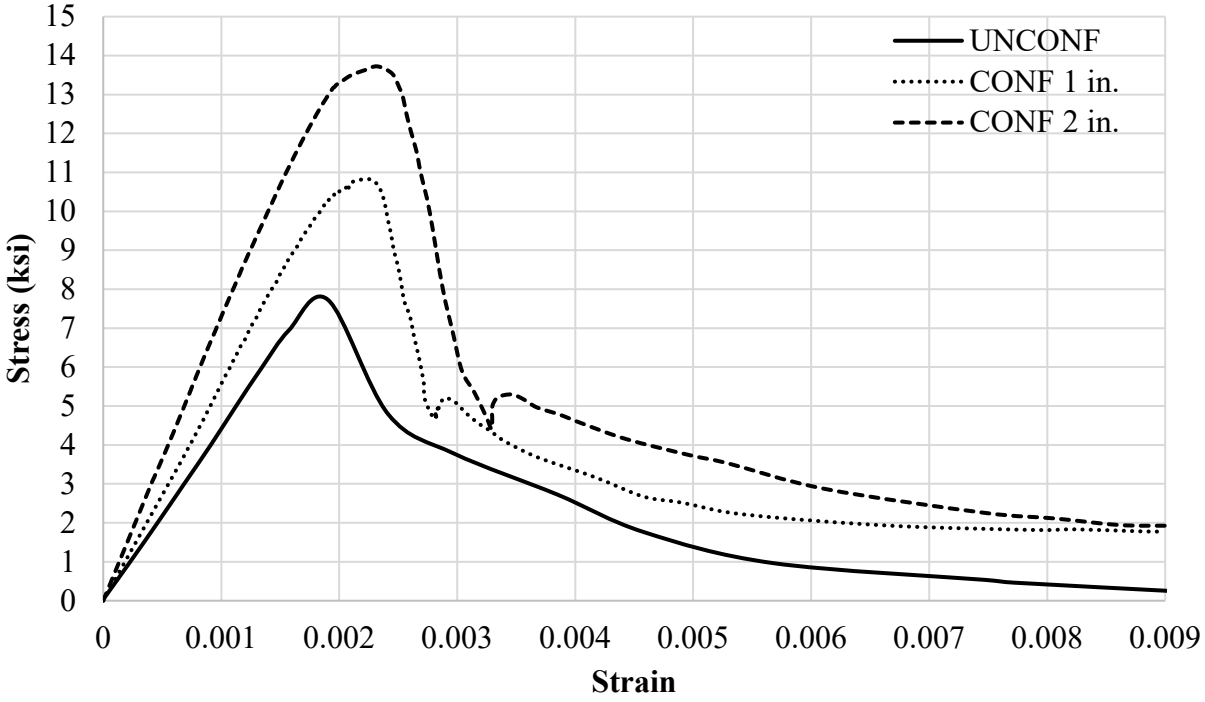

Figure 4.26 Average stress-strain curve of CC6 ksi specimens

Table 4.8 Results of first phase specimens

Specimen ID	Specimen #	Maximum Stress (ksi)	Stress increase	Strain at Maximum stress	Strain increase	MOE (ksi)	MOE increase
CC6		**6.1**		**0.00144**		**4,242**	
CC6-UHPC 1	1	8.5		0.00254		5,205	
	2	7.8		0.00230		5,300	
	3	8.0		0.00290		5,793	
Average		**8.1**	**33%**	**0.00238**	**65%**	**5,433**	**28%**
Standard deviation		**0.36**		**0.00030**		**315.6**	
COV		**0.044**		**0.126**		**0.058**	
CC6- UHPC 2	1	10.2		0.00264		5,492	
	2	10.0		0.00220		7,005	
	3	10.2		0.00248		6,713	
Average		**10.13**	**66%**	**0.00244**	**69%**	**6,404**	**51%**
Standard deviation		**0.115**		**0.00022**		**802.6**	
COV		**0.011**		**0.091**		**0.125**	
CC7.5		**7.7**		**0.00190**		**4,324**	
CC7.5- UHPC 1	1	10.5		0.00308		5,390	
	2	10.0		0.00316		5,809	
	3	10.8		0.00313		4,665	
Average		**10.43**	**35%**	**0.00312**	**64%**	**5,288**	**23%**
Standard deviation		**0.4**		**0.00004**		**578.8**	
COV		**0.038**		**0.013**		**0.11**	
CC7.5- UHPC 2	1	11.8		0.00312		7,973	
	2	11.1		0.00322		7,257	
	3	12.9		0.00330		7,599	
Average		**11.93**	**55%**	**0.00321**	**69%**	**7,610**	**76%**
Standard deviation		**0.9**		**0.00009**		**358.1**	
COV		**0.075**		**0.029**		**0.047**	

4.6.1.2 Modes of failure

The observed mode of failure in all specimens was crack localization failure within the UHPC jacket as shown in Figure 4.27 and Figure 4.29.

Cracks initiate at approximately 60% of the peak load in the UHPC jacket in specimens confined with a 1.0 in. UHPC jacket and at 65% of the peak load in those confined with a 2.0 in UHPC jacket. These values are observed visually during testing of specimens. Initially, hairline cracks formed at the top of the jacket and propagated downward through the UHPC. Failure primarily results from the development of a single dominant crack that originates at the top or

bottom of the UHPC jacket and extends toward the opposite end. Despite the formation of cracks within the UHPC jacket, the specimens continue to sustain increasing loads due to the fiber-bridging mechanism. As the steel fibers within the UHPC engage, they provide resistance and distribute the load across the fractured sections. However, once more than 50% of the fibers rupture, a sudden drop in load capacity occurs. Following this drop, the specimen exhibits some load recovery as the remaining fibers continue to resist deformation. Ultimately, as the remaining fibers fail, the specimen undergoes complete failure. Figure 4.27 and Figure 4.29 shows the modes of failure of all specimens confined with 1-in.- and 2-in.-thick UHPC, respectively. As per literature the mode of failure would be the same when CC compressive strength is lower than or equal to 3 ksi (Poncetti et al., 2023).

a) Failure mode of specimen CC6-UHPC1#1

b) Failure mode of specimen CC6-UHPC1#2

Figure 4.27 Failure modes of specimens confined with 1-in.-thick of UHPC

c) Failure mode of specimen CC6-UHPC1#3

d) Failure mode of specimen CC7.5-UHPC1#1

e) Failure mode of specimen CC7.5-UHPC1#2

Figure 4.27 Failure modes of specimens confined with 1-in.-thick of UHPC

f) Failure mode of specimen CC7.5-UHPC1#3

Figure 4.27 Failure modes of specimens confined with 1-in.-thick of UHPC

a) Failure mode of specimen CC6-UHPC2#1

b) Failure mode of specimen CC6-UHPC2#2

Figure 4.28 Failure modes of specimens confined with 2-in.-thick of UHPC

c) Failure mode of specimen CC6-UHPC2#3

d) Failure mode of specimen CC7.5-UHPC2#1

e) Failure mode of specimen CC7.5-UHPC2#2

Figure 4.28 Failure modes of specimens confined with 2-in.-thick of UHPC

f) Failure mode of specimen CC7.5-UHPC2#3

Figure 4.28 Failure modes of specimens confined with 2-in.-thick of UHPC

As illustrated in Figure 4.29, the failure crack consistently propagates from the intersection between the CC core and the UHPC jacket. When the crack initiates at the top, it extends downward to the base, whereas when it originates at the bottom, it propagates upward toward the top. This failure mechanism highlights the role of fiber reinforcement in delaying ultimate failure and influencing the axial load behavior of the UHPC-confined specimens.

Figure 4.29 Cracks initiation in specimens during testing

4.6.1.3 Verification of the proposed confinement model

In this section, the experimental results of the specimens are compared with the predicted values obtained using the confinement model proposed in Section 3.4.2 in Chapter 3. The

comparison demonstrates a strong correlation between measured and predicted performance with the calculated compressive strength averaging 3.5% lower and the predicted strain averaging 10% higher than the corresponding experimental values. These results indicate the robustness of the modified confinement model developed in this study. Table 4.9 present the average strength, strain of each phase of specimens and the ratio between the measured and the calculated values.

Table 4.9 Comparison between measured and calculated stresses and strain

Sub-group ID	Measured confined compressive strength (ksi)	Calculated confined compressive strength (ksi)	Measured to Predicted Ratio	Measured strain corresponding to measured confined compressive strength	Calculated strain corresponding to calculated confined compressive strength	Measured to Predicted Ratio
CC6-UHPC1	8.1	7.7	1.05	0.00238	0.0022	1.08
CC6-UHPC2	10.13	9.8	1.03	0.00244	0.0028	0.87
CC7.5-UHPC1	10.43	9.9	1.05	0.00312	0.0035	0.90
CC7.5-UHPC2	11.93	11.8	1.01	0.00320	0.0044	0.75

4.6.2 Phase II

This phase consists of eight specimens, divided into four groups, each containing two specimens. The primary objective is to investigate the effect of surface preparation techniques on shear transfer and bond strength between CC and UHPC in compression members, effect of adding transverse reinforcement at the ends of the UHPC jacket and investigate the behavior under axial and flexural loading.

The first group includes two specimens undergo sandblasting as a surface preparation method. The second, third and fourth groups, each comprising two specimens, are subjected to cover removal surface roughening, a common roughening technique. These methods are selected due to their widespread application in improving bond performance. The specimens in the first

three groups are tested under axially loading test while the specimens in the fourth group are tested under flexural loading.

Among the specimens prepared using cover removal, the UHPC jacket in the specimens in the third group are transversely reinforced at the top end to enhance structural integrity, whereas the second and fourth group remains unreinforced. The application of transverse reinforcement is intended to mitigate jacket failure, as the tests of the specimens that do not have transverse reinforcement demonstrate that specimens without reinforcement exhibit failure due to localized cracking in the UHPC jacket. The transverse reinforcement is strategically placed within the top 6.0 in. of the jacket, aligning with observed failure patterns. In unreinforced specimens, failure typically initiates as a primary crack at the top, which then propagates downward for approximately 6.0 in. before branching into multiple cracks, ultimately leading to complete failure. By reinforcing this critical region, the experiment aims to enhance the confinement effect of the UHPC jacket and improve shear transfer efficiency at the CC-UHPC interface. This study does not evaluate partially wrapped (non-continuous) UHPC jackets. For such partial jackets, confinement effects should be neglected, and the jacket must be anchored to the CC using either mechanical anchors or by engaging the existing longitudinal bars and stirrups into UHPC or both.

4.6.2.1 Results of axial testing

The slippage of the CC column relative to the UHPC jacket is monitored using the instrumentation setup described in the test setup section and shown in Figure 4.30. The average diagram of the load-slippage of each group, AS, AR, and ART, is presented in Figure 4.30.

Although some slippage readings are recorded, the results indicate that no significant relative movement (less than 0.01 in.) occurs between CC core and the UHPC jacket which indicates a perfect bond between both materials confirming the assumption that is assumed in the

analytical proposed model in Chapter 3. The observed values are minimal and can be attributed primarily to the compression of the specimen, which leads to shortening the element rather than actual interface slippage. Consequently, the measured displacement is likely a result of structural deformation rather than a true loss of bond between the CC and UHPC.

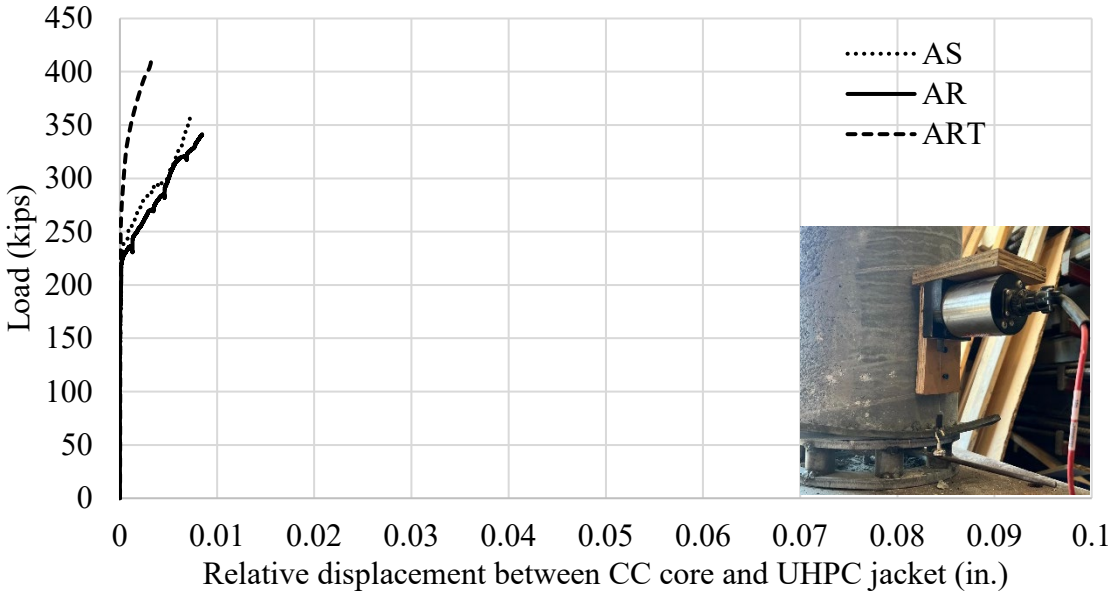

Figure 4.30 Load-slippage diagram of all specimens

The failure mode observed in all specimens is crack localization failure within the UHPC jacket, as illustrated in Figure 4.31. The cracks form due to splitting stresses from the CC core.

Crack initiation occurs at approximately 65% of the peak load in all specimens, as visually observed during testing. Initially, hairline cracks develop at the top of the UHPC jacket and gradually propagate downward. The failure mechanism is primarily governed by the formation of dominant cracks that extend downward for approximately 6.0 in. before branching into multiple cracks, as depicted in Figure 4.31.

Despite the presence of cracks, the specimens continue to sustain increasing loads due to the fiber-bridging effect of the UHPC. The embedded steel fibers play a crucial role in resisting

crack propagation and distributing the load across fractured sections. However, once a significant portion of the fibers rupture, a sudden drop in load-carrying capacity occurs, leading to failure.

This failure mechanism is specifically addressed in the design of specimens ART#1 and ART#2, where transverse reinforcement is incorporated into the UHPC jacket to enhance confinement and increase the load capacity. The inclusion of transverse reinforcement effectively improves the jacket's ability to sustain stresses, as both UHPC and reinforcement contribute to the confinement effect. The testing of ART#1 and ART#2 demonstrate no signs of cracking or failure, as shown in Figure 4.31, confirming the effectiveness of the additional confinement provided by transverse reinforcement within the UHPC jacket.

a) AR#1

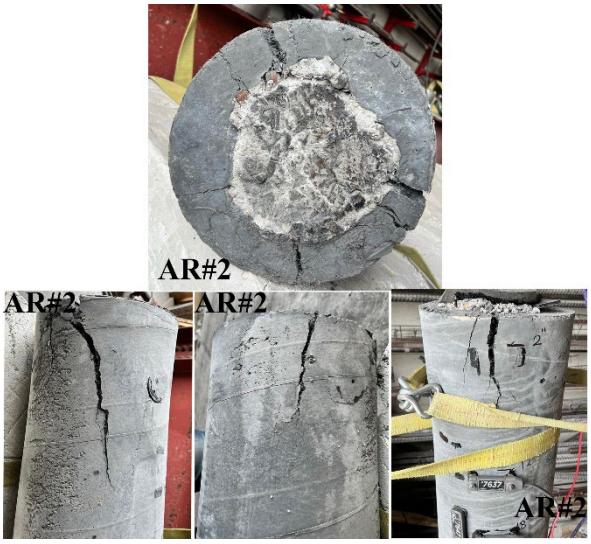

b) AR#2

c) AS#1

d) AS#2

e) ART#1

f) ART#2

Figure 4.31 Modes of failure of axially loaded specimens a) AR#1, b) AR#2, c) AS#1, d) AS#2, e) ART#1 and f) ART#2

Table 4.10 presents the test results for the specimens, highlighting the influence of surface preparation on axial capacity. The findings indicate that sandblasting provides slightly higher load capacity compared to the roughened surface achieved through cover removal using jackhammering. This difference arises because jackhammering results in uneven surface

dimensions, reducing the effective contact area between the CC core and the UHPC jacket. From a structural standpoint, both techniques provide comparable performance; however, sandblasting is recommended due to its simplicity and consistency.

Table 4.10 includes the calculated axial capacity of the CC core based on AASHTO LRFD 2020, incorporating the confinement effect of UHPC for specimens AS#1, AS#2, AR#1, and AR#2. For specimens ART#1 and ART#2, where transverse reinforcement is included within the UHPC jacket, the confinement effect is determined by adding the tensile contribution of transverse steel to the UHPC in the lateral confining pressure formula. The comparison between measured and predicted failure loads demonstrates strong agreement, verifying the accuracy of the proposed UHPC confinement model. These results confirm that the model can be effectively applied to various compression members confined by UHPC.

In specimens ART#1 and ART#2, the maximum load is limited by the capacity of the steel testing frame, rather than the failure of the specimens themselves. No cracks or signs of impending failure are observed during testing, indicating these specimens can sustain additional loading beyond the measured values.

Table 4.10 Results of the second phase of testing

Surface Preparation	Transversely reinforced	Column ID	Calculated axial capacity of unconfined CC core (kip)	Calculated axial capacity of confined CC core (kip)	Measured failure load (kip)	Ratio between measured and calculated confined axial capacities
Sand Blasting (S)	N/A	AS#1	293	367	360.6	1.00
		AS#2			360	1.00
Roughened By Cover Removal (R)	N/A	AR#1			347	0.97
		AR#2			337	0.94
Roughened By Cover Removal (R)	#3 @ 1 in. at the top	ART#1			407*	0.70
		ART#2			410*	0.70

* Specimens reached the maximum capacity of the steel frame with no failure.

The shear transfer strength is calculated in accordance with the AASHTO (2024), and the results are presented in Table 4.11. These results further validate the bonding efficiency between UHPC and CC, demonstrating that interface shear failure is not a governing failure mode in the tested specimens.

Table 4.11 Measured failure load of the second phase of testing and interface shear strength

Surface Preparation	Transversely reinforced	Column ID	Calculated interface shear strength (kip)	Measured Failure Load (kip)	Ratio between measured and calculated interface shear capacities
Sand Blasting (S)	N/A	AS#1	277.5	376	1.35
		AS#2		360	1.30
Roughened By Cover Removal (R)	N/A	AR#1		347	1.25
		AR#2		337	1.22
Roughened By Cover Removal (R)	#3 @ 1 in. at the top	ART#1		407*	1.47
		ART#2		410*	1.48

* Specimens reached the maximum capacity of the steel frame with no failure.

Figure 4.32 presents the transverse strain profiles for each group of the second phase. Transverse strains are recorded using strain gauges mounted along the height of the UHPC jacket for each specimen. The gauges are positioned starting at 2.0 in. from the top of the jacket, followed by one at 12.0 in. from the top, and then at 6.0 in. intervals down to 36.0 in. An additional gauge is placed at 46.0 in. from the top to capture strain behavior near the lower end of the jacket. The figure shows the average transverse strain recorded at the failure load for each group.

The results indicate that transverse strains are highest near the top and bottom regions of the columns, where failure of the UHPC jacket is observed. Values of strains reach a minimum near the mid-height of the specimens, creating a V-shaped strain distribution along the height. This distribution can be attributed to a combination of arching action and confinement effects driven by the geometry of the test setup and the nature of the applied axial loading. As the concrete core is initially compressed, the load is primarily carried by the core itself, without significant contribution from the UHPC jacket. At this stage, the section behaves as a CC column rather than a composite system, and the core tends to expand laterally due to the axial load. The UHPC jacket restrains this expansion, particularly at the top and bottom. This restraint generates significant transverse tensile stresses in the UHPC jacket at these locations, leading to higher strain concentrations. Meanwhile, the mid-height region, being less restrained, experiences lower lateral pressure and thus reduced transverse strain. This is likely because, at mid-height, the interaction between the concrete core and the UHPC jacket becomes more effective, allowing the section to behave more as a composite column, distributing the load more evenly between the two materials. The observed strain profile reflects the internal transverse stress flow within the jacket, where the load path curves outward from top- to mid-height and from bottom- to mid-height, generating peak tension at both ends and minimal tension at mid-span.

Specimens AR exhibited higher transverse strains compared to those prepared by sandblasting (AS), particularly at the critical zones near the top and bottom. This can be attributed to the non-uniform cross-sectional area of the concrete core after cover removal in the roughened specimens, which results in a smaller area and leads to higher axial stress and consequently elevated arching forces in the UHPC jacket, which leads to higher transverse strain.

Moreover, the specimen RT exhibit relatively high transverse strains without showing signs of jacket failure. This highlights the beneficial role of transverse reinforcement in resisting crack localization and enhancing the jacket's ductility and confinement capacity, even under high loads that exceed the failure loads of the unreinforced specimens.

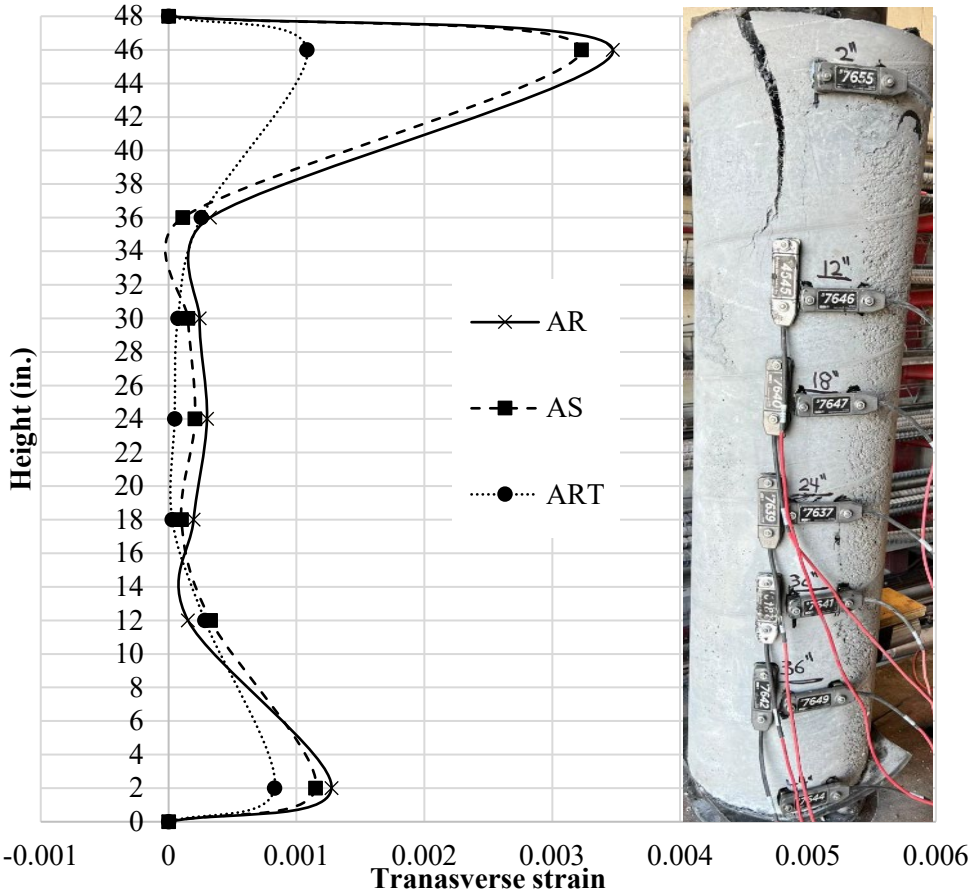

Figure 4.32 Average transverse strain profile alonge the UHPC jacket

4.6.2.2 Results of flexural testing

Figure 4.33 illustrates the load-deflection responses of specimens FR#1 and FR#2 under three-point bending. Both specimens exhibited linear elastic behavior followed by gradual stiffness degradation as flexural cracking propagated. Upon yielding the longitudinal reinforcement in the CC core and progressive pullout of the bridging steel fibers at crack localization, a noticeable reduction in stiffness and load capacity marked the onset of failure. Notably, specimen FR#2 sustained a slightly higher load than FR#1 and experienced a shear failure as demonstrated by the diagonal tension cracking in addition to flexure cracking.

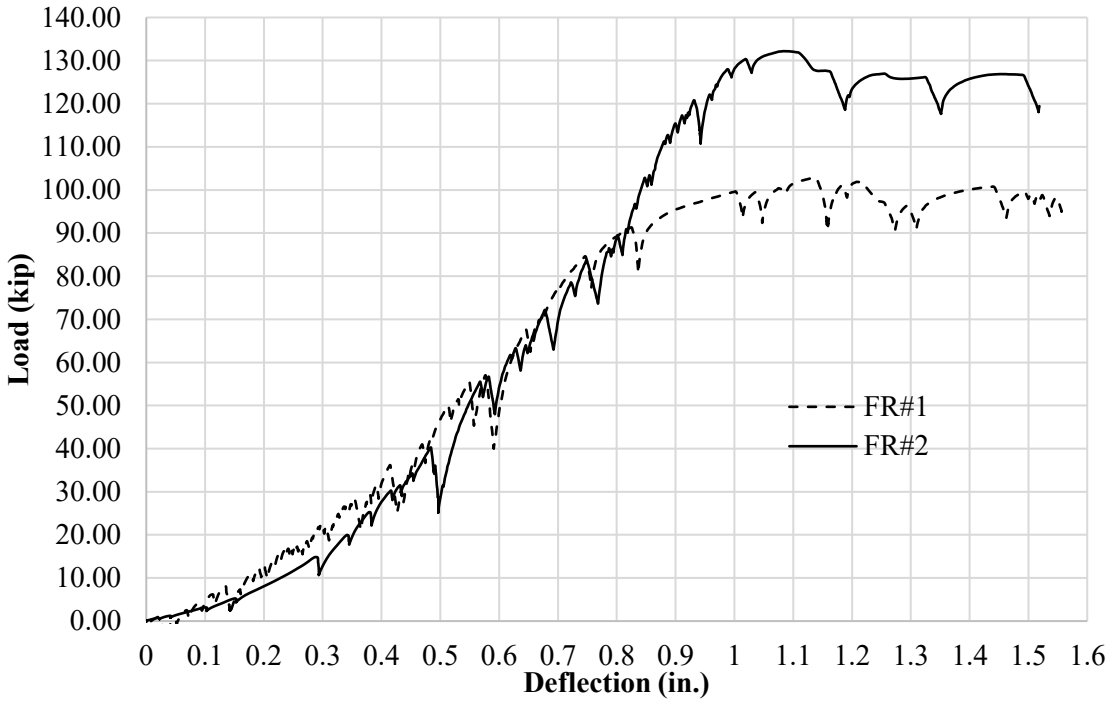

Figure 4.33 Load deflection relation curve of all specimens

Specimen FR#1 failed under pure flexure, with a single dominant crack mid-span, the region of maximum bending moment, as shown in Figure 4.34-a. In specimen FR#2, shear failure was observed; however, the specimen underwent flexural cracks developed at the bottom in the

mid-span with one dominant crack as shown Figure 4.34-b. As the load increased, audible sounds associated with fiber pullout were noted, indicating active engagement of the steel fibers within the UHPC jacket prior to crack formation. The 2% steel fibers by volume plays a critical role in controlling crack propagation. In specimen FR#1, microcracks gradually merged into a dominant flexural crack, while in specimen FR#2, a critical shear crack developed, ultimately governing the failure mode even though the presence of flexural cracks. The shear failure in FR#2 is due to the reinforcement orientation in the CC core, which lead to more rebars in the tension zone, thereby enhancing flexural resistance and shifting the failure mechanism toward shear. Crack initiation was observed at an average load of 51.0 kip in both specimens. Cracks propagated in the UHPC jacket and extended into the CC core, indicating effective bond between the two materials. No signs of sliding or debonding were observed at the UHPC-CC interface throughout the test. The structural collapse was not immediate, as residual load capacity was maintained briefly due to the fiber bridging effect and presence of steel reinforcement in the CC core.

a) FR#1

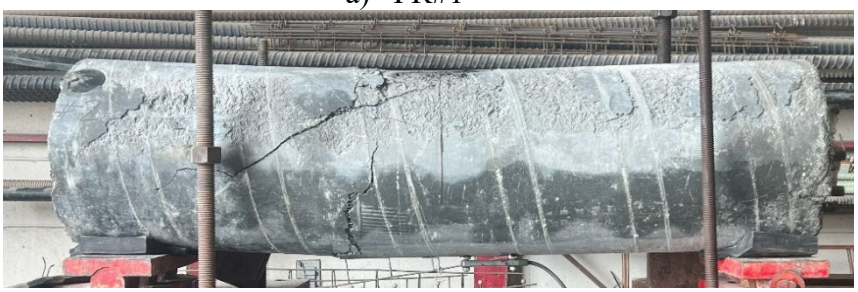

b) FR#2

Figure 4.34 Modes of failure of a) specimen FR#1 and b) specimen FR#2

Table 4.12 provides a comparison between the experimentally measured moment capacities and theoretical flexural strengths, calculated for both the CC core alone and the composite CC- UHPC section using the analytical approach proposed in Chapter 3. For specimen FR#1, the experimental moment capacity reached 1,104.56 kip.in, corresponding to a ratio of 1.76 relative to the calculated capacity of the CC core alone, and 1.35 relative to the composite section calculated capacity. Specimen FR#2 achieved the highest moment capacity of 1,255.78 kip.in, corresponding to a ratio of 2.00 relative to the calculated capacity of the CC core alone, and 1.53 relative to the composite section calculated capacity. The results demonstrate the substantial contribution of the UHPC jacket to the overall flexural performance, leading to an average moment capacity enhancement of approximately 88% compared to the CC core alone, as calculated per AASHTO LRFD (2020) provisions. The comparison between the measured and predicted capacities showed an average ratio of 1.44, suggesting that the method presented in Chapter 3 provides a safe and conservative design approach. However, the flexural capacity appeared to be influenced by factors such as the specimen orientation and the placement of reinforcement during testing—details that were not documented. As a result, the actual ratio may, in practice, be lower than reported. Both specimens exhibited no signs of slip or debonding at the UHPC–CC interface throughout the loading process, confirming excellent bond performance. This observation is consistent with the interface shear strength predictions presented in Table 4.11, which were not exceeded during testing.

Table 4.12 Results of flexural testing

Specimen ID	Measured failure load P (kip)	Measured moment capacity M (kip.in)	Calculated flexural capacity of the CC core M_o (kip.in)	$\frac{M}{M_o}$	Calculated flexural capacity of composite section M_{co} (kip.in)	$\frac{M}{M_{co}}$
FR#1	114.75	1,104.56	627.30	1.76	820.0	1.35

FR#2	132.18	1,255.78		2.0		1.53
Average	123.50	1,173.0		1.88		1.44

Figure 4.35 illustrates the relationship between the applied load and the tensile strain recorded at the bottom surface of the UHPC jacket for specimens FR#1 and FR#2. Strain gauges were installed at mid-span in the extreme tension zone to capture the response of the UHPC under flexural loading. The vertical dashed line represents the value of crack localization strain from Table 4.7. In specimens FR#1 and FR#2, the maximum tensile strain reached approximately 0.0035 and 0.0031, respectively, which are close to crack localization strain. This behavior is consistent with the observed flexural failure mode, in which tensile strains in the UHPC jacket are maximized at the bottom fiber. The slight differences in strains between FR#1 and FR#2 could be due to unintentional strain gage dislocation and steel reinforcement positioning. The absence of slip or separation confirms a perfect bond and composite action between the UHPC and CC core.

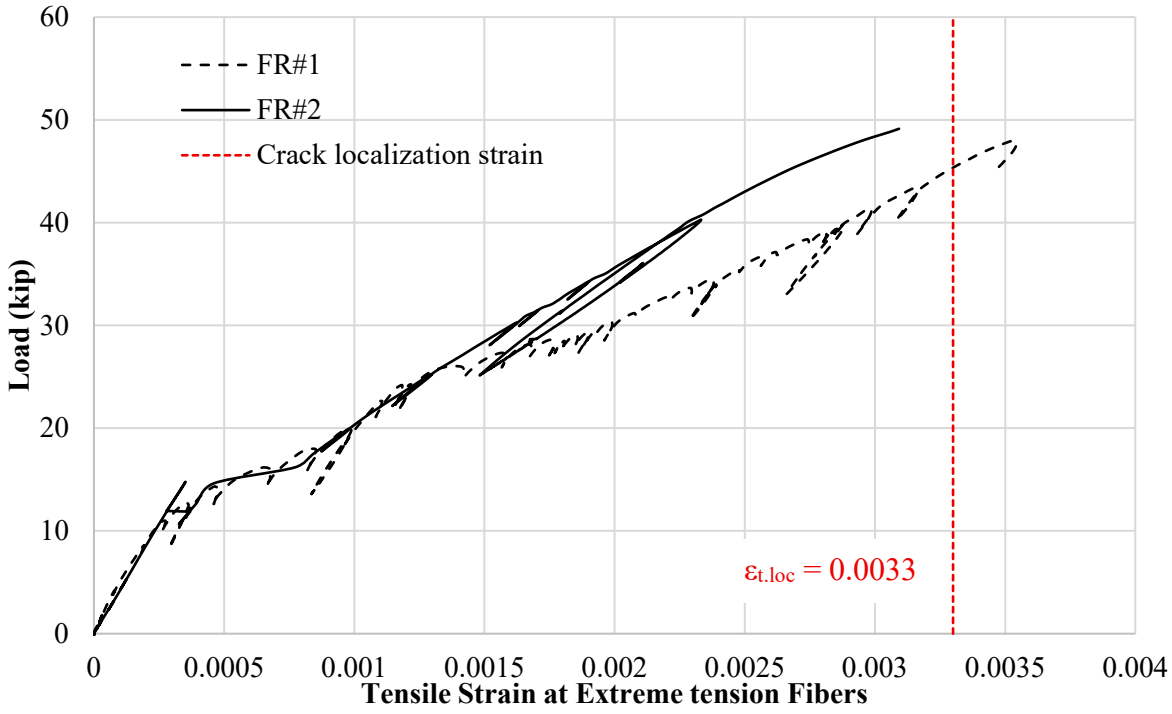

Figure 4.35 Load-strain relationship of the two specimens tested in flexure

Chapter 5 Summary, Conclusions and Recommendations

5.1 Summary

As of 2024, approximately 36% of bridges across the United States require repair or replacement, with 7% classified as structurally deficient, according to the Bridge Report (2024). The estimated cost to restore these structures and extend their service life is projected to exceed $260 billion. This growing need for infrastructure rehabilitation has prompted interest in advanced materials such as UHPC for structural repair and strengthening of CC members. The behavior of composite UHPC and CC members presents significant challenges due to the considerable disparity in their mechanical properties. UHPC exhibits a much higher elastic modulus than CC, which leads to disproportionate stress distribution within composite sections. Currently, there is a lack of predictive models and standardized design methodologies for CC compression members repaired or strengthened using UHPC jacket. Additionally, construction procedures for applying UHPC jacket in compression member rehabilitation are not well established.

To address these challenges, this report proposes a comprehensive design methodology and construction framework for utilizing UHPC in the repair and preservation of CC compression members. The main objectives of this research are to:

1. Develop a predictive model capable of estimating the axial and lateral load capacity of compression members encased in UHPC.
2. Demonstrate the proposed model through a case study involving a bridge pier strengthened with UHPC encasement.
3. Investigate the shear transfer and bond strength between CC and UHPC in compression members.
4. Investigate the confinement effect provided by UHPC jacket for compression members.

5. Investigate the flexural behavior of CC compression member repaired with UHPC jacket.
6. Propose construction procedures for implementing UHPC in bridge repair projects.

5.2 Conclusions

This study is divided into analytical and experimental work. The analytical work is proposed to be used to calculate the capacity and construct the interaction diagram for compression members with composite CC-UHPC sections and calculate the effect of confinement. The experimental study investigates the axial and flexural behavior of compression members repaired or strengthened using UHPC in terms of shear transfer and bond capacity between UHPC and CC and investigates the effect of UHPC confinement. The following are the key findings and original contributions of the research:

1. The proposed model in Chapter 3 is suitable for application to composite CC-UHPC sections of compression members and aligns with the design philosophy of AASHTO and PCI guidelines.
2. UHPC jacketing significantly enhances the axial capacity of concrete members, with the degree of improvement dependent on the jacket thickness.
3. A moderate increase in flexural capacity is observed, although the axial strength enhancement is more pronounced.
4. Richart's confinement model can be used to predict the modified strength of CC confined with UHPC. The model shows good agreement with the experimental results, having less than 3.5% deviation in compressive strength and over 10% deviation in strain
5. The inclusion of transverse reinforcement within the UHPC jacket leads to additional enhancement in axial strength beyond that provided by UHPC alone

6. UHPC confinement improved the compression behavior of unreinforced CC as compressive strength increased by 34% with a 1-inch UHPC jacket and by 60% with a 2-inch jacket. Axial strain at peak stress increased by 45% with a 1-inch jacket and by 50% with a 2-inch jacket. Modulus of elasticity (MOE) increased by 24% with a 1-inch jacket and by 62% with a 2-inch jacket.
7. No significant difference between specimens with surface prepared using sandblasting and those with concrete cover removal. Sandblasting is preferred due to its efficiency, simplicity and ability to produce consistent and uniform surface texture.
8. Full composite action between UHPC and the concrete substrate was achieved in all specimens, regardless of the surface preparation technique used (sandblasting or cover removal).
9. The predicted interface shear capacity, as calculated using the AASHTO UHPC Design Specifications, is found to be conservative when compared with experimental results.
10. In specimens ART#1 and ART#2, which included transverse steel reinforcement in the UHPC jacket, no cracking or failure was observed, even at the maximum capacity of the test frame. This confirms that combining UHPC and transverse reinforcement significantly enhances both strength and ductility.
11. Most specimens failed due to crack localization in the UHPC jacket, initiating around 65% of the peak load. These cracks were caused by splitting stresses and propagated downward. However, fiber bridging delayed failure, demonstrating UHPC's post-cracking behavior and toughness.

12. The highest transverse strains in the UHPC jacket were recorded near the column ends. This observation supports the use of transverse reinforcement in the top and bottom of the UHPC jacket to improve composite member performance.

13. Based on the results, no slippage appears at the interface between UHPC jacket and CC core of a circular compression member when loaded in flexure with a measured capacity exceeds the predicted flexural capacity.

5.3 Recommendations for Construction

- For effective bond performance between CC and the UHPC jacket, it is recommended to roughen the surface of the existing concrete using sandblasting or jackhammering techniques. Additionally, the substrate should be pre-wetted prior to casting UHPC. Mechanical anchors are not required when these procedures are applied.
- In strengthening applications, transverse steel ties should be installed within the UHPC jacket near the column/pile ends where transverse stresses are highest. Open ties may be inserted and overlapped to provide adequate anchorage and development.
- UHPC may be cast by free-fall placement for heights up to 4 ft without segregation. For taller members, intermediate pour openings should be incorporated into the formwork to ensure complete filling and to minimize the risk of void formation or segregation.

5.4 Recommendations for Future Research

- Evaluate the performance of UHPC-encased compression members under cyclic loading conditions, such as those encountered in fatigue loading scenarios.
- Conduct a life cycle cost analysis comparing UHPC and FRP confinement methods for reinforced or prestressed concrete structures, to better understand which technique offers greater long-term value in terms of durability, maintenance, and overall cost-effectiveness.

References

AASHTO. (2020). *AASHTO LRFD bridge design specifications* (9th ed.). Washington, DC: American Association of State Highway and Transportation Officials.

ACI Committee 318. (2019). *Building code requirements for structural concrete and commentary (ACI CODE-318-19) (Reapproved 2022)*. Farmington Hills, MI: American Concrete Institute.

Ali Dadvar, S., Mostofinejad, D., & Bahmani, H. (2020). Strengthening of RC columns by ultra-high performance fiber reinforced concrete (UHPFRC) jacketing. *Construction and Building Materials*, *235*, 117485. https://doi.org/10.1016/j.conbuildmat.2019.117485

American Association of State and Highway Transportation Officials. (2022). *AASHTO T 397-22: Standard method of test for uniaxial tensile response of ultra-high performance concrete*. Washington, DC: AASHTO.

American Association of State Highway and Transportation Officials (AASHTO). 2024. "*Guide specification: Structural design with ultra-high performance concrete"*. Developed for consideration by AASHTO CBS T-10 Committee. American Association of State Highway and Transportation Officials.

Binard, J. P. (2017). UHPC: A game-changing material for PCI bridge producers. *PCI Journal*.

Black, A. P. (2022). *Bridge report*. American Road and Transportation Builders Association (ARTBA), Federal Highway Administration (FHWA) National Bridge Inventory (NBI). Retrieved from https://artbabridgereport.org/reports/2022-ARTBA-Bridge-Report.pdf

Bousalem, B., Chikh, N. (2007) "Development of a confined model for rectangular ordinary reinforced concrete columns", Materials and Structures 40(6), 605–613.

Cao, J., Shao, X., Deng, L., & Gan, Y. (2017). Static and fatigue behavior of short-headed studs embedded in a thin ultrahigh-performance concrete layer. *Journal of Bridge Engineering, 22*(5), 04017005.

Collins, M. P., & Mitchell, D. (1991). *Prestressed concrete structures* (Vol. 9). Englewood Cliffs, NJ: Prentice Hall.

De Normalisation, C. E. (2004). *Eurocode 2: Design of concrete structures—Part 1-1: General rules and rules for buildings*. Brussels, Belgium.

Devalupura, R. K., & Tadros, M. K. (1992). Critical assessment of ACI 318 Eq. (18-3) for prestressing steel stress at ultimate flexure. *Structural Journal, 89*(5), 538–554. https://doi.org/10.14359/9641

Doiron, G. (2017). UHPC pier repair/retrofit: Examples of completed projects in North America. In *AFGC-ACI-fib-RILEM International Symposium on Ultra-High Performance Fibre-Reinforced Concrete*.

Ductal. (2020, March). *Ductal website*. Retrieved from https://www.ductal.com/en/

El-Helou, R. G., & Graybeal, B. A. (2019). The ultra girder: A design concept for a 300-foot single span prestressed ultra-high performance concrete bridge girder. *International Interactive Symposium on Ultra-High Performance Concrete, 2*(1). Iowa State University Digital Press.

El-Tawil, S., Tai, Y., Meng, B., Hansen, W., & Liu, Z. (2018). *Commercial production of non-proprietary ultra-high performance concrete* (Report No. RC-1670). Michigan Department of Transportation.

Farouk, A. I. B., Rong, W., & Zhu, J. (2023). Compressive behavior of ultra-high-performance-normal strength concrete (UHPC-NSC) column with the longitudinal grooved contact surface. *Journal of Building Engineering*, *68*, 106074. https://doi.org/10.1016/j.jobe.2023.106074

Farzad, M., Rastkar, S., Sadeghnejad, A., & Azizinamini, A. (2019). Simplified method to estimate the moment capacity of circular columns repaired with UHPC. *Infrastructures, 4*(3), 45. https://doi.org/10.3390/infrastructures4030045

Farzad, M., Shafieifar, M. & Azizinamini, A., 2019. Retrofitting of Bridge Columns Using UHPC. *Journal of Bridge Engineering*, 24(12), p.04019121. https://doi.org/10.1061/(ASCE)BE.1943-5592.0001497

Farzad, M., Shafieifar, M., & Azizinamini, A. (2019). Experimental and numerical study on an innovative sandwich system utilizing UPFRC in bridge applications. *Engineering Structures, 180*, 349–356. https://doi.org/10.1016/j.engstruct.2018.11.052

Farzad, M., Shafieifar, M., & Azizinamini, A. (2019). Retrofitting of bridge columns using UHPC. *Journal of Bridge Engineering, 24*(12), 04019121. https://doi.org/10.1061/(ASCE)BE.1943-5592.0001497

Federal Highway Administration. (2015). *Bridge maintenance reference manual* (Publication No. FHWA-NHI-14-050).

French National Standard (NF) P18-470. (2016). *Ultra-high performance fiber-reinforced concrete – Specifications, performance, production and conformity*. Association Française de Normalisation (AFNOR), Paris, France.

French Standard, NF P 18-710. (2016). *National addition to Eurocode 2 — Design of concrete structures: Specific rules for ultra-high performance fibre-reinforced concrete (UHPFRC)*.

GB 50010-2010. (2010). *Code for design of concrete structures*. Standardization Administration of China: Beijing, China.

Haber, Z. B., & Graybeal, B. A. (2019). Advancing bridge repair and preservation using ultra-high-performance concrete. *ASPIRE Magazine*.

Haber, Z. B., De la Varga, I., Graybeal, B. A., Nakashoji, B., & El-Helou, R. (2018). *Properties and behavior of UHPC-class materials* (Report No. FHWA-HRT-18-036). U.S. Federal Highway Administration, Office of Infrastructure Research and Development.

Haber, Z. B., Foden, A., McDonagh, M., Ocel, J. M., Zmetra, K., & Graybeal, B. A. (2022). *Design and construction of UHPC-based bridge preservation and repair solutions* (Report No. FHWA-HRT-22-065). U.S. Department of Transportation, Federal Highway Administration, Turner-Fairbank Highway Research Center.

Hain, A., & Zaghi, A. (2021). Learnings from the field implementation of a novel UHPC beam end repair on a corroded steel girder bridge in Connecticut. Retrieved from https://www.youtube.com/watch?v=wIU9CgIlTmI&t=111s

Hedia, M. H., & Morcous, G. (2024). Capacity of Reinforced/Prestressed Concrete Compression Members Strengthened/Repaired Using Ultra-High-Performance Concrete Encasement. Transportation Research Record, 2678(11), 1020-1035. https://doi.org/10.1177/03611981241242776

Hossain, K. M. A., Yeganeh, A. E., & Loh, P. (2023, June). Axial load behavior of repaired piers with ultra high-performance concrete jacket. *International Interactive Symposium on Ultra-High-Performance Concrete, 3*(1). https://doi.org/10.21838/uhpc.16730

Hu, J., Marcus, G., & Aitbayeva, A. (2023). Production of cast-in-place UHPC for bridge applications. *NDOT Research Report SPR-FY22(008)*.

Hung, C. C., Kuo, C. W., & Shao, Y. (2021). Cast-in-place and prefabricated UHPC jackets for retrofitting shear-deficient RC columns with different axial load levels. *Journal of Building Engineering, 44*, 103305. https://doi.org/10.1016/j.jobe.2021.103305

Kodsy, A., & Morcous, G. (2023). Predicting strength of non-prestressed concrete I-beams repaired/strengthened in flexure and shear using ultra-high-performance concrete (UHPC). *Structures, 58*, 105670. https://doi.org/10.1016/j.istruc.2023.105670

Lopes Poncetti, B., Brother dos Santos, V., Coelho de Magalhães Grossi, C., Dezotti Tolentino, L., & Dias Vanderlei, R. (2023). Experimental investigation of the performance of normal and high-strength concrete confined by UHPFRC jacketing. *Engineering Structures*, *289*, 116321. https://doi.org/10.1016/j.engstruct.2023.116321

Mander, J. B., Priestley, M. J., & Park, R. (1988). Theoretical stress-strain model for confined concrete. *Journal of Structural Engineering, 114*(8), 1804–1826. https://doi.org/10.1061/(ASCE)0733-9445(1988)114:8(1804)

Mander, J.B., Priestley, M.J.N., Park, R. (1988) "Theoretical Stress-Strain Model for Confined Concrete", Journal of Structural Engineering 1804–1825.

Mattock, A. H. (1979). Flexural strength of prestressed concrete sections by programmable calculator. *PCI Journal, 24*(1), 32–54. https://doi.org/10.15554/pcij.01011979.32.54

Mendonça, F., Abo El-Khier, M., Morcous, G., & Hu, J. (2020). *Feasibility study of development of ultra-high performance concrete (UHPC) for highway bridge applications in Nebraska*.

Rabehi, B., Ghernouti, Y., Li, A., & Boumchedda, K. (2014). Comparative behavior under compression of concrete columns repaired by fiber reinforced polymer (FRP) jacketing and ultra high-performance fiber reinforced concrete (UHPFRC). *Journal of Adhesion Science and Technology, 28*(22–23), 2327–2346. https://doi.org/10.1080/01694243.2014.966885

Richart, F. E., Brandtzæg, A., & Brown, R. L. (1928). *A study of the failure of concrete under combined compressive stresses* (Bulletin No. 185). University of Illinois Engineering Experiment Station.

Ronanki, V. S., & Aaleti, S. (2022). Experimental and analytical investigation of UHPC confined concrete behavior. *Construction and Building Materials, 325*, 126710.

Scott, B.D., Park, R., Priestley, M.J.N. (1982) “Stress-Strain Behavior of Concrete Confined by Overlapping Hoops at Low and High Strain Rates”, ACI Journal Proceedings 79(1) 13–27.

Seibert, P. J., Perry, V., Roy, S., & Bruce, R. (2020). Performance evaluation of field-cast UHPC connections for precast bridge elements. *ACI Materials Journal, 117*(2), 155–167.

SETRA-AFGC. (2002). *Ultra-high-performance fibre-reinforced concretes: Interim recommendations*.

Shehab, H., Eisa, A., Wahba, A. M., Sabol, P., & Katunský, D. (2023). Strengthening of Reinforced Concrete Columns Using Ultra-High Performance Fiber-Reinforced Concrete Jacket. *Buildings*, *13*(8), 2036. https://doi.org/10.3390/buildings13082036

Sim, C., Tadros, M., Gee, D., & Asaad, M. (2020). Flexural design of precast, prestressed ultra-high-performance concrete members. *PCI Journal, 65*(6).

Susilorini, R. M., & Kusumawardaningsih, Y. (2023). Advanced Study of Columns Confined by Ultra-High-Performance Concrete and Ultra-High-Performance Fiber-Reinforced Concrete Confinements. *Fibers*, *11*(5), 44. https://doi.org/10.3390/fib11050044

Tadros, M. K., Lawler, J., Abo El-Khier, M., Gee, D., Kurt, A., Lucier, G., & Wagner, E. (2022). *Implementation of ultra-high-performance concrete in long-span precast pretensioned elements for concrete buildings and bridges: Phase II report v2.0*. Precast/Prestressed Concrete Institute.

Thorenfeldt, E. (1987). Mechanical properties of high-strength concrete and applications in design. In *Symposium Proceedings, Utilization of High-Strength Concrete*. Norway.

Wibowo, H., & Sritharan, S. (2018). Use of ultra-high-performance concrete for bridge deck overlays (No. IHRB Project TR-683).

Wight, J. K., & MacGregor, J. G. (2017). *Reinforced concrete: Mechanics and design* (7th ed.). Pearson Education.

Yuan, W., Chen, Z., Zhang, H., Li, Q., & Zhang, J. (2022). Cyclic performance of RC bridge piers retrofitted with UHPC jackets: Experimental investigation. *Engineering Structures, 259*, 114139. https://doi.org/10.1016/j.engstruct.2022.114139

Zhang, Y., Yang, J., Li, T., & Deng, M. (2022). Mechanical behavior of RC columns strengthened with thin UHPC jacket under cyclic loads. *Journal of Building Engineering*, *49*, 104065. https://doi.org/10.1016/j.jobe.2022.104065

Appendix A Design of Column with UHPC Encasement

Unit Weight of Concrete $\gamma_{uc} := 155\ pcf$

UHPC Compression Model

Design Compressive Strength $f_{uc}' := 21.1\ ksi$

Correction Factor for MOE $K_1 := 1$

Modulus of Elasticity $E_{uc} := 2500\ ksi\ K_1 \cdot \left(\frac{f_{uc}'}{ksi}\right)^{0.33} = 6838\ ksi$

Reduction Factor for Compression $\alpha_u := 0.85$

Elastic Compressive Strain $\varepsilon_{ucp} := \frac{\alpha_u \cdot f_{uc}'}{E_{uc}} = 0.0026$

Ultimate Compressive Strain $\varepsilon_{ucu} := 0.0035$

Compressive Stress-Strain Relationship

$$f_{uc}(\varepsilon_{uc}) := \text{if}\left(0 \le \varepsilon_{uc} < \varepsilon_{ucp}, \varepsilon_{uc} \cdot E_{uc}, \text{if}\left(\varepsilon_{ucp} \le \varepsilon_{uc} \le \varepsilon_{ucu}, \alpha_u \cdot f_{uc}', 0\ ksi\right)\right)$$

UHPC Tension Model

Effective Cracking Strength $f_{t.cr} := 1.1\ ksi$

Crack Localization Stress $f_{t.loc} := 1.18\ ksi$

Check for Strain Hardening $f_{t.loc} := \text{if}\left(f_{t.loc} < 1.2 \cdot f_{t.cr}, f_{t.cr}, f_{t.loc}\right) = 1.1\ ksi$

Elastic Tensile Strain $\varepsilon_{t.cr} := \frac{f_{t.cr}}{E_{uc}} = 0.000161$

Crack Localization Strain $\varepsilon_{t.loc} := 0.0033$

Tensile Stress-Strain Relationship

$$f_t(\varepsilon_t) := \text{if}\left(0 \le \varepsilon_t \le \varepsilon_{t.cr}, \varepsilon_t \cdot E_{uc}, \text{if}\left(\varepsilon_{t.cr} < \varepsilon_t \le \varepsilon_{t.loc}, f_{t.cr} + (\varepsilon_t - \varepsilon_{t.cr}) \cdot \frac{f_{t.loc} - f_{t.cr}}{\varepsilon_{t.loc} - \varepsilon_{t.cr}}, 0\ ksi\right)\right)$$

$\varepsilon_{uc} := 0, 0.0001 .. \varepsilon_{ucu}$ $\varepsilon_t := 0, 0.00001 .. \varepsilon_{t.loc}$

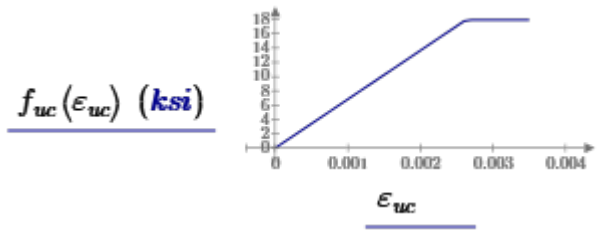

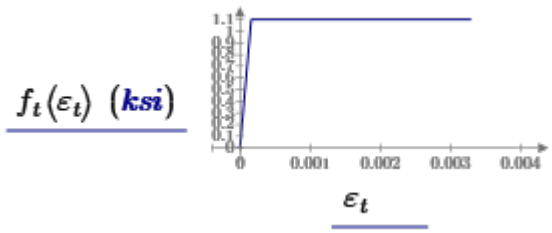

CC Compression Model

Specified Concrete Compressive Strength $f_{cc}' := 5400\ psi$

Unit Weight $\gamma_{cc} := 145\ pcf$

Concrete MOE $E_{cc} := 120\ psi \cdot K_1 \cdot \left(\frac{\gamma_{cc}}{1\ pcf}\right)^2 \cdot \left(\frac{f_{cc}'}{ksi}\right)^{0.33} = 4402\ ksi$

Peak Concrete Strain $\varepsilon_{ccu} := 0.003$

Section Properties

$$\alpha_1 := min\left(0.85, \max\left(0.75, 0.85 - \left(\frac{f_{cc}'}{ksi} - 10\right) \cdot 0.02\right)\right) = 0.85$$

Section Height

$$n := 0.8 + \frac{f_{cc}'}{2500\ psi} = 2.96$$

$$\varepsilon_{cc}' := \frac{f_{cc}'}{E_{cc}} \cdot \frac{n}{n-1} = 0.00185277297883$$

$$k := 0.67 + \frac{f_{cc}'}{9000\ psi} = 1.27$$

Stress-Strain Relationship

$$f_{cc}(\varepsilon_{cc}) := \text{if}\left(0 \le \varepsilon_{cc} \le \varepsilon_{ccu}, f_{cc}' \cdot \left(\frac{n \cdot \frac{\varepsilon_{cc}}{\varepsilon_{cc}'}}{n - 1 + \left(\frac{\varepsilon_{cc}}{\varepsilon_{cc}'}\right)^{n \cdot k}}\right), 0\ psi\right)$$

$\varepsilon_{cc} := 0, 0.0001 .. \varepsilon_{ccu}$

$Q := \varepsilon_{cc} = \begin{bmatrix} 0 \\ \vdots \end{bmatrix} \frac{1}{m} \cdot in$

$f_{cc}(\varepsilon_{cc})\ (ksi)$

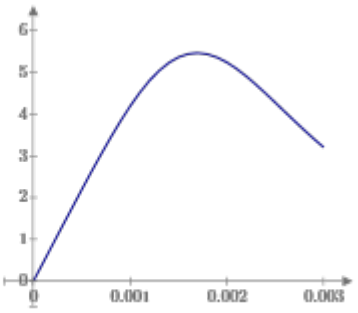

ε_{cc}

Section Properties

Section Height

$$h := 12\ in$$

Outer Section Width (function of distance z from compression side)

$$b_o(z) := \begin{cases} \text{if } 0\ in < z \le 7\ in \\ \quad 10\ in + 14\ in \cdot \frac{z}{7\ in} \\ \text{else if } 7\ in < z \le 17\ in \\ \quad 24\ in \\ \text{else if } 17\ in < z \le h \\ \quad 24\ in - 14\ in \cdot \frac{z - 17\ in}{7\ in} \\ \text{else} \\ \quad 0\ in \end{cases}$$

If Circular

$$b_o(z) := \text{if}\left(0 < z < h, 2 \cdot \sqrt{z \cdot h - z^2}, 0\ in\right)$$

CC Radius

$$r := 4\ in$$

CC Width (function of distance z from compression side)

$$b_h(z) := \text{if}\left(\left(\frac{h}{2} - r\right) < z < \left(\frac{h}{2} + r\right), 2 \cdot \sqrt{r^2 - \left(z - \frac{h}{2}\right)^2}, 0\ in\right)$$

$$b(z) := b_o(z) - b_h(z)$$

$$z := 0, 0.01\ in .. h + 0.01\ in$$

$$b_h(6\ in) = 8\ in$$

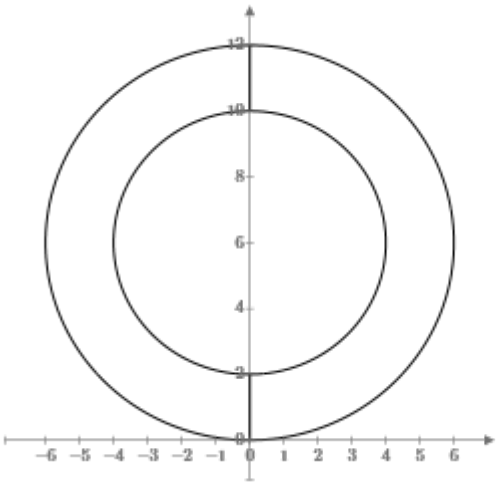

$h - z\ (in)$

$0.5\ b_o(z)\ (in)$

$-0.5 \cdot b_o(z)\ (in)$

$0.5\ b_h(z)\ (in)$

$-0.5\ b_h(z)\ (in)$

UHPC Encasement Thickness

$$t_{uhpc} := \frac{h}{2} - r = 2\ in$$

UHPC Shell

Section Area

$$A_g := \int_{0\,in}^{h} b(z)\,dz = 62.83\ in^2$$

Section C.G. from Compression Side

$$cg := \frac{\int_{0\,in}^{h} b(z)\cdot z\,dz}{A_g} = 6\ in$$

Section Inertia

$$I_g := \int_{0\,in}^{h} b(z)\cdot(cg - z)^2\,dz = 812.1385\ in^4$$

Section Modulus

$$S_g := \frac{I_g}{cg} = 135.36\ in^3$$

Weight per unit length

$$w_g := A_g \cdot \gamma_{uc} = 0.068\ klf$$

CC Core

Section Area

$$A_{gc} := \int_{t_{uhpc}}^{h - t_{uhpc}} b_h(z)\,dz = 50.27\ in^2$$

Section C.G. from Compression Side

$$cg_c := \frac{\int_{t_{uhpc}}^{h - t_{uhpc}} b_h(z)\cdot z\,dz}{A_{gc}} = 6\ in$$

Section Inertia

$$I_{gc} := \int_{t_{uhpc}}^{h - t_{uhpc}} b_h(z)\cdot(cg_c - z)^2\,dz = 201.1\ in^4$$

Section Modulus

$$S_{gc} := \frac{I_{gc}}{cg_c} = 33.513\ in^3$$

Weight per unit length

$$w_{gc} := A_{gc} \cdot \gamma_{cc} = 0.051\ klf$$

Perimeter

$$pr := 2 \cdot \pi \cdot r = 25.133\ in$$

Steel Properties

Steel Yield Strength $f_y := 60\ ksi$

Steel MOE $E_s := 29000\ ksi$

Steel Yield Stain $\varepsilon_y := \frac{f_y}{E_s} = 0.002$

Strain at Service Stress Limit $\varepsilon_{sl} := \frac{0.8\ f_y}{E_s} = 0.00166$

Rupture Strain of Steel $\varepsilon_{su} := 9\%$

Stress of Non-pre-stressing steel

$$f_s(\varepsilon_s) := \text{if}(\varepsilon_s > \varepsilon_{su}, 0\ ksi, \text{if}(\varepsilon_s \geq 0, min(\varepsilon_s \cdot E_s, f_y), \max(\varepsilon_s \cdot E_s, -f_y)))$$

Steel Layers (at least 2)
(from compression side)

A_s (in^2)	d (in)
$1 \cdot 0.307$	2.75
$2 \cdot 0.307$	3.625
$2 \cdot 0.307$	6
$2 \cdot 0.307$	8.375
$1 \cdot 0.307$	9.375

$$\left(\frac{5}{8}\ in\right)^2 \cdot \frac{\pi}{4} = 0.307\ in^2$$

$$6 \cdot \left(\frac{8}{8}\ in\right)^2 \cdot \frac{\pi}{4} = 4.712\ in^2$$

Diameter of bar $d_b := \frac{5}{8}\ in$

$4.712 \cdot 60 = 282.72$

Total Area of Steel $\sum A_s = 2.456\ in^2$

$2.456 \cdot 60 = 147.36$

Steel Reinforcement Ratio $\rho := \frac{\sum A_s}{A_g + A_{gc}} = 2.17\%$

$\varepsilon_s := 0, 0.0001 .. \varepsilon_{su}$

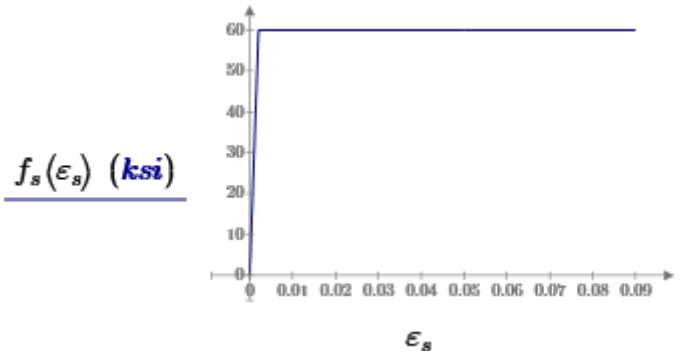

Resistance Factor

Comp-Control Strain Limit	$\varepsilon_{cl} := 0.002$	
Tension-Control Strain Limit	$\varepsilon_{tl} := 0.005$	
Lower Limit of Phi Factor	$\phi_l := 0.65$	0.75 for spiral and 0.65 for tied
Upper Limit of Phi Factor	$\phi_\mu := 0.9$	For Curvature Ductility
Upper Limit of Phi Factor	$\phi_u := 0.9$	Use 1.0 for Prestressed and 0.9 for reinforced
Resistance Reduction Factor	$\phi(\varepsilon_t) := min\left(\phi_u, \max\left(\phi_l, \phi_l + (\phi_u - \phi_l) \cdot \frac{\varepsilon_t - \varepsilon_{cl}}{\varepsilon_{tl} - \varepsilon_{cl}}\right)\right)$	
Ductility Ratio Limit	$\mu_l := 3.0$	

Interaction Diagram

Transverse Reinforcement Factor $k := 0.8$ Use 0.8 for ties and 0.85 for spirals

Pure Compression $P_{no} := k \cdot \left(\alpha_u \cdot f_{uc}' \cdot A_g + \alpha_1 \cdot f_{cc}' \cdot \left(A_{gc} - \sum A_s \right) + f_y \cdot \sum A_s \right) = 1195\ kip$

Curvature Function $$\psi(c) := \text{if}\left(c \le \frac{\varepsilon_{ucu}}{\varepsilon_{ucu} + \varepsilon_{t.loc}} \cdot h, \frac{\varepsilon_{t.loc}}{h - c}, min\left(\frac{\varepsilon_{ucu}}{c}, \frac{\varepsilon_{ccu}}{c - t_{uhpc}} \right) \right)$$

UHPC Compression Force $$C_{uc}(c) := \int_{0\ in}^{c} b(c-y) \cdot f_{uc}(\psi(c) \cdot y)\, dy$$

UHPC Comp. Force Arm from Top $$Z_{uc}(c) := \text{if}\left(0 < c, \frac{\int_{0\ in}^{c} b(c-y) \cdot f_{uc}(\psi(c) \cdot y) \cdot (c-y)\, dy}{C_{uc}(c)}, 0\ in \right)$$

UHPC Tension Force $$T_c(c) := \int_{0\ in}^{h-c} b(c+y) \cdot f_t(\psi(c) \cdot y)\, dy$$

UHPC Tension Force Arm from Top $$X(c) := \text{if}\left(c < h, \frac{\int_{0\ in}^{h-c} b(c+y) \cdot f_t(\psi(c) \cdot y) \cdot (c+y)\, dy}{T_c(c)}, 0\ in \right)$$

CC Compression Force $$C_{cc}(c) := \int_{0}^{c} b_h(c-y) \cdot f_{cc}(\psi(c) \cdot y)\, dy$$

CC Comp. Force Arm from Top $$Z_{cc}(c) := \frac{\int_{0}^{c} b_h(c-y) \cdot f_{cc}(\psi(c) \cdot y) \cdot (c-y)\, dy}{C_{cc}(c)}$$

Strain in Non-Pre-stressing Steel $\varepsilon_s(c) := (d - c) \cdot \psi(c)$

Stress in Non-Pre-stressing Steel

$$f_{ss}(c) := \left\| \begin{array}{l} \text{for } i \in 0 .. \text{last}(d) \\ \quad \left\| \begin{array}{l} R_i \leftarrow \text{if } d_i > c \\ \qquad \left\| f_s\left(\varepsilon_s(c)_i\right) - f_t\left(\varepsilon_s(c)_i\right) \right. \\ \qquad \text{else} \\ \qquad \left\| f_s\left(\varepsilon_s(c)_i\right) + f_{uc}\left(\varepsilon_s(c)_i\right) \right. \end{array} \right. \\ R \end{array} \right.$$

Force in Non-Pre-stressing Steel $T_s(c) := \overrightarrow{A_s \cdot f_{ss}(c)}$

Nominal Axial Force $P_n(c) := min\left(C_{uc}(c) + C_{cc}(c) - T_s(c) - \sum T_s(c), P_{no} \right)$

Nominal Moment

$$M_n(c) := C_{uc}(c)\cdot\left(cg - Z_{uc}(c)\right) + C_{cc}(c)\cdot\left(cg_c - Z_{cc}(c)\right) + T_c(c)\cdot\left(X(c) - cg\right) + T_s(c)\cdot\left(d - cg\right)$$

Depth of most tension Steel $d_t := \max(d) = 9.375\ in$

Strain Resistance Factor $\phi(c) := \phi\left(\left(d_t - c\right)\cdot\psi(c)\right)$

Service Stress Limit Curvature $\psi_l(c) := \dfrac{\varepsilon_{sl}}{d_t - c}$ Use $\varepsilon_{pl} - \varepsilon_{pe}$ for prestressed, ε_{sl} for reinforced

Curvature Ductility Ratio $\mu(c) := \dfrac{\psi(c)}{\psi_l(c)}$

Curvature Ductility Resistance Factor $\phi_\mu(c) := \text{if}\left(\mu(c) < 1, \phi_l, \text{if}\left(\mu(c) > \mu_l, \phi_\mu, \phi_l + \left(\phi_\mu - \phi_l\right)\cdot\dfrac{\left(\mu(c) - 1\right)}{\left(\mu_l - 1\right)}\right)\right)$

For Pure Flexure $c_{eq} := \text{root}\left(C_{uc}(c) + C_{cc}(c) - T_c(c) - \sum T_s(c), c, 0, h\right) = 3.593\ in$

Range of Plot $c := c_{eq}, c_{eq} + 0.05\ in\ldots 3\ h$

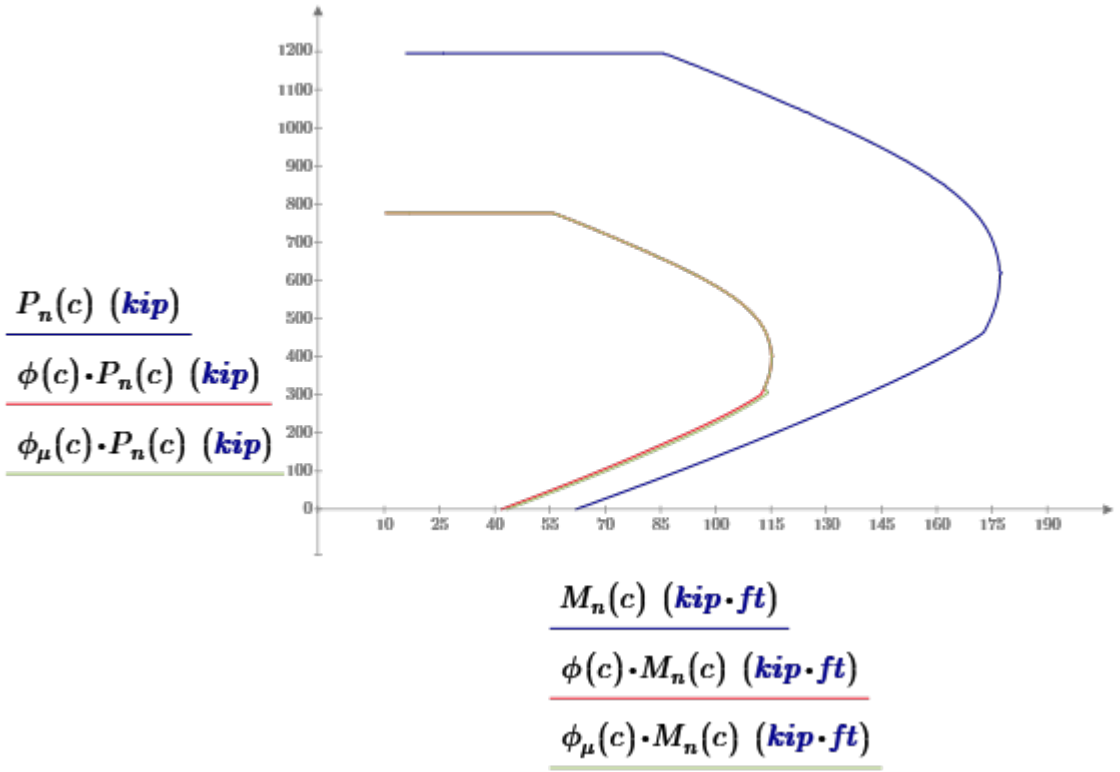

Check Slenderness

Height of column $l := 4\ ft$ $l_u := 4\ ft$

Moment at the top $M_1 := 1\ kip \cdot ft$

Moment at the bottom $M_2 := 1\ kip \cdot ft$

Radius of Gyration $r := \sqrt{\frac{I_{gc} + I_g}{A_{gc} + A_g}} = 2.99\ in$ 0.3h for rectangular, 0.25h for circular

Effective Length Factor $k_s := 1.0$ For pinned-pinned condition

Column Slenderness $sl := \frac{k_s \cdot l_u}{r} = 16$

Short Column Limit $lim := min\left(34 - 12 \cdot \frac{M_1}{M_2}, 40\right) = 22$ braced column with min moment at the top and bottom

$$check := \text{if}\left(sl \le lim, \text{“Short Column”}, \text{“Slender Column”}\right) = \text{“Short Column”}$$

Axial Capacity of CC only

$$P_{n.cc} := k \cdot \left(\alpha_1 \cdot f_{cc}' \cdot \left(A_{gc} - \sum A_s\right) + f_y \cdot \sum A_s\right) = 293.4\ kip$$

Axial Capacity of UHPC only

$$P_{n.uhpc} := k \cdot \left(\alpha_u \cdot f_{uc}' \cdot A_g\right) = 901.5\ kip$$

$$Primeter := 2 \cdot 4\ in \cdot \pi = 25.133\ in$$

Concrete Confinement Formula (Richart, 1928, Brandzaeg, 1928, Brown, 1934)

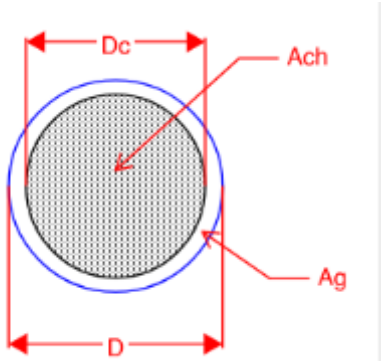

CC Compressive Strength $f_c' := 5.4\ ksi$

Gross Section Diameter $D := b_o(6\ in) = 12\ in$

Gross Section Area $A_t := A_g + A_{gc} = 113.1\ in^2$

UHPC Tensile Strength $f_t := f_{t.loc} = 1.1\ ksi$

UHPC Cover Thickness $c := t_{uhpc} = 2\ in$

Area of Longitudinal Steel $\sum A_s = 2.456\ in^2$

Steel Yield Strength $f_y := 60\ ksi$

Spiral (Core) Diameter $D_c := b_h(6\ in) = 8\ in$

Core Area $A_{cc} := A_{gc} = 50.27\ in^2$

Area of UHPC per unit length $A_u := c \cdot 1\ in = 2\ in^2$

Area of tie $A_{st} := \left(\frac{3}{8}\ in\right)^2 \cdot \frac{\pi}{4} = 0.11\ in^2$

Tension Force in Unreinforced UHPC $T_u := A_u \cdot f_t = 2.2\ kip$

Tension Force in reinforced UHPC $T_{u2} := A_u \cdot f_t + A_{st} \cdot f_y = 8.827\ kip$

Unreinforced UHPC Confinement Stress $f_2 := \frac{2 \cdot T_u}{D_c \cdot 1\ in} = 0.55\ ksi$

Reinforced UHPC Confinement Stress $f_{22} := \frac{2 \cdot T_{u2}}{D_c \cdot 1\ in} = 2.207\ ksi$

Unreinforced UHPC Confined Concrete Strength $f_{cc}' := f_c' + 4.1 \cdot f_2 = 7.66\ ksi$

Reinforced UHPC Confined Concrete Strength $f_{cc2}' := f_c' + 4.1 \cdot f_{22} = 14.447\ ksi$

Unconfined Core Capacity $P_o := \left(A_{cc} \cdot 0.85\ f_c' + \sum A_s \cdot (f_y - 0.85\ f_c')\right) \cdot 0.8 = 293\ kip$

Unreinforced UHPC Confined Core Capacity $P_{cc} := \left(A_{cc} \cdot 0.85\ f_{cc}' + \sum A_s \cdot (f_y - 0.85\ f_{cc}')\right) \cdot 0.8 = 367\ kip$

Reinforced UHPC Confined Core Capacity $P_{cc} := \left(A_{cc} \cdot 0.85\ f_{cc2}' + \sum A_s \cdot (f_y - 0.85\ f_{cc2}')\right) \cdot 0.8 = 588\ kip$

Interface shear

No. of Anchors $n := 0 \cdot 4 = 0$

Area of each Anchor $A_{vf1} := \left(\frac{2}{8}\ in\right)^2 \cdot \frac{\pi}{4} = 0.049\ in^2$

Area of interface reinforcement crossing the shear plane within the area **Acv** $A_{vf} := n \cdot A_{vf1} = 0\ in^2$

Yield strength of **Avf** $f_y := 60\ ksi$

Normal clamping force provided by steel reinforcement $C_1 := A_{vf} \cdot f_y = 0\ kip$ Article 1.7.4.4

Normal clamping force provided by UHPC $C_2 := 0\ kip$ Article 1.7.4.4

Limiting interface shear resistance $K := 0.8\ ksi$ 1.8 ksi for intentionally roughened
0.8 ksi for not intentionally roughened

Permanent net compressive force normal to shear plane $P_c := 0\ kip$

Friction factor $\mu := 0.6$ 1.0 for intentionally roughened
0.6 for not intentionally roughened

Cohesion factor $c := 0.075\ ksi$ 0.24 ksi for intentionally roughened
0.075 ksi for not intentionally roughened

Interface Length considered to be engaged in shear transfer $L_v := l_u - 2\ in = 46\ in$

Interface width considered to be engaged in shear transfer $b_v := pr = 25.133\ in$ Article 1.7.4.4

Area of UHPC engaged in interface shear transfer $A_{cv} := (b_v \cdot L_v) - (A_{vf}) = 1156.106\ in^2$

Nominal shear resistance of interface plane $V_n := min\left(\left(c \cdot A_{cv} + \mu \cdot \left(C_1 + C_2 + P_c\right)\right), K \cdot A_{cv}\right) = 86.708\ kip$

Development Length of Longitudinal bars $l_{db} := \max\left(\frac{0.63 \cdot f_y \cdot d_b}{\sqrt{f_{cc}' \cdot ksi}}, 0.3\ d_b \cdot \frac{f_y}{ksi}\right) = 11.25\ in$

Tie diameter $d_{bs} := \frac{3}{8}\ in$

Extension length of ties $l_s := \max\left(6 \cdot d_{bs}, 75\ mm\right) = 3\ in$

Appendix B Supplementary Experimental Results

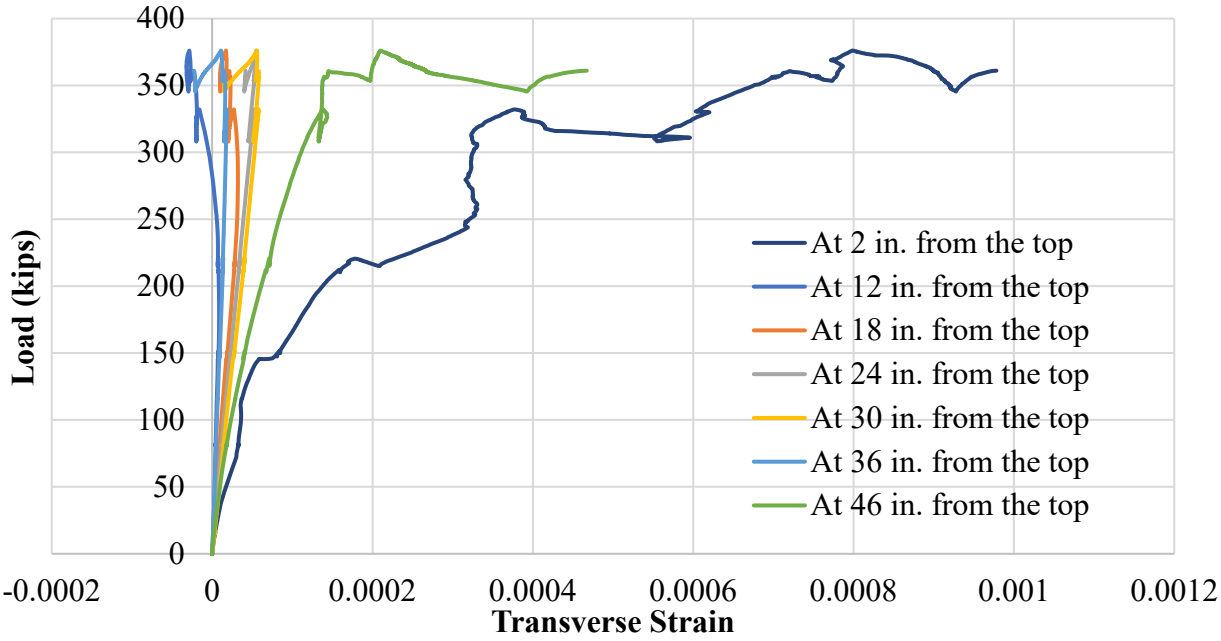

Figure B.1 Transverse strain results of Specimen AS#1

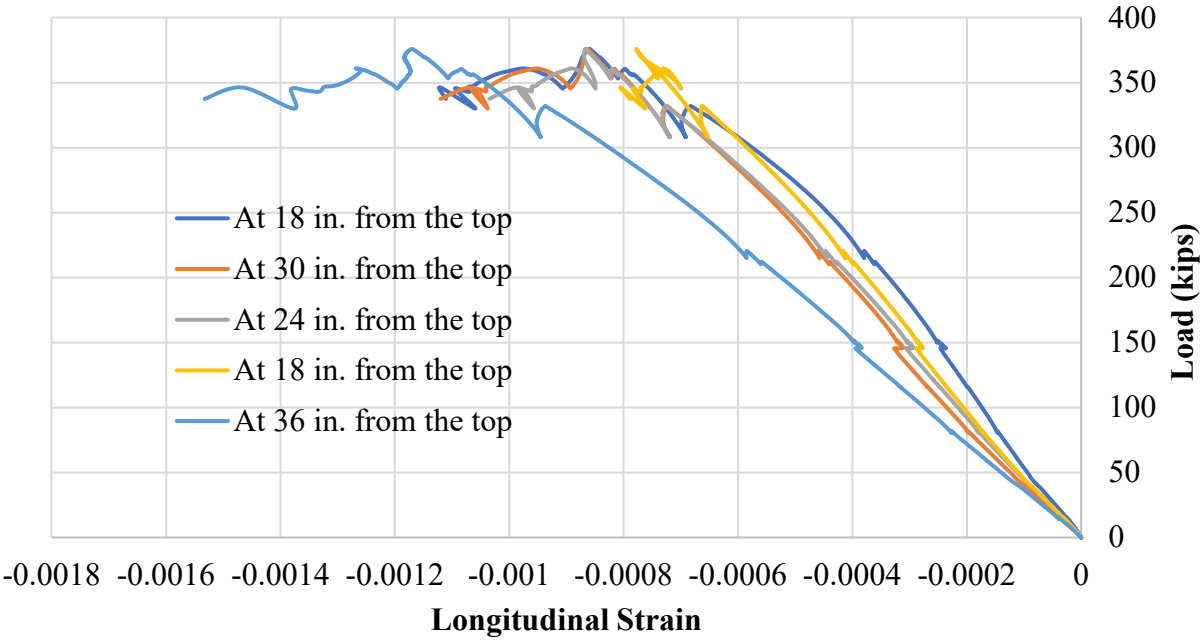

Figure B.2 Longitudinal strain results of Specimen AS#1

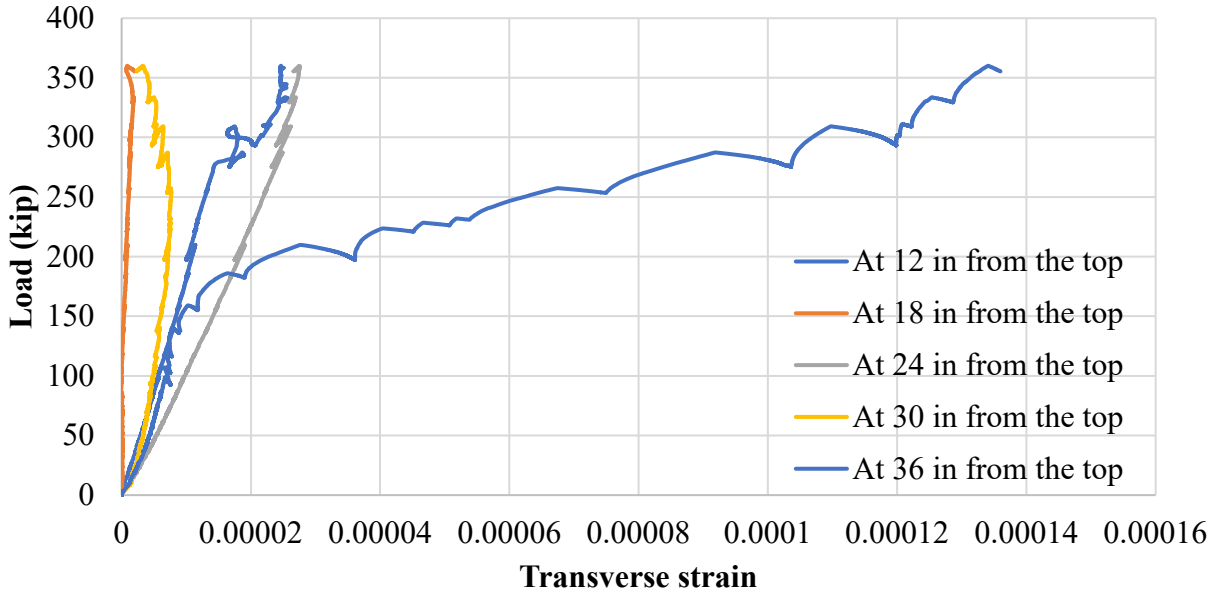

Figure B.3 Transverse strain results of Specimen AS#2

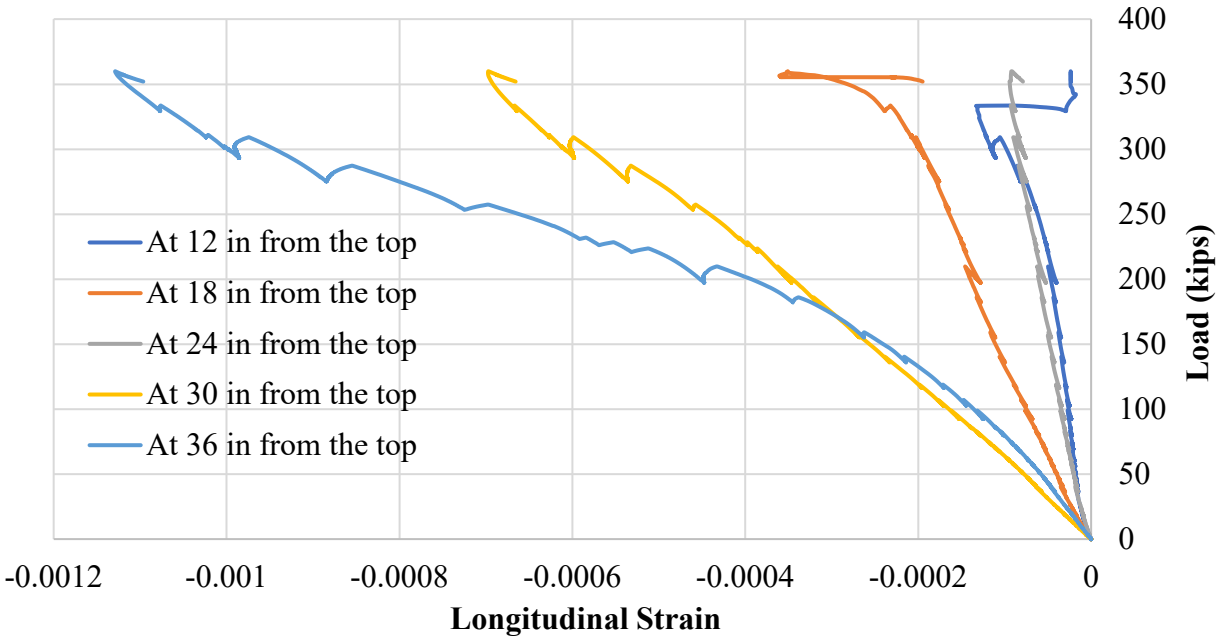

Figure B.4 Longitudinal strain results of Specimen AS#2

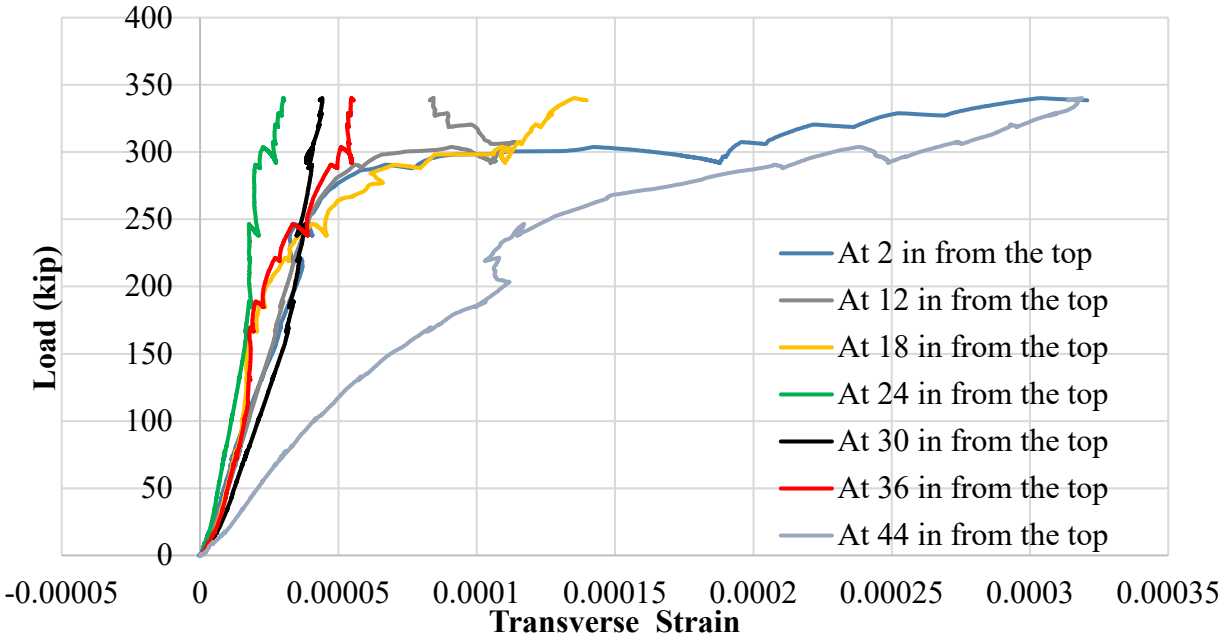

Figure B.5 Transverse strain results of Specimen AR#1

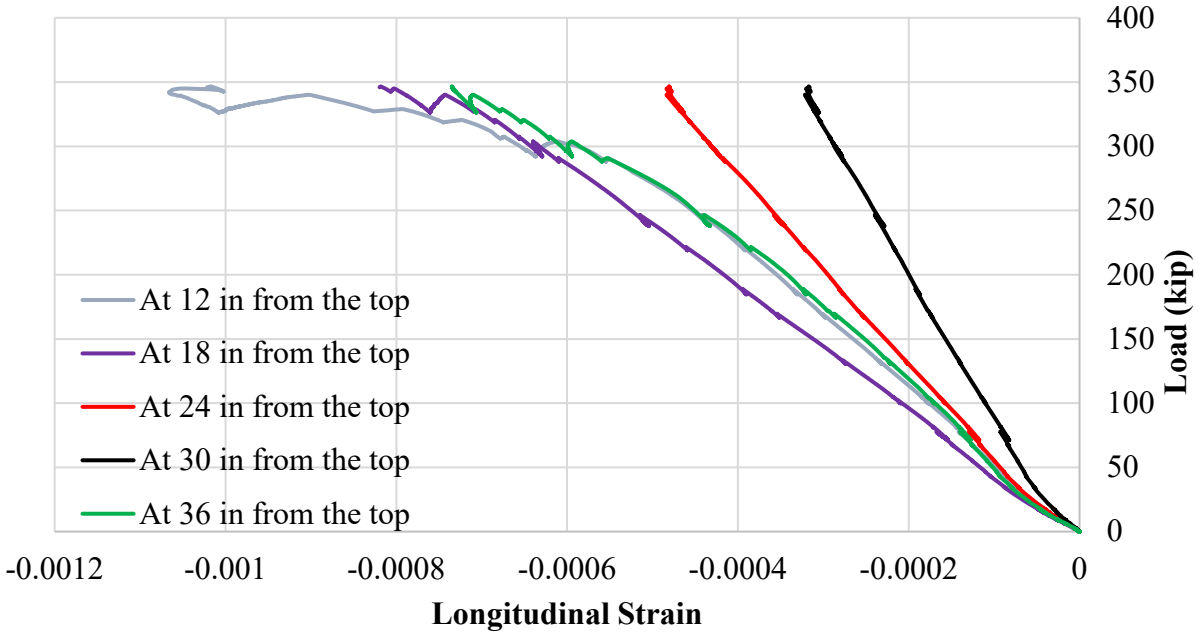

Figure B.6 Longitudinal strain results of Specimen AR#1

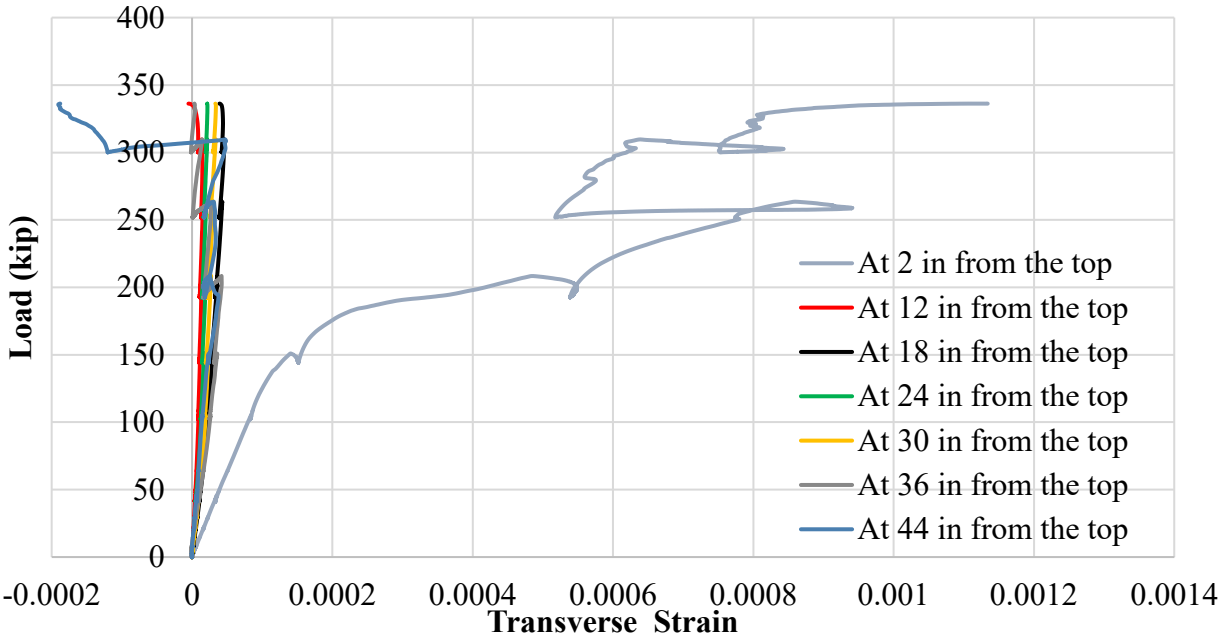

Figure B.7 Transverse strain results of Specimen AR#2

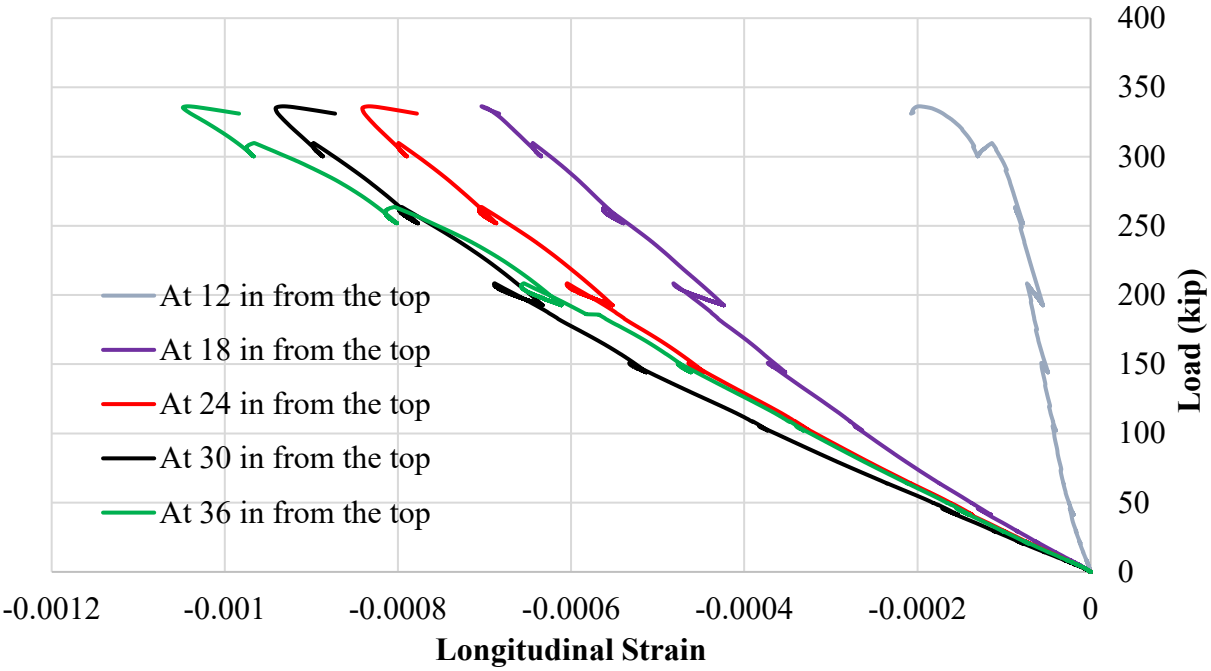

Figure B.8 Longitudinal strain results of Specimen AR#2

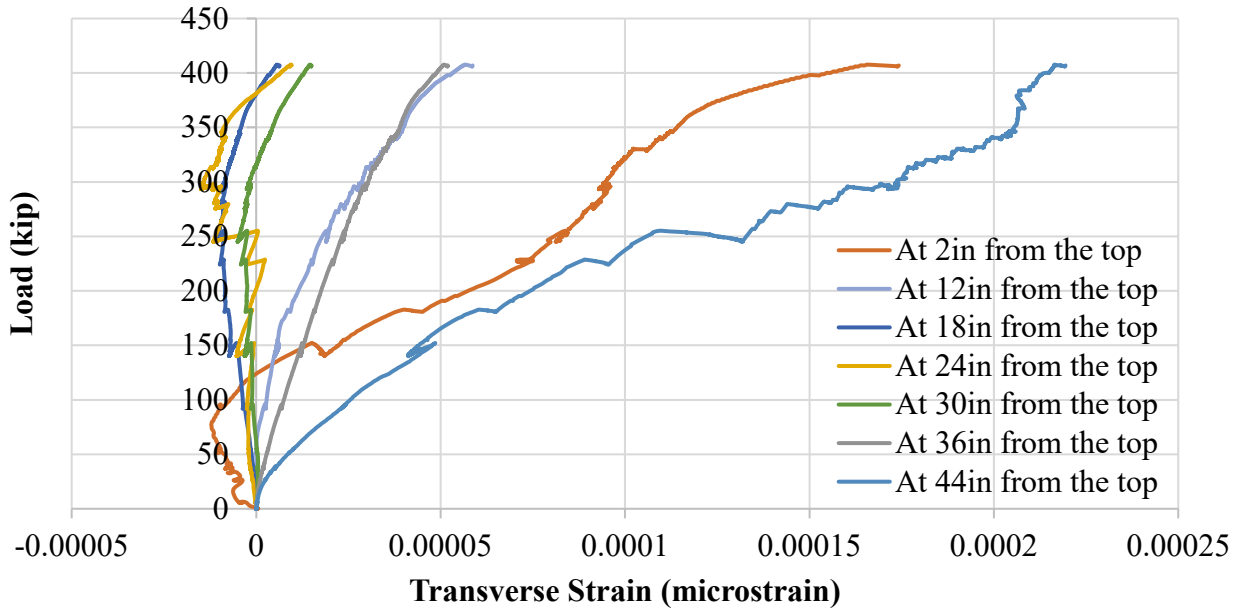

Figure B.9 Transverse strain results of Specimen ART#1

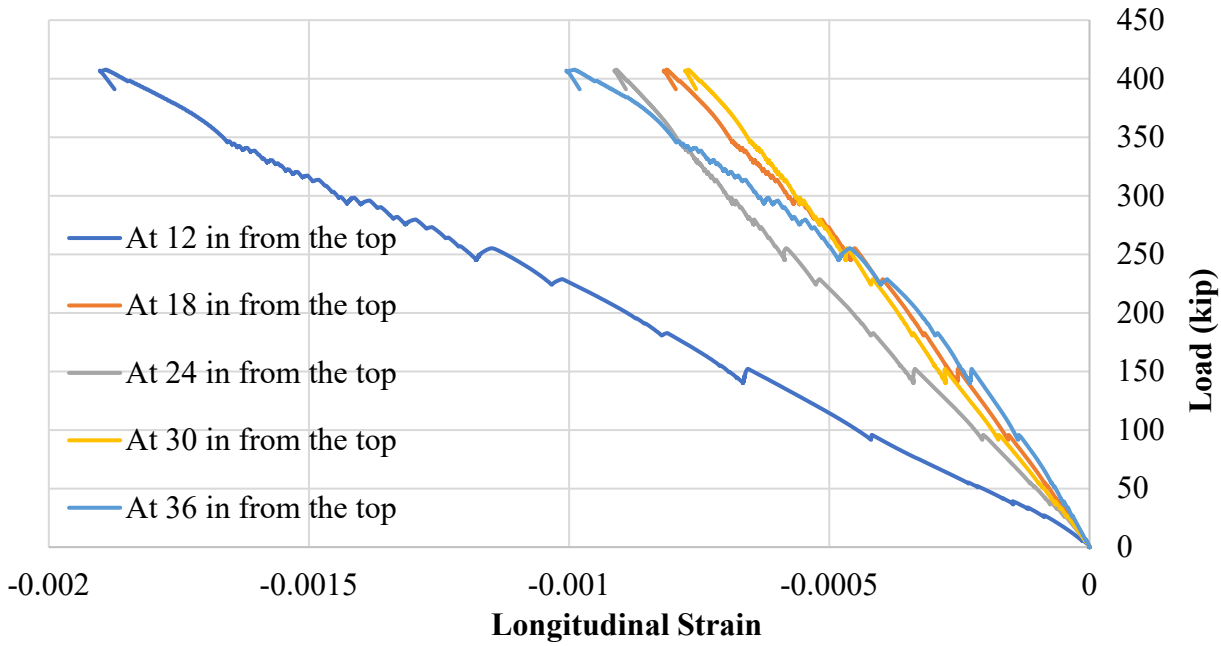

Figure B.10 Longitudinal strain results of Specimen ART#1